7th IAA Planetary Defense Conference

26-30 April 2021, Online Event

Hosted by UNOOSA in collaboration with ESA

Session 9a: Impact Effects

Chairs: Olga Popova | Michael Aftosmis | Mark Boslough | Jessie Dotson | David Morrison

Presenters: A. Losiak | S. Haihao | S. Liu | D. Glazachev | O. Popova

Environmental Effects of Very Small Crater Formation

wildFIRE lab

A. Losiak[1,2], C. Belcher[1],

J. Plado[3], A. Jõeleht[3], C. D. K. Herd[4], R. S. Kofman[4], M. Szokaluk[5], W. Szczuciński[5], A. Muszyński[5], M. Szyszko, E. M. Wild[6]

[1]wildFIRE Lab, Hatherly Laboratories, University of Exeter, UK; [2]Institute of Geological Sciences, PAS, Poland; [3]Department of Geology, University of Tartu, Estonia, [4]Institute of Geology, Adam Mickiewicz University in Poznan; [6]VERA Laboratory, Faculty of Physics, University of Vienna;

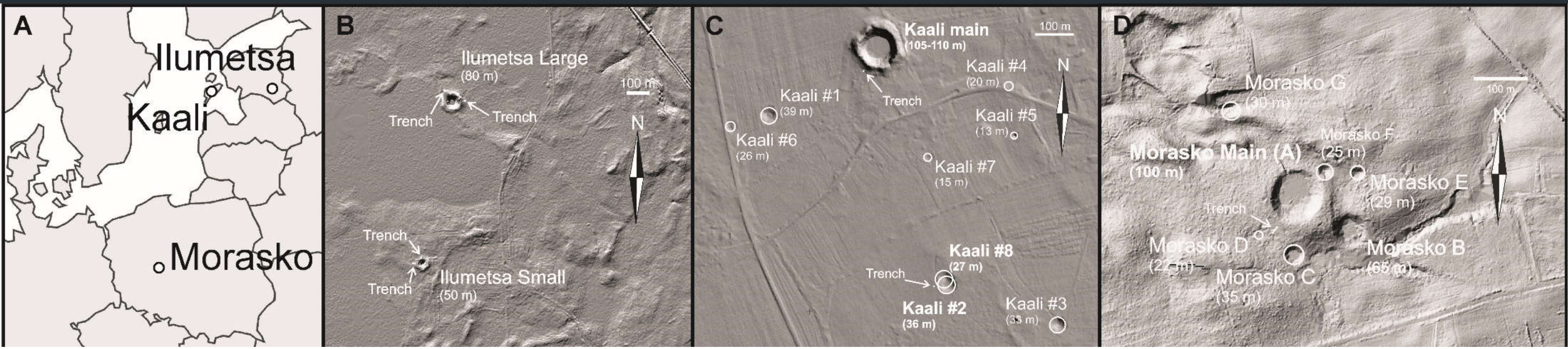


Chixulub
10 km asteroid
180 km crater

What about very small craters?

wildFIRE lab

- 17 known craters <200 m

Schmieder and Kring 2020

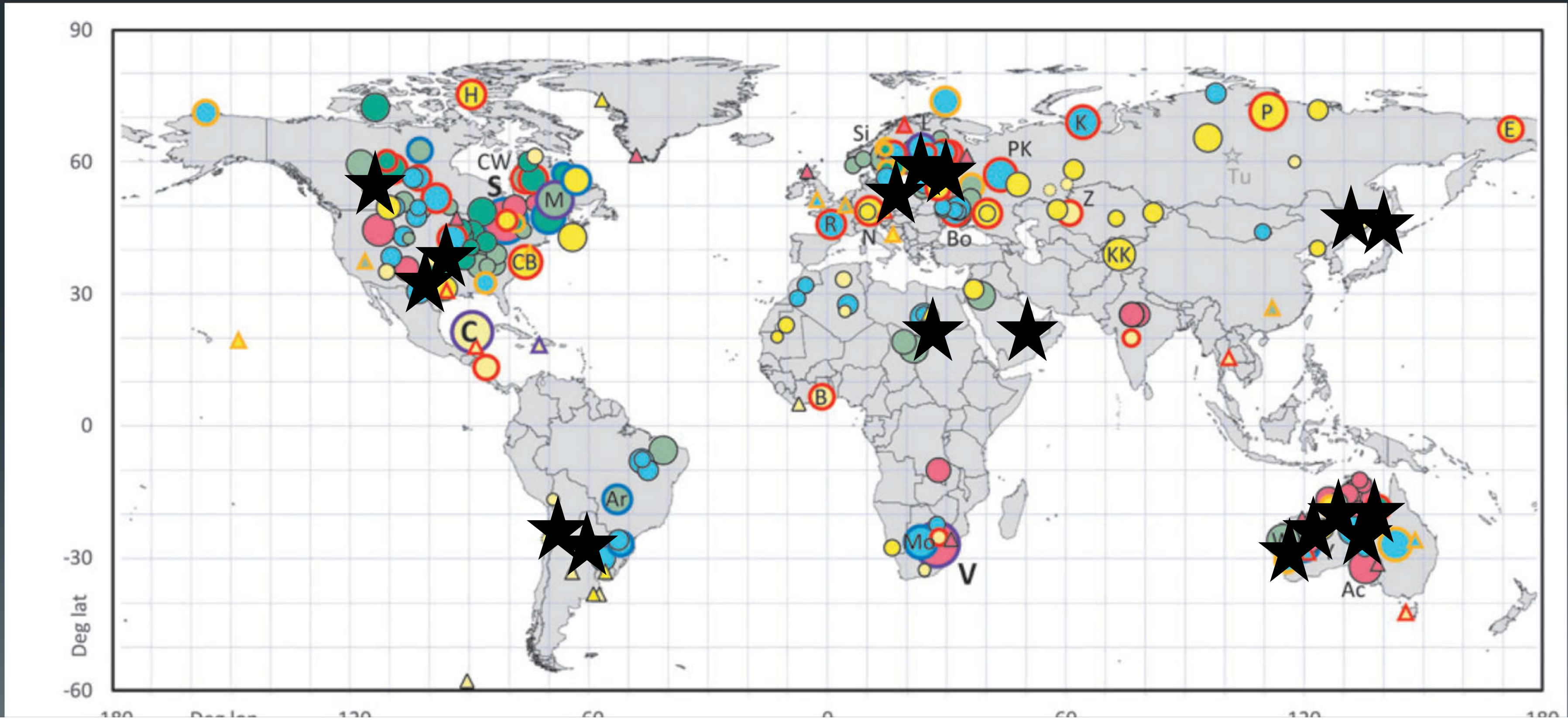

What about very small craters?

- 17 known craters <200 m
- Should be >20 Holocene ~100m craters
  - There are 5 (80-120m)

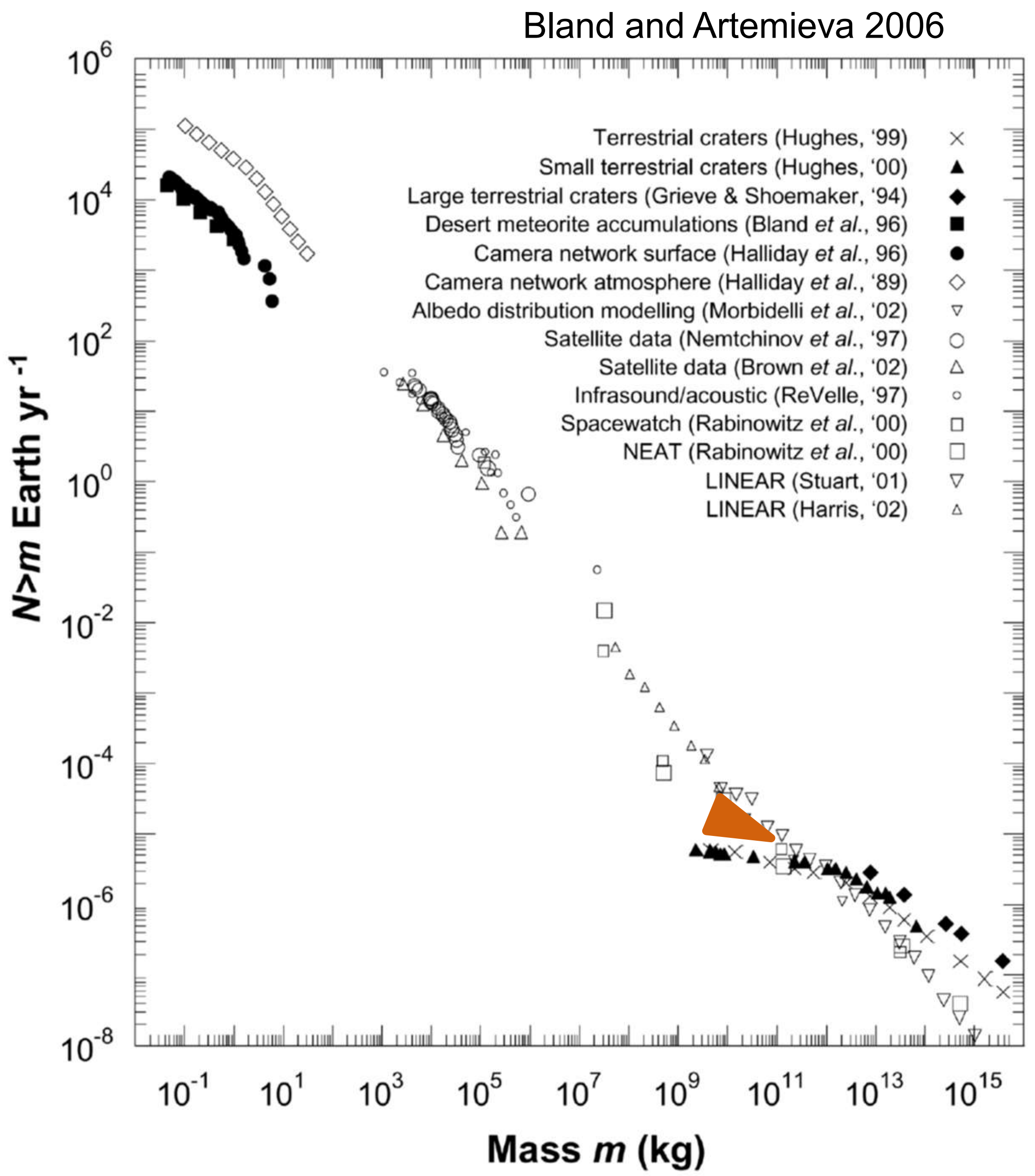

Environmental effects: Kaali

- Strewn field
  - Up to 100 m

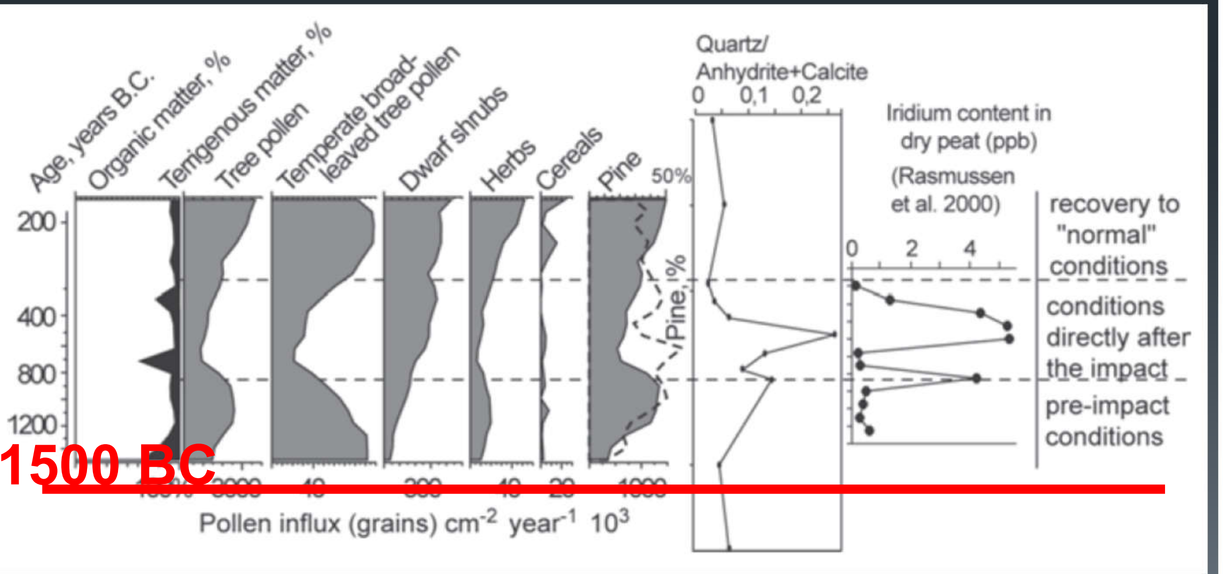

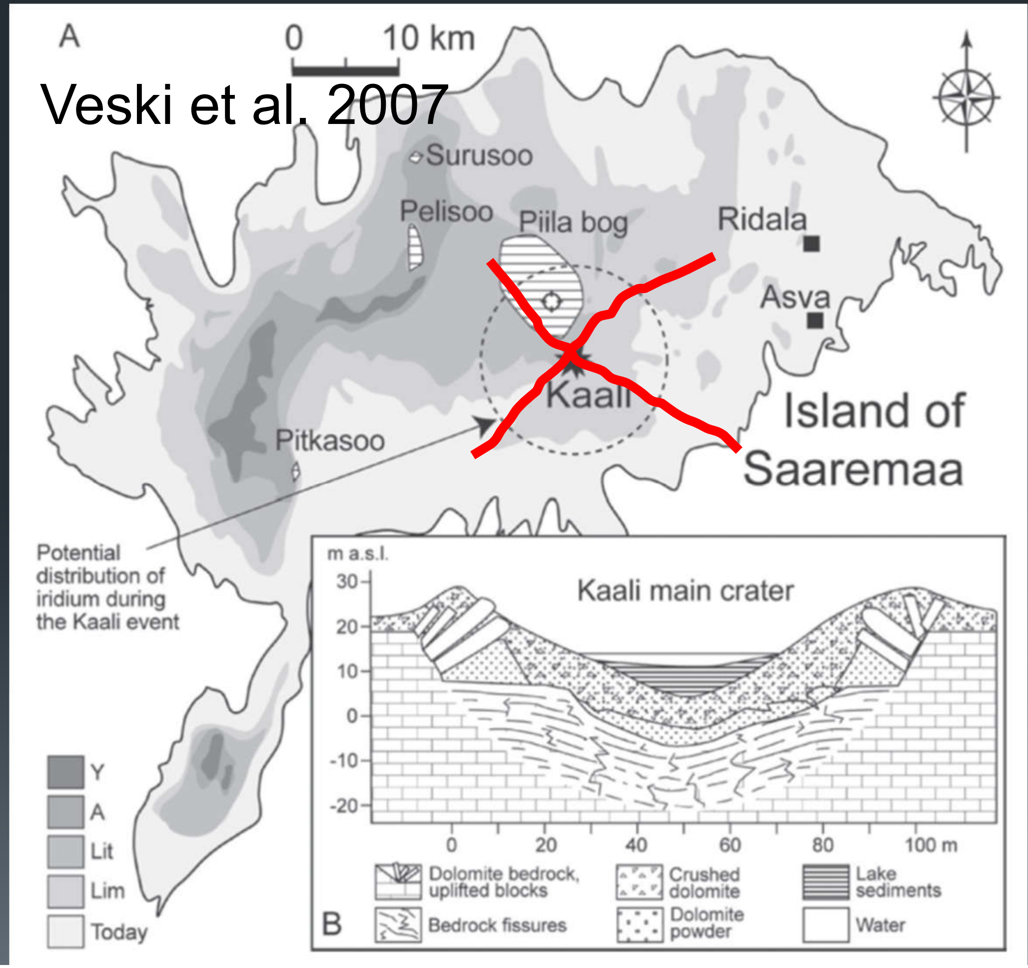

Environmental effects: Morasko

- Strewn field
  - Up to 100 m

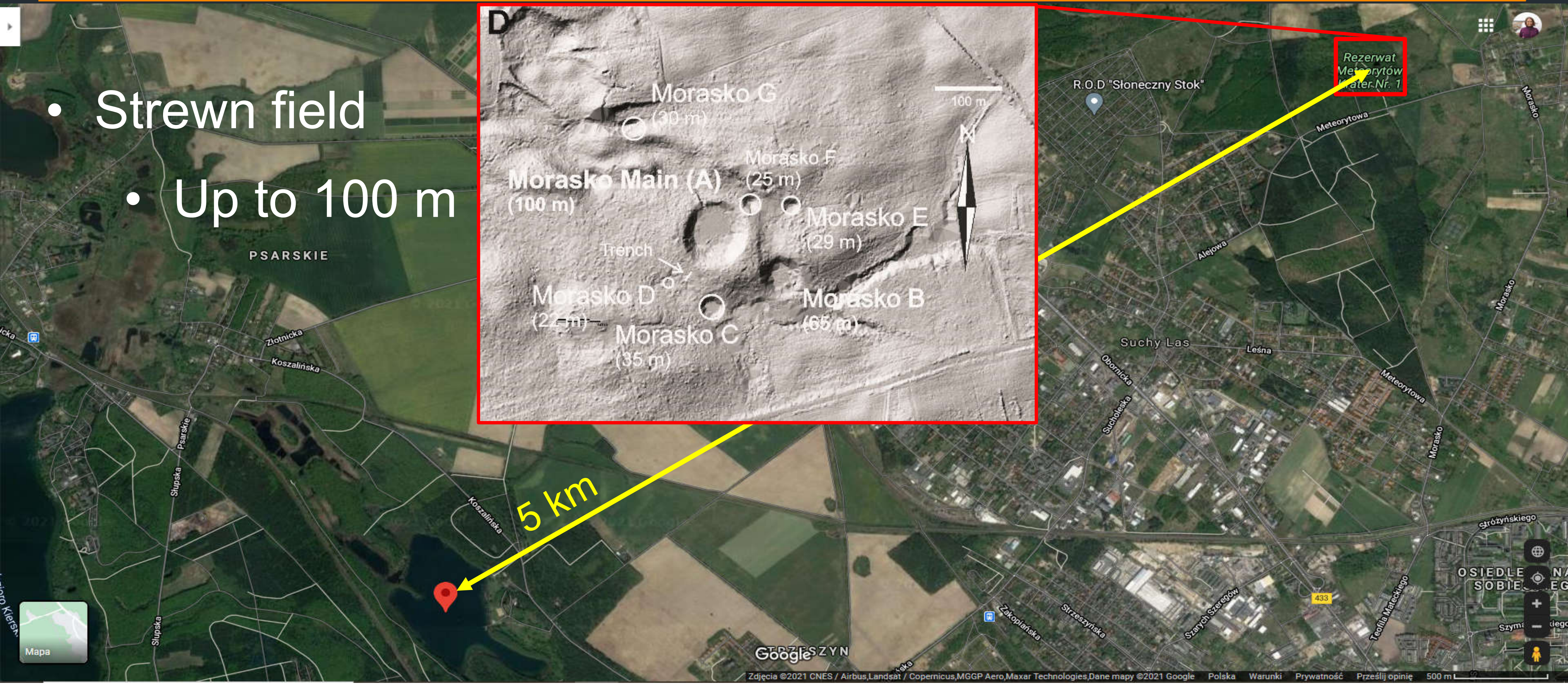

Environmental effects: Morasko

- Strewn field
  - Up to 100 m

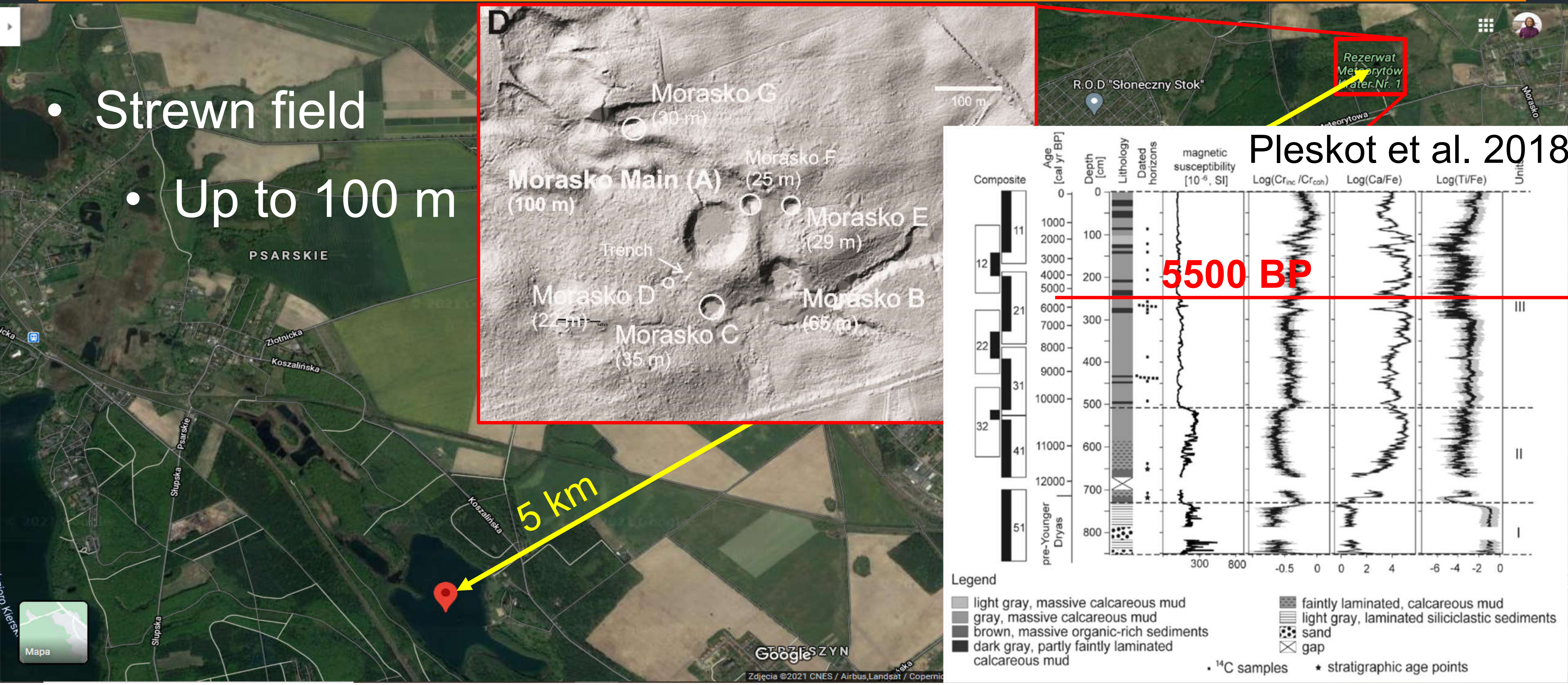

Charcoal in proximal ejecta of small impact craters

wildFIRE Lab

Charcoal in proximal ejecta of small impact craters

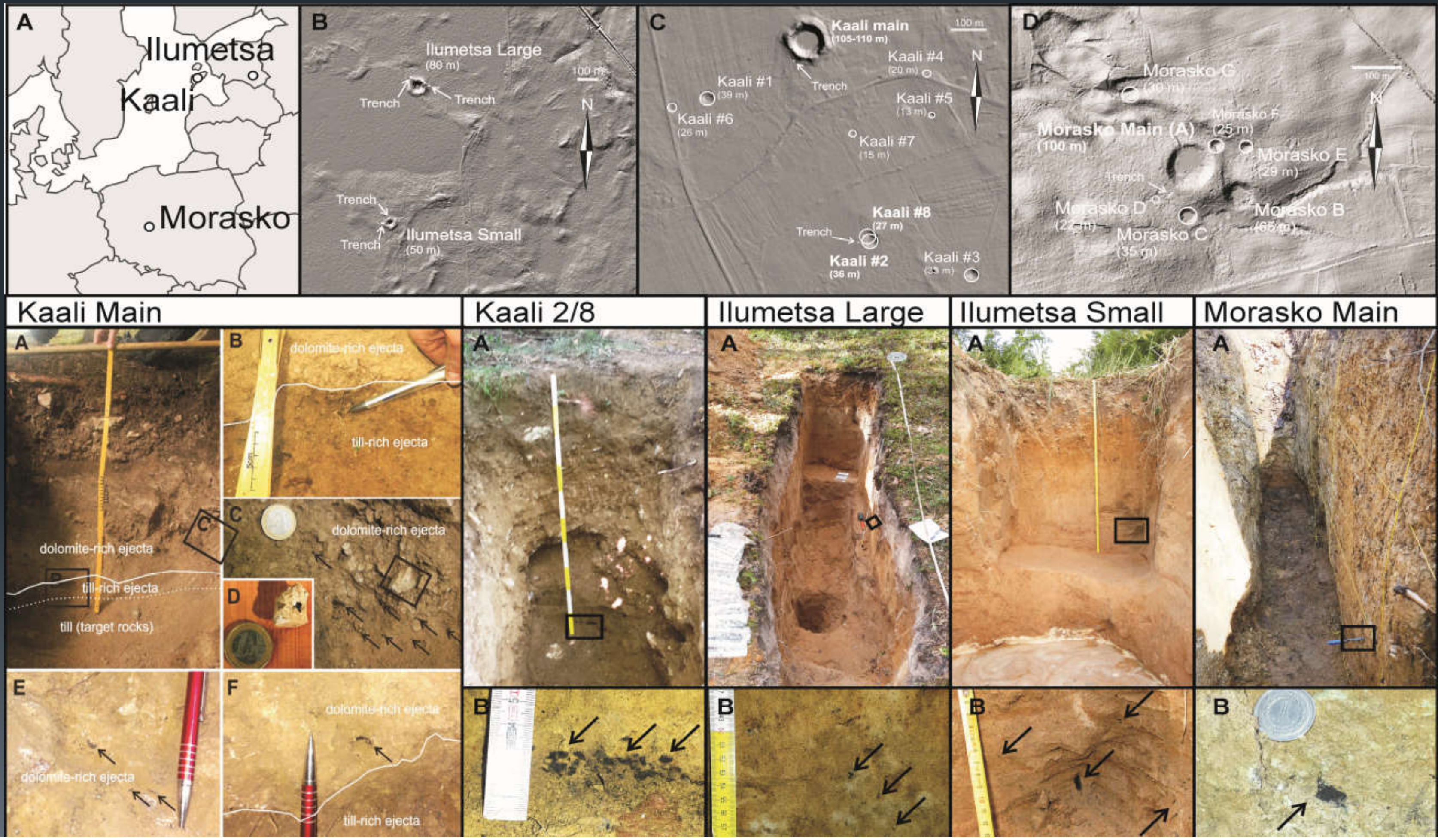

Small impacts charcoal: distribution

- Horizontal distribution:
  - Ring <rim to < ~0.1 R
- Vertical distribution:
  - Depth > 50 cm
  - Most close to ejecta base
- Double charcoal layer at overlapping craters

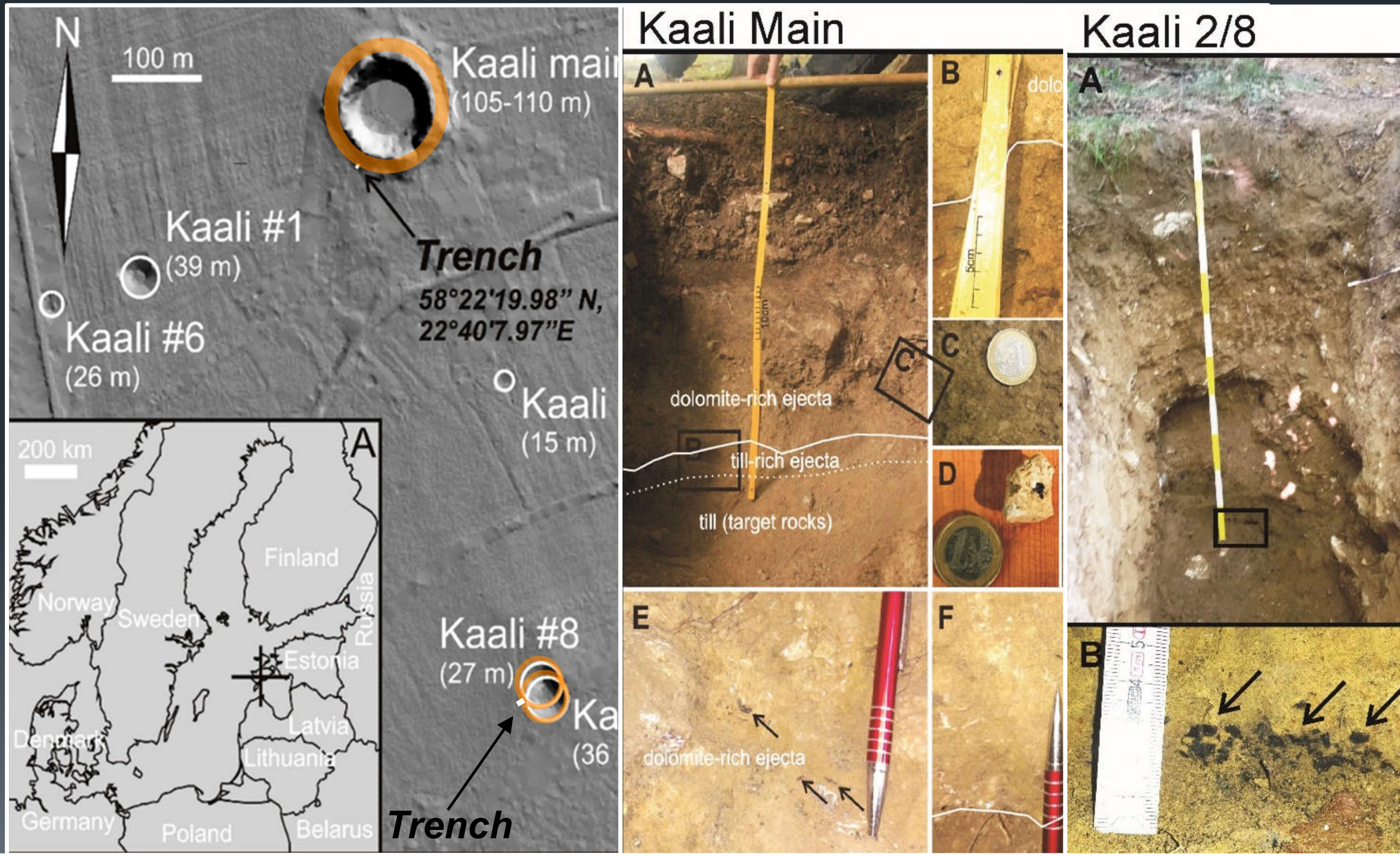

Small impacts charcoal: ages

- ± same age
  - Oldest sediments inside craters and proximal ejecta charcoals
  - Proximal ejecta charcoals from different craters of the same strewn field

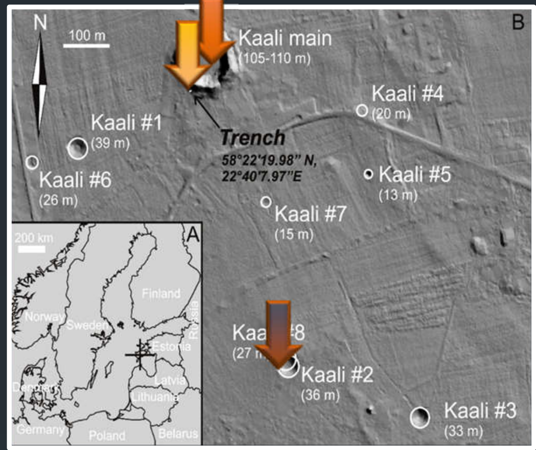

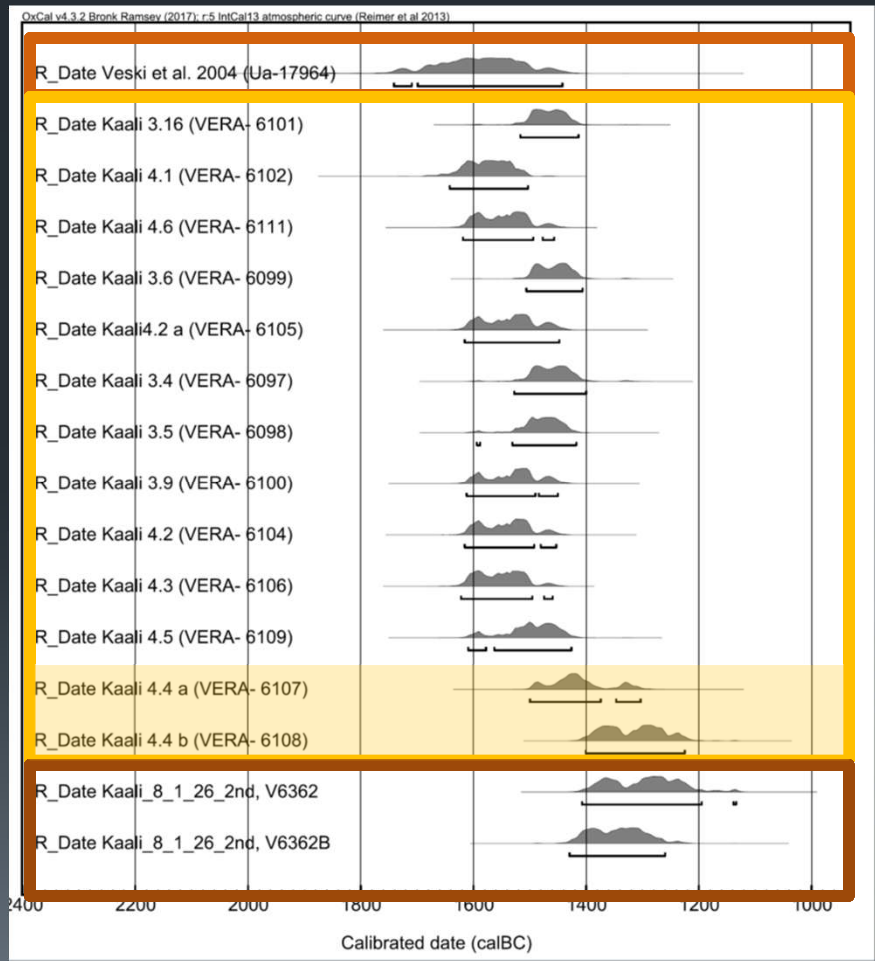

Small impacts charcoal: REFLECTANCE

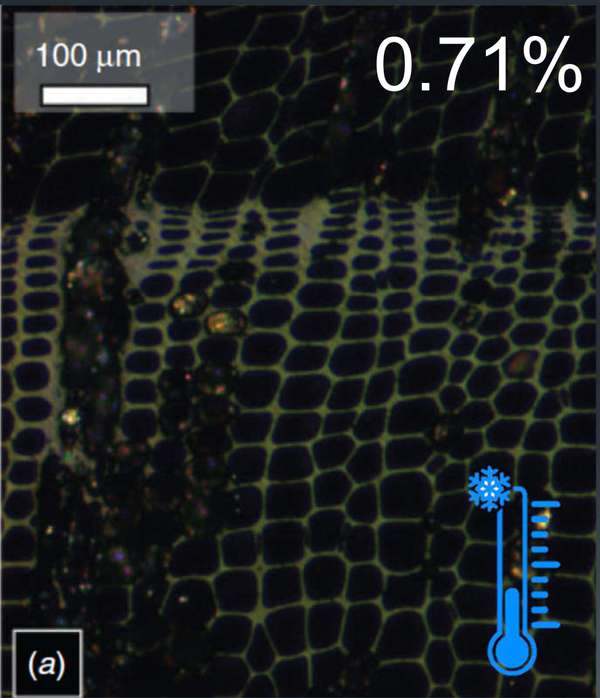

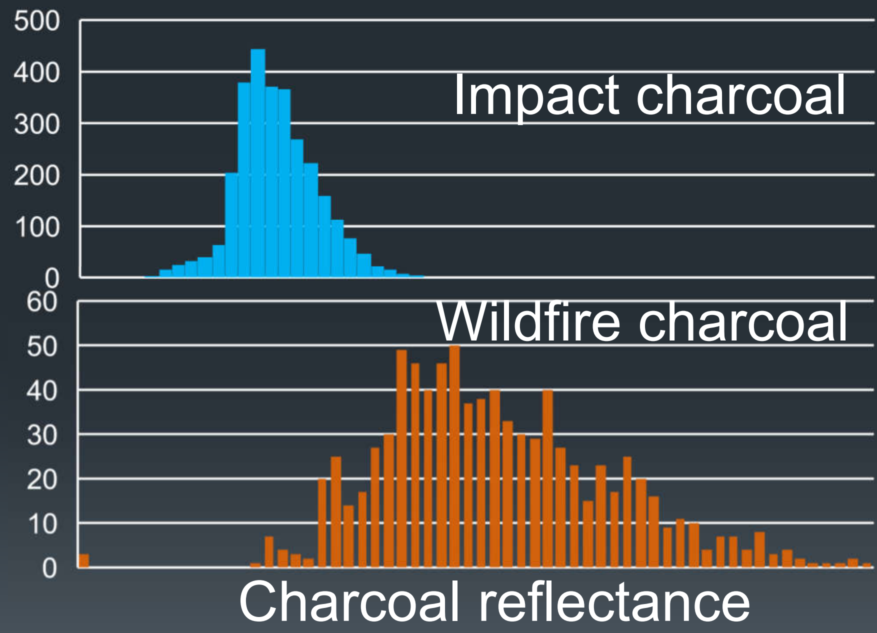

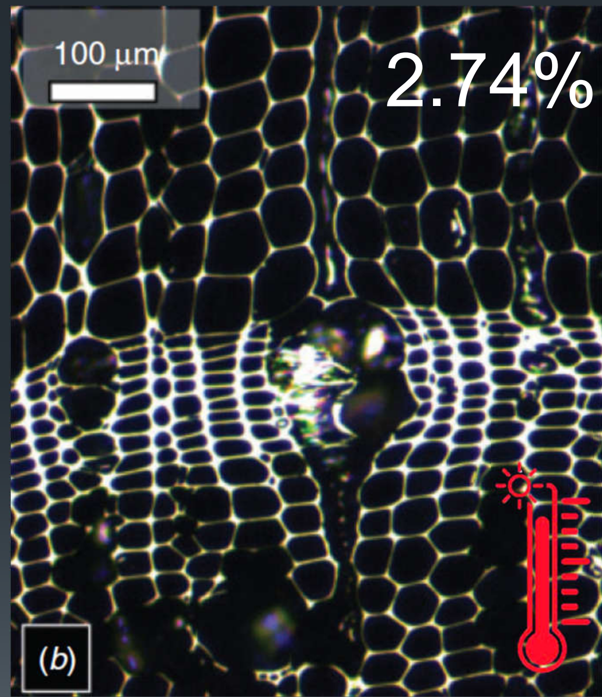

Belcher and Hudspith 2016

Heated sand experiments

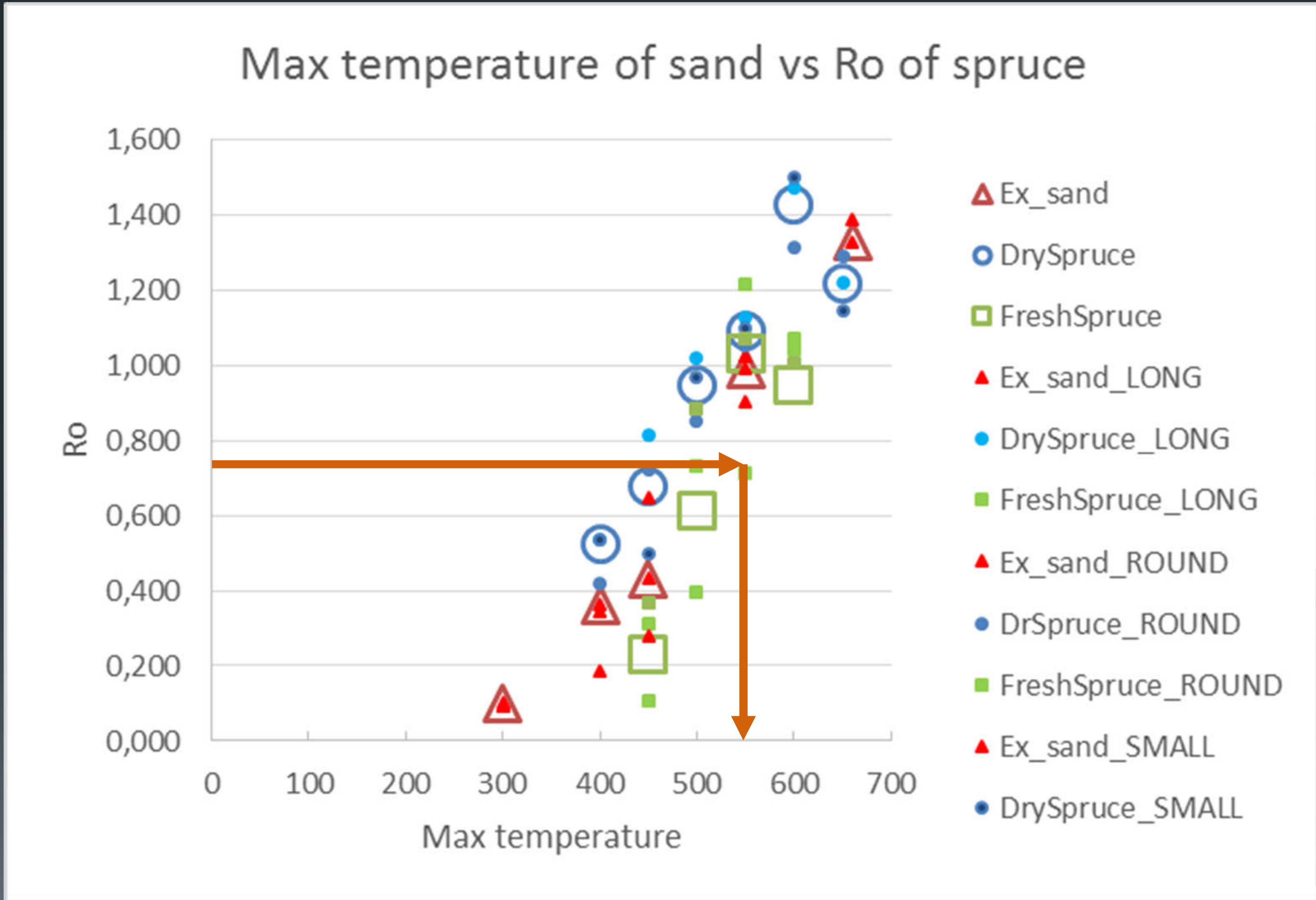

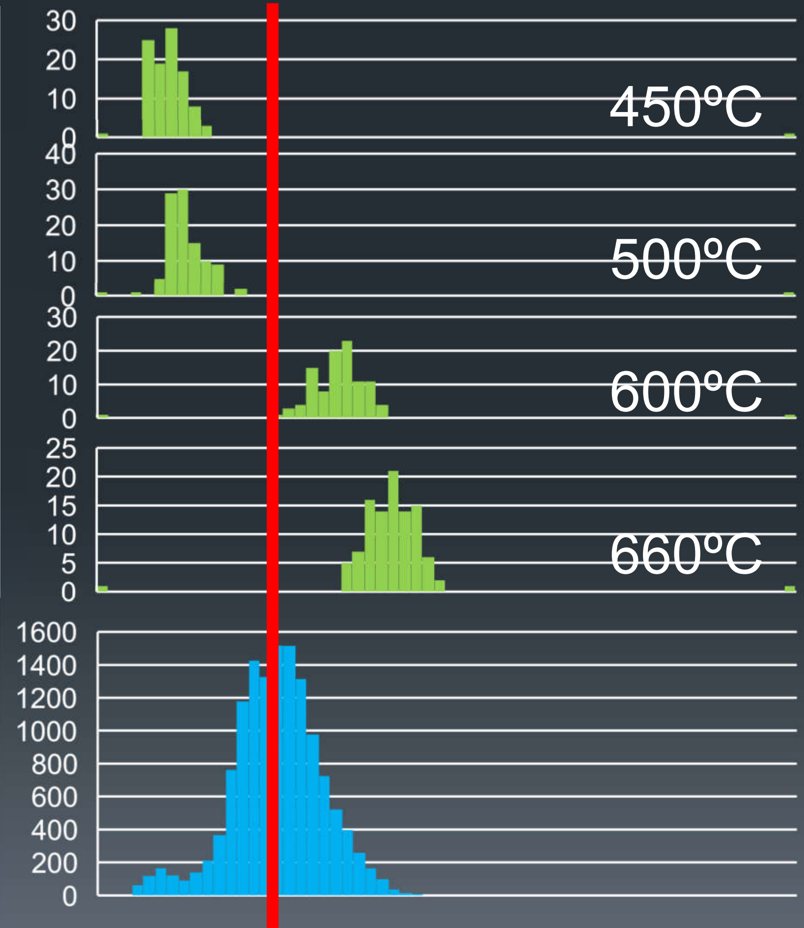

Environmental Effects of Very Small Crater Formation

A. Losiak[1,2], C. Belcher[1],

J. Plado[3], A. Jõeleht[3], C. D. K. Herd[4], R. S. Kofman[4], M. Szokaluk[5], W. Szczuciński[5], A. Muszyński[5], M. Szyszko, E. M. Wild[6]

[1]wildFIRE Lab, Hatherly Laboratories, University of Exeter, UK; [2]Institute of Geological Sciences, PAS, Poland; [3]Department of Geology, University of Tartu, Estonia, [4]Institute of Geology, Adam Mickiewicz University in Poznan; [6]VERA Laboratory, Faculty of Physics, University of Vienna;

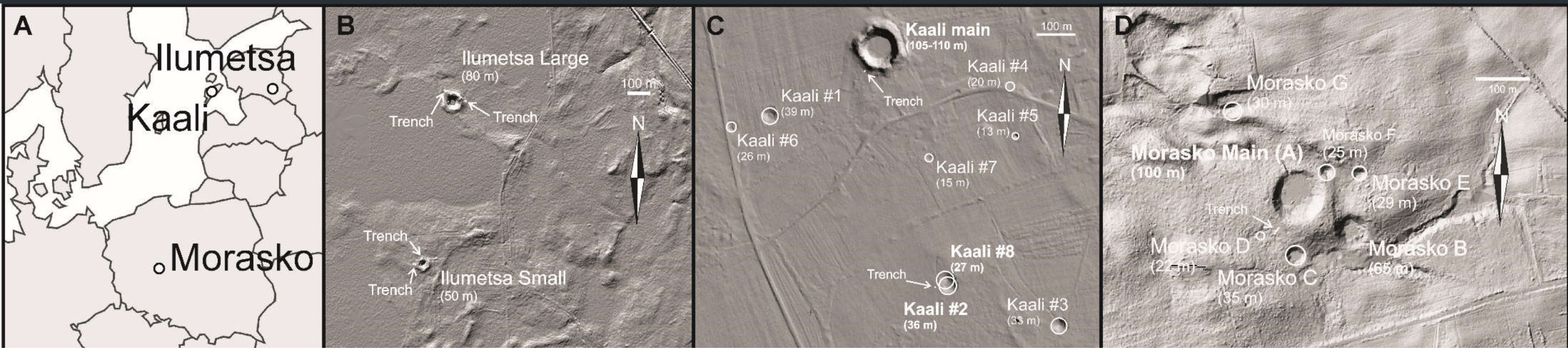

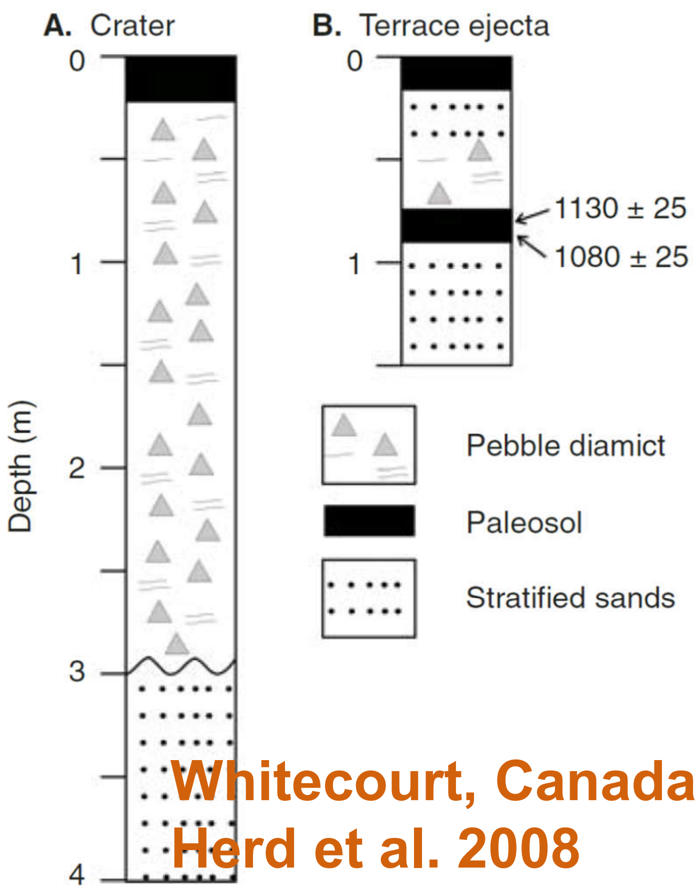

Whitecourt, Canada
Herd et al. 2008

Figure 2. Stratigraphy of sediments at the Whitecourt meteorite impact crater. A: Stratigraphy beneath crater floor at its approximate center. B: Stratigraphy of interpreted ejecta and buried paleosol from adjacent terrace ~11.5 m east of crater rim. Radiocarbon ages in ^{14}C yr B.P. are shown for the buried paleosol.

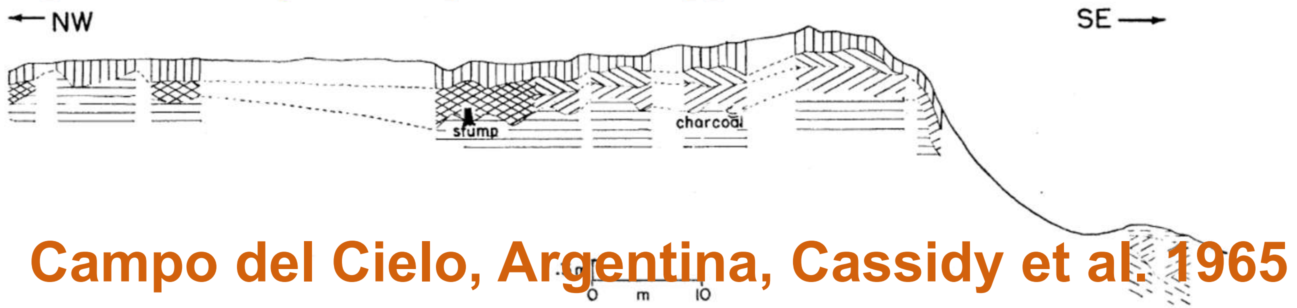

Campo del Cielo, Argentina, Cassidy et al. 1965

Fig. 9. Sectional diagram of trench along northwest radius, crater 2.

Symbol	Zone	Description	Interpretation
	a	Soft dark-colored soil with much vegetable matter Lumpy texture	Modern soil developed in throwout material
		Gradational boundary	
	b	Light-tan, clayey material, in part cemented by caliche Lumpy texture	Modern subsoil developed in throwout material
		Sharply defined boundary	
	c	Compact, dark-colored, organic-rich zone	Pre-impact soil
		Gradational boundary	
	d	Compact, tan-colored, clayey material	Pre-impact subsoil
	b′	Darker, less clayey material than *b*, with material suggesting zone *c* occasionally near its base.	Transitional zone between *b* and *c* found at distances greater than 25 m from the crest, where the sharply defined boundary between *b* and *c* disappears
	e	Light-tan, clayey material	Recent wash from crater walls
		Gradational boundary	
	f	Dark, organic-rich zone, becoming redder and containing decreasing amounts of organic material with greater depth	Older wash from crater walls that accumulated relatively slowly and allowed some degree of soil formation
		Gradational boundary	
	g	Apparent "clay conglomerate" or "clay breccia" or both, consisting of dark brown or red clay containing apparent clasts of darker and harder clay fragments and variable amounts of caliche and veinlike and patchy green clay. Small meteorite fragments, oxide flakes, and rust spots also noted within a lenslike zone at depth (Fig. 8)	Older wash from crater walls that accumulated fast enough that soil formation did not occur. May grade downward into fallback material and autochthonous breccia

Ries
1 km asteroid
24 km crater

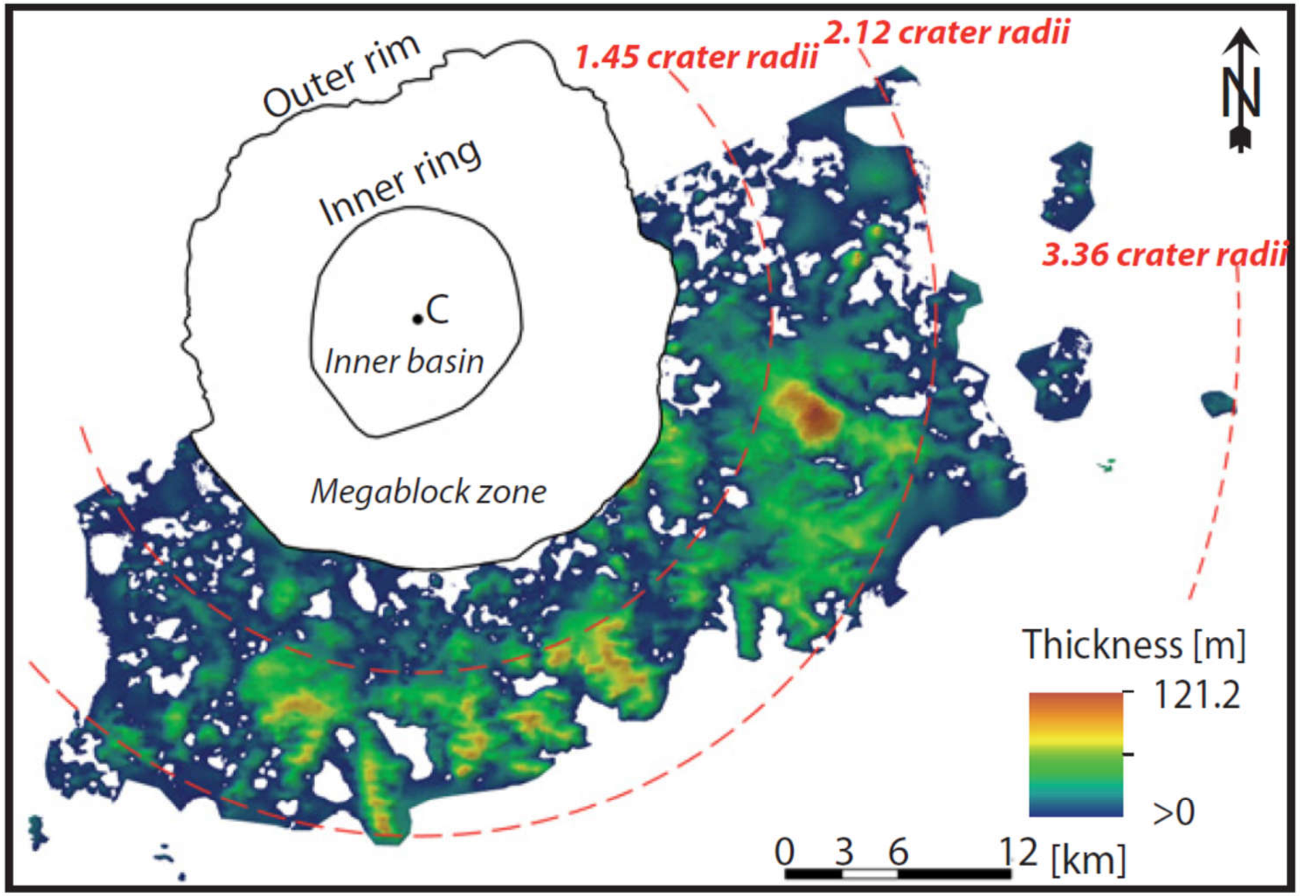

Figure 2. Results of the interpolated morphology of the Bunte Breccia thickness. White areas represent out-cropping weathered autochthonous units (e.g., Malmian limestone) or post-impact sediments (e.g., loess) (C—crater center).

Sturm et al. 2013

50-100 m in diameter

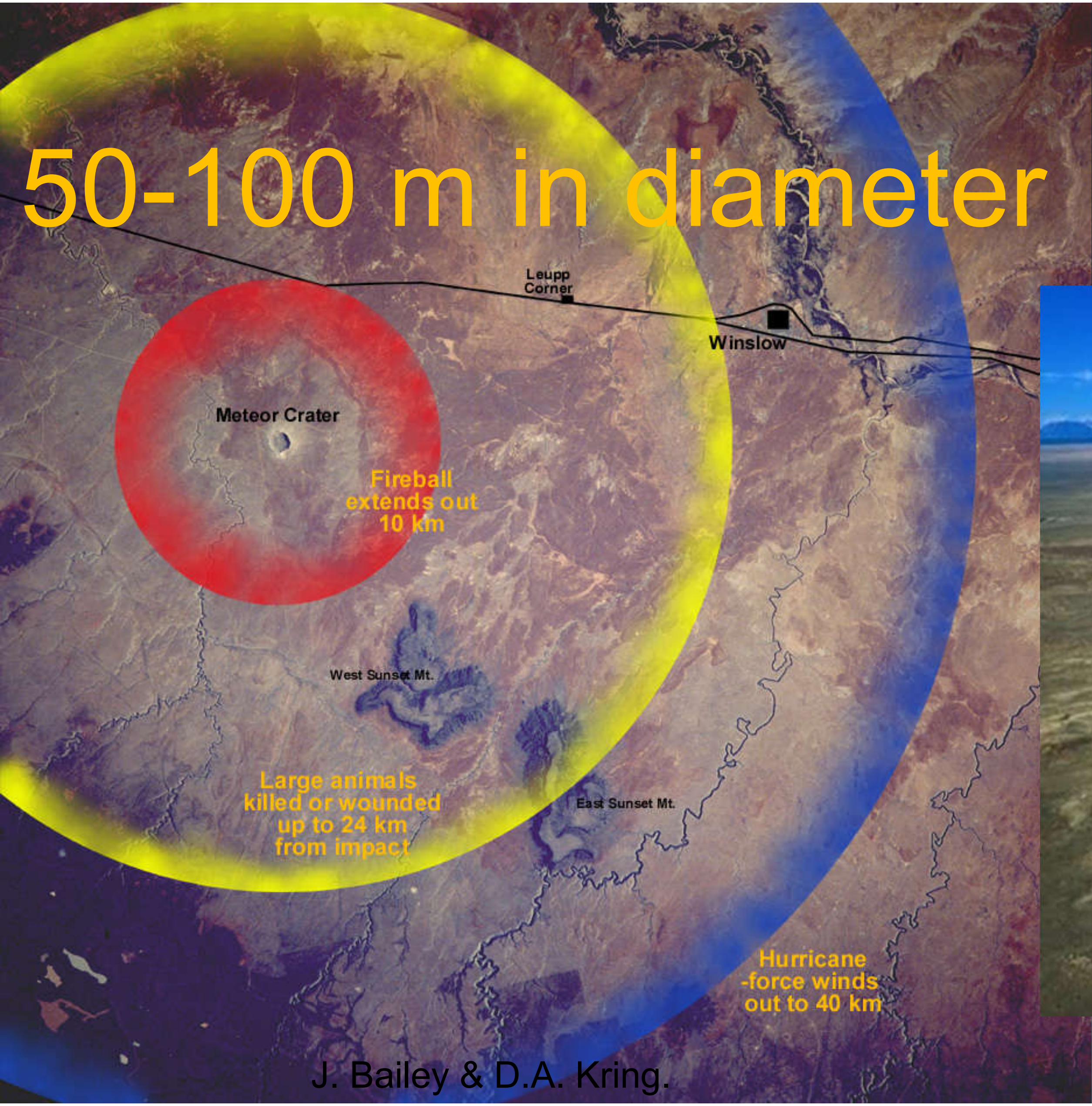

J. Bailey & D.A. Kring.

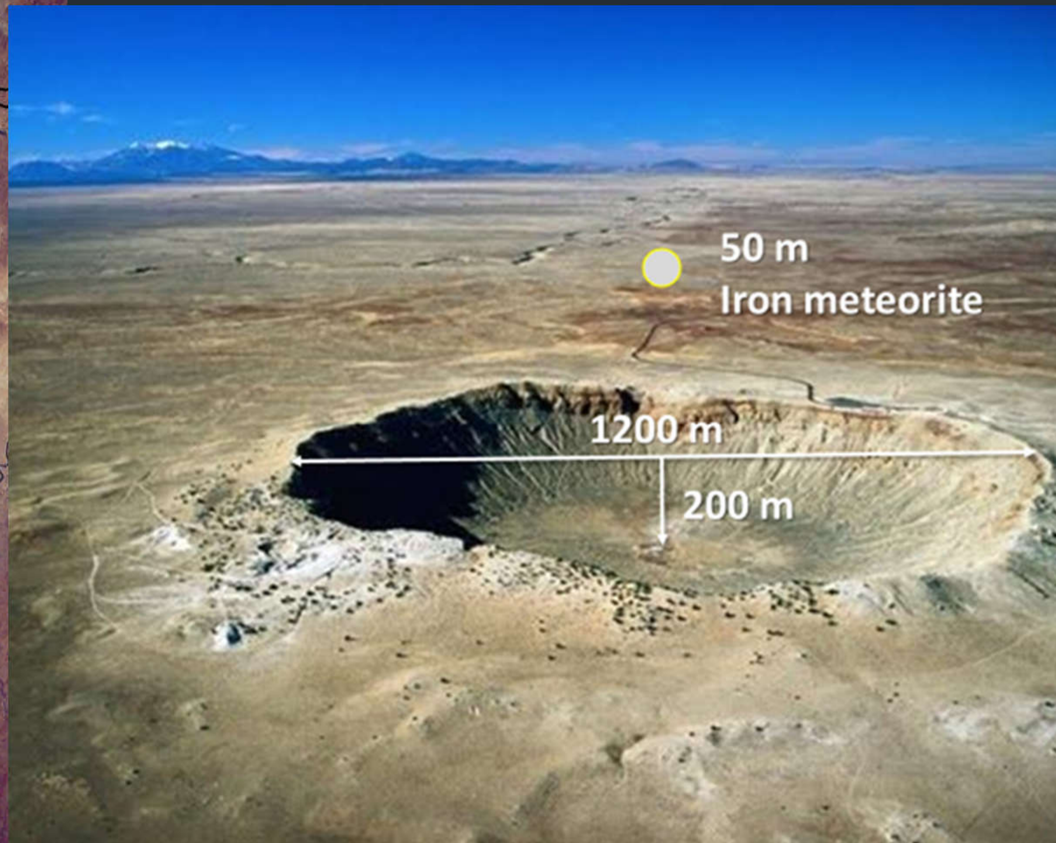

~50 m diameter

Tunguska

Russia

30.06.1908

No crater, Forest damaged

X injured

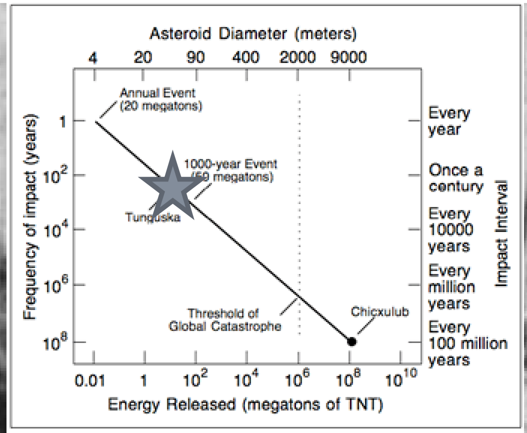

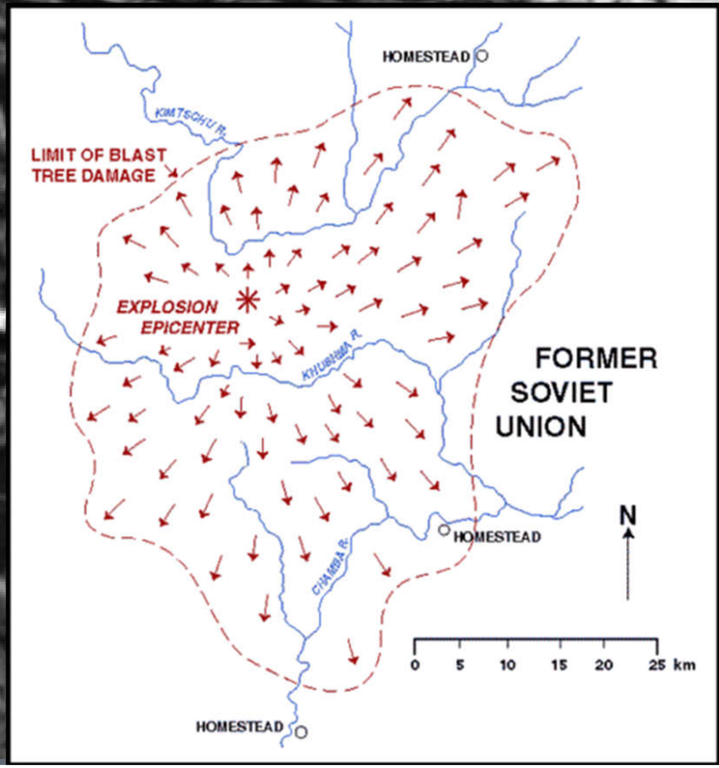

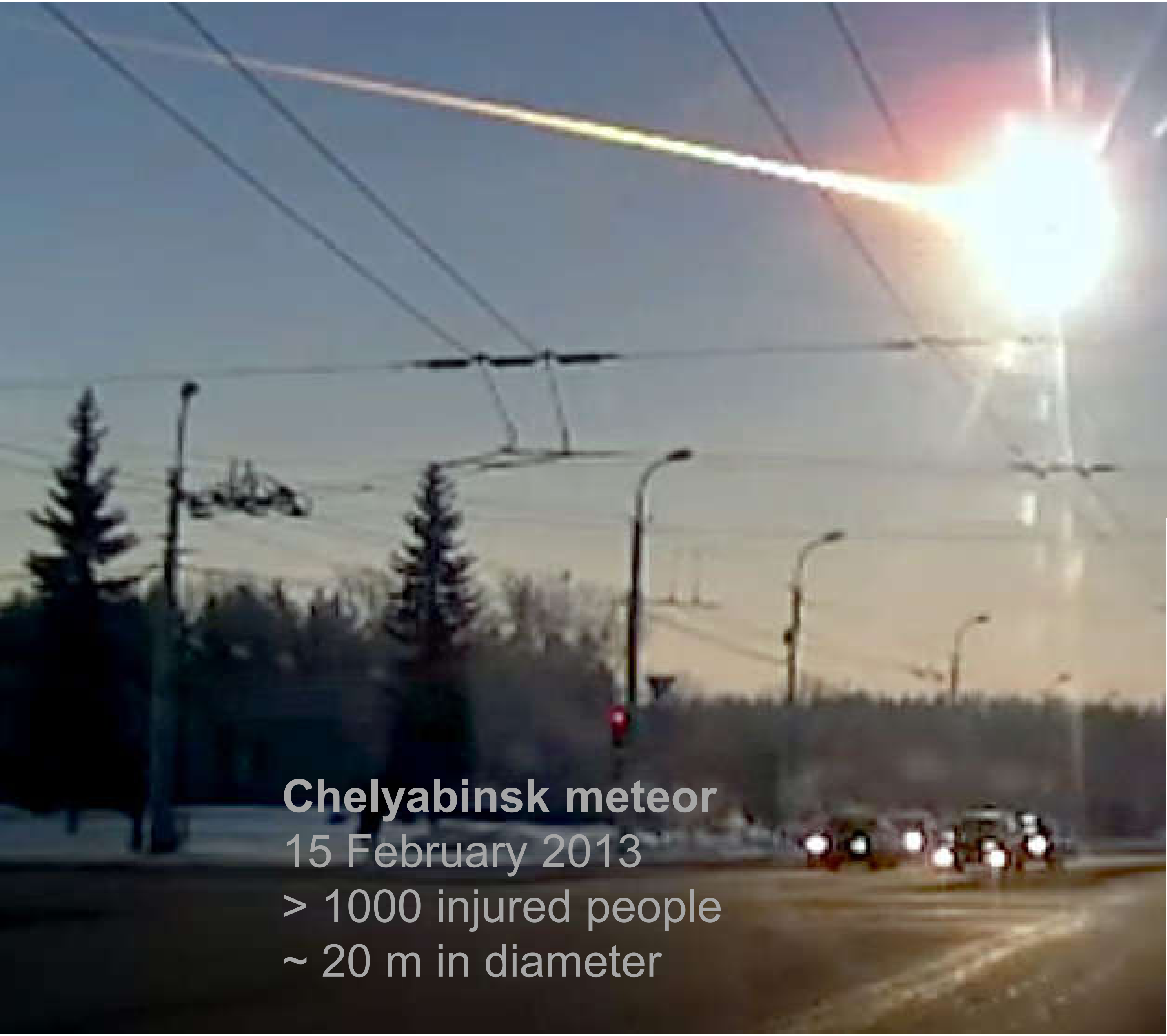
Chelyabinsk meteor
15 February 2013
> 1000 injured people
~ 20 m in diameter

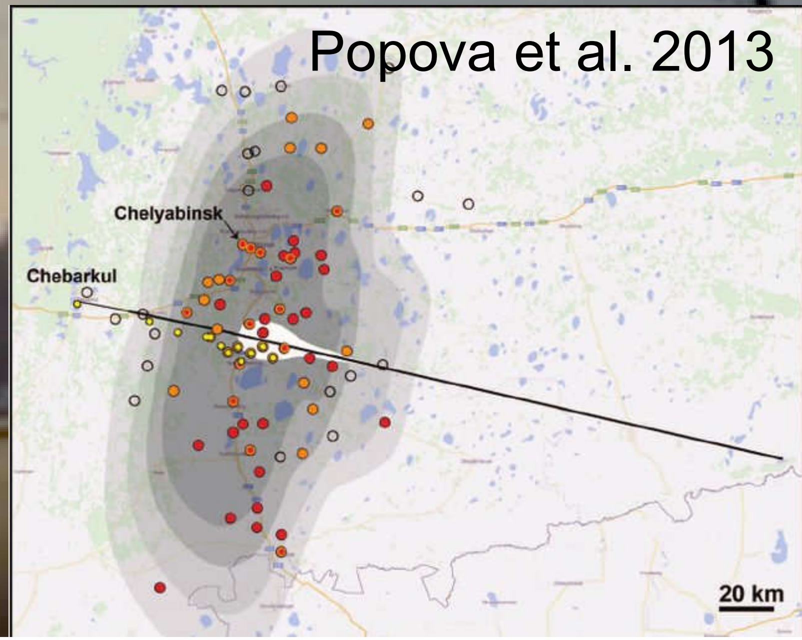
Popova et al. 2013
Chelyabinsk
Chebarkul
20 km

Methods: Charcoal reflectance

- Temperature of formation
- Time of heating
- Ignition
- Fuel moisture
  - Fuel type

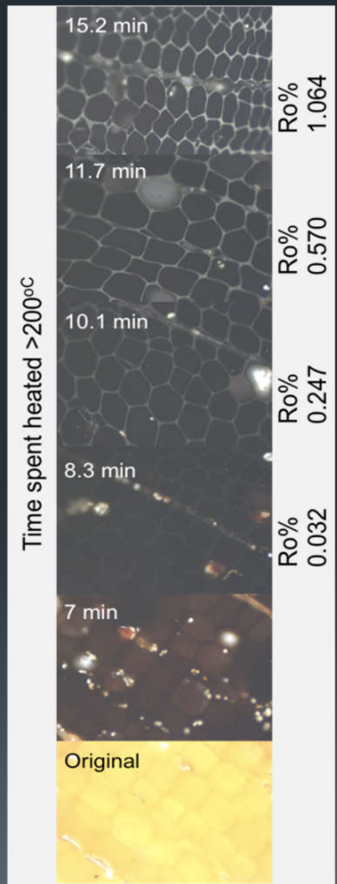

Belcher et al. 2018

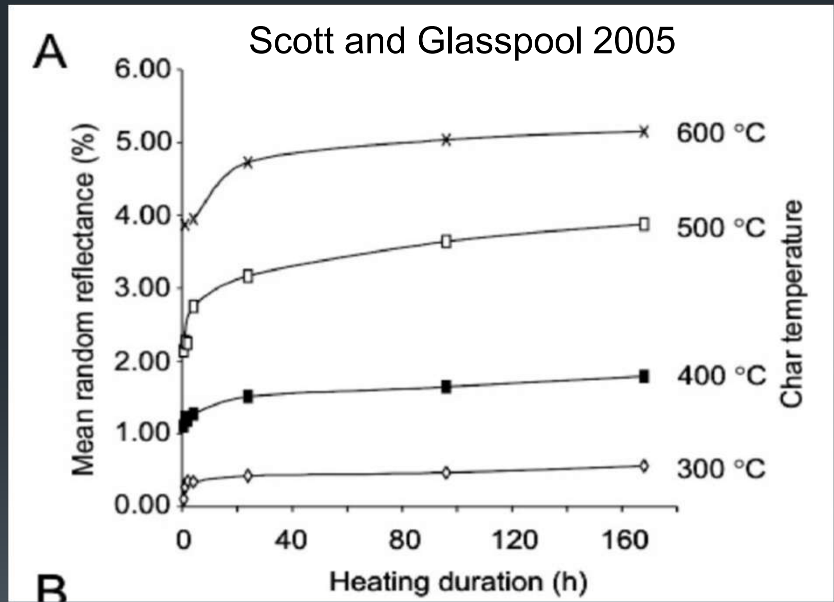

The Melting Ablation Analysis of Meteorites in High Temperature Flow

Sun Haihao, Luo Yue, Dang Leining, Su Siyao, Shi Weibo, Shi Yilei, Liu Sen
Hypervelocity Aerodynamics Institute of
China Aerodynamics Research and Development Center

1. Background
2. Introduction to the Experiments at CARDC
3. Description of Melting Ablation Model
4. Results and Discussions

1. Background

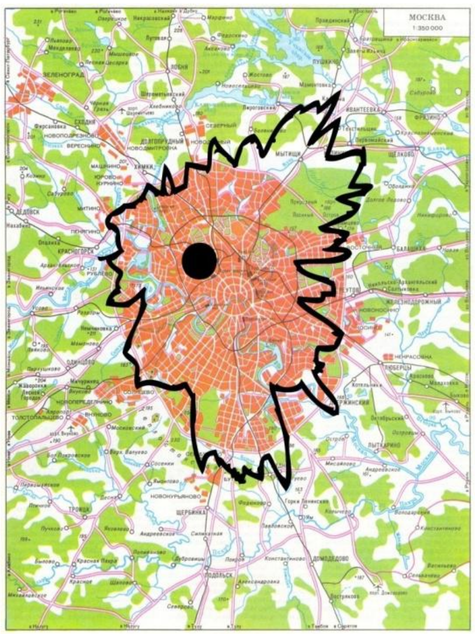

Tunguska event, Russia, 1908 , ~70m，~15km/s

Chelyabinsk event, Russia, 2013, ~20m，~19km/s

K/T event, Chicxulub, Mexico, 65 millions years ago, extinction of dinosaurs, ~10km，~14km/s

1. Background

- Ablation of meteoroid caused by aerodynamic heating leads to massive mass loss, affects trajectory and radiation characteristics during Earth entry with hypervelocity speed .
- Ablation coefficient of meteoroid is under large uncertainty , and gives rise to unfavorable effects in risk assessment.

  range: 3.5×10^{-10} - 7×10^{-8} kg/J

- Aiming to reveal mechanism and predict ablation of meteoroid, ground experiments, modeling and computation had been carried out by NASA, VKI, University of Stuttgart, et. al.
- The preliminary work in this field by CARDC will be presented in this paper.

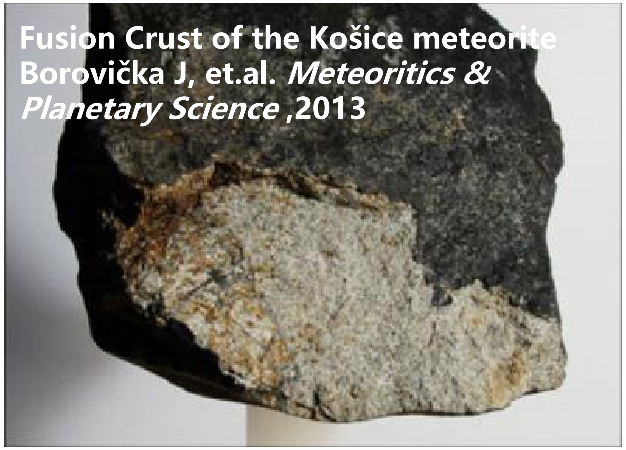
Fusion Crust of the Košice meteorite
Borovička J, et.al. *Meteoritics & Planetary Science* ,2013

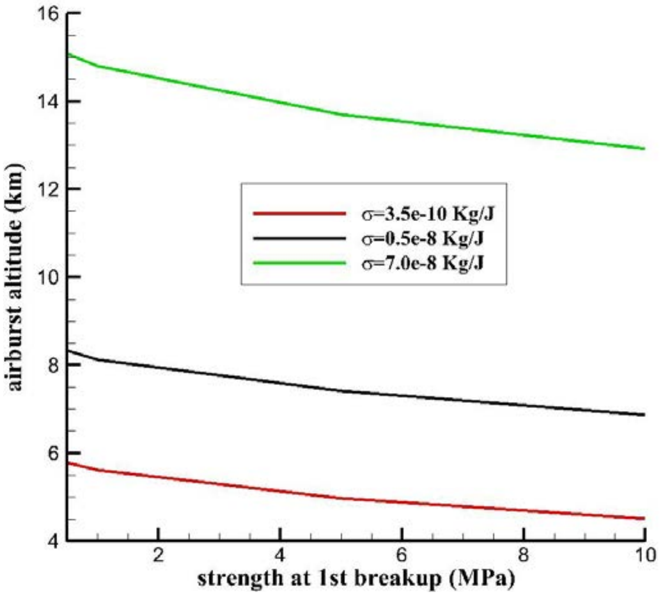

Dang Leining, et.al. Chinese Journal of Theoretical and Applied Mechanics,2020.12

2. Introduction to the Experiments at CARDC

Meteorite material

- NWA 13132, 2007, Niger, Northwest Africa
- Ordinary chonrite (L5/6)
- The meteorite is mainly consisting of olivine, pyroxene, plagioclase, Fe-Ni metal, with minor chromite and phosphates.

The raw meteorite material

State	I
Enthalpy (MJ/kg)	7.7
Stagnation heat flux (MW/m^2)	13.1
Stagnation Pressure (MPa)	0.51

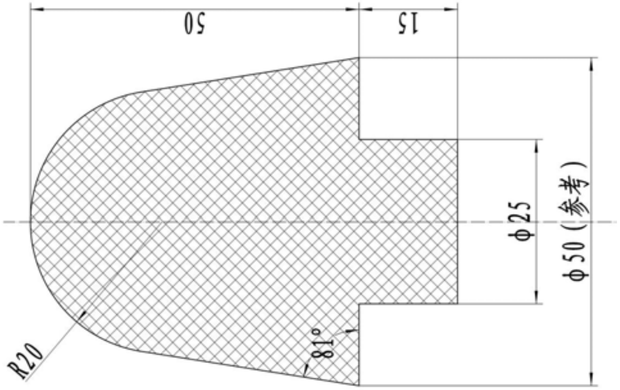

The test model

2. Introduction to the Experiments at CARDC

- **Experiment facility: 20 MW arcjet wind tunnel at CARDC**

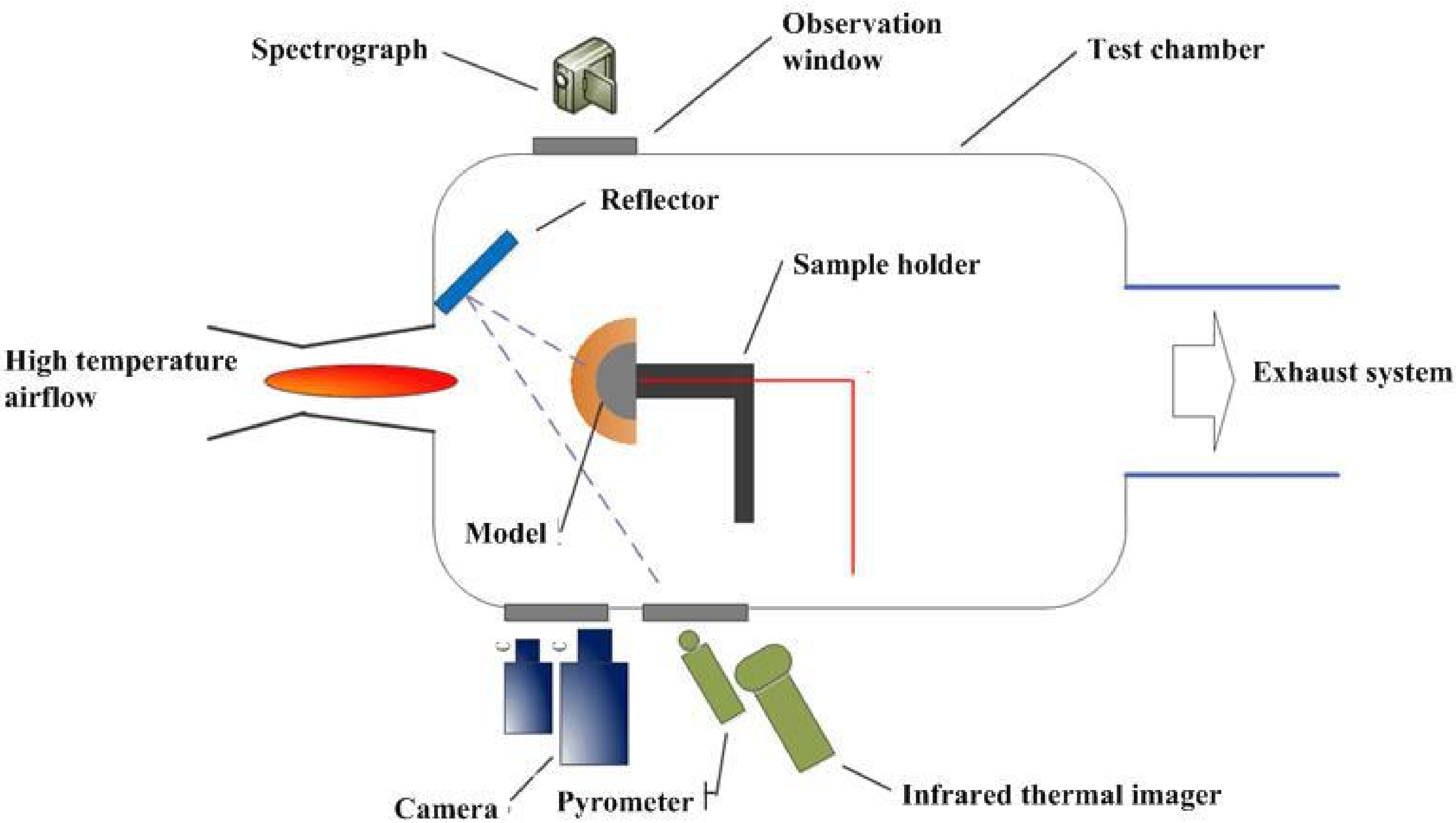

■ Sample #4 of Stony meteorite

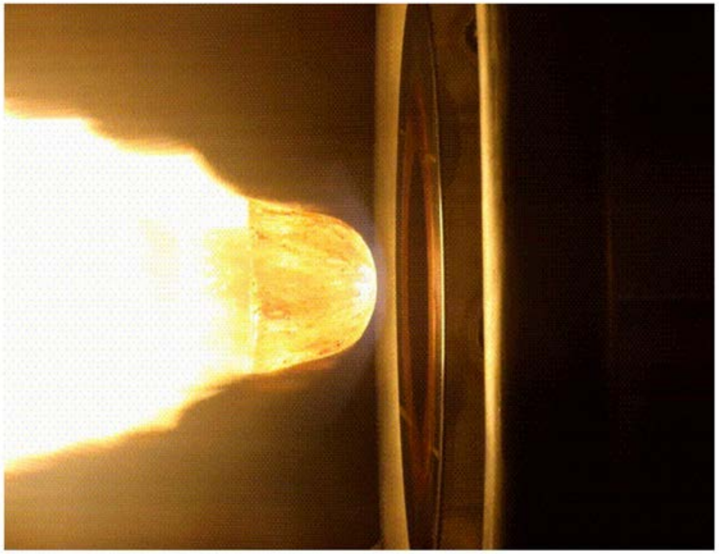

Melt flow over stony meteorite model during arc-jet exposure

The posttest shape (Sample #4)

■ Sample #4 of Stony meteorite

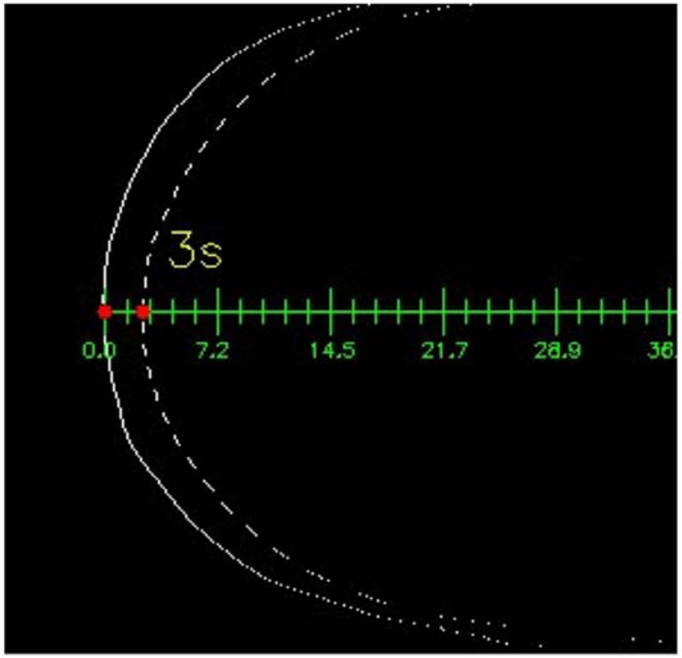

The ablation shape change during the experiment

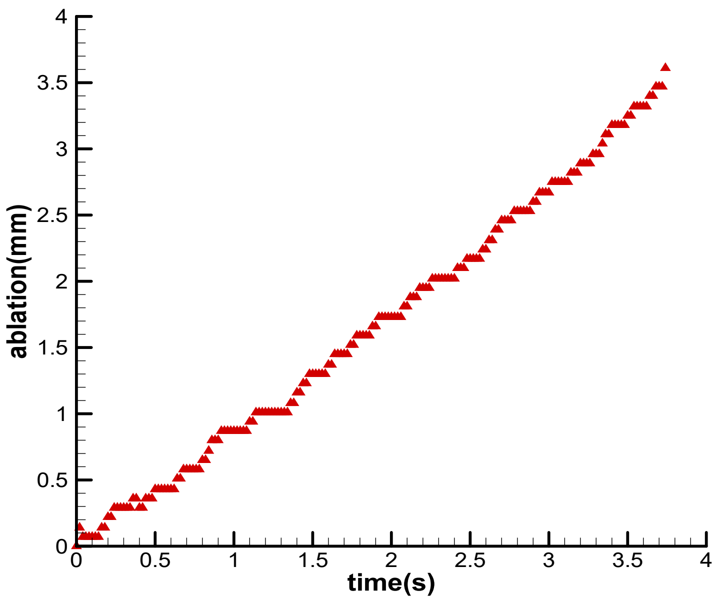

The surface recession with time at the stagnation

1. Background
2. Introduction to the Experiments at CARDC
3. **Description of Melting Ablation Model**
4. Results and Conclusions

3. Description of Melting Ablation Model

■ The main phenomena

1. The heat conduction in the solid region
2. The energy taken off by the motion of the melt layer;
3. The latent heat absorbed during the evaporation process;
4. The thermal blocking effect induced by the sio_2 injected into the boundary layer.

■ The assumption of Model

1. Steady state;
2. Incompressible flow;
3. Inertia term is ignored in the momentum equation;
4. The transverse temperature gradient is ignored in the energy equation.

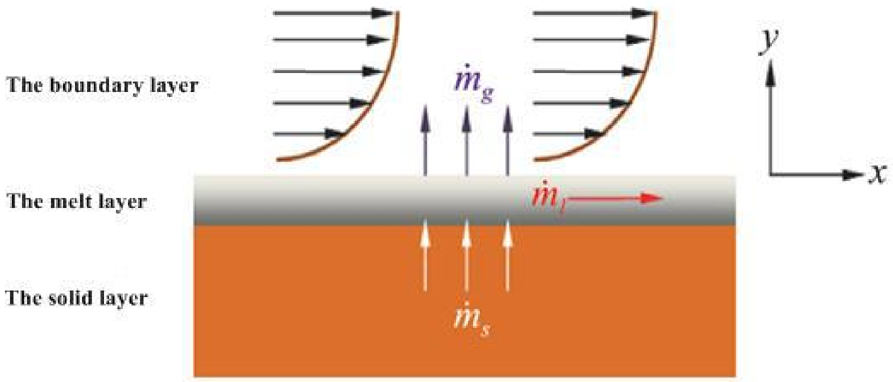

3. Description of Melting Ablation Model

Melting Ablation Mode

Evaporation rate

$$\mathrm{SiO_2(l)} \rightarrow \mathrm{SiO_2(g)}$$

$$\mathrm{SiO_2(g)} \rightarrow \mathrm{SiO_2} + \frac{1}{2}\mathrm{O_2}$$

$$p_s = p_0 \exp\left(18.48 - \frac{57780}{T_w}\right)$$

$$C_w = \left[1 + M_{av}\left(\frac{P_e}{P_s} - 1\right)\right]^{-1}$$

$$\dot{m}_v = \left(\frac{C_w}{1 - C_w}\right)\left(\frac{\varphi q_{or}}{h_r}\right)$$

Equations of steady state liquid layer

$$\frac{\partial u}{\partial x} + \frac{\partial v}{\partial y} = 0$$

$$\frac{\partial}{\partial y}\left(\mu \frac{\partial u}{\partial y}\right) = \frac{dp}{dx}$$

$$v\frac{\partial T}{\partial y} = \frac{k_l}{\rho_l c_{pl}} \frac{\partial^2 T}{\partial y^2}$$

$$\mu = \exp\left(\frac{a}{T} - b\right)$$

stagnation: $$v_w - v_{-\infty} = -\frac{2\delta^2}{\mu_w}\left(\tau_w^{'} - 2p^{''}\delta\right)$$

other zone: $$\int_0^x \left(v_{-\infty} - v_w\right) r dx = r\frac{\delta^2}{\mu_w}\left(\tau_w - 2p_x\delta\right)$$

Bethe H, Adams M C. A Theory for the Ablation of Glassy Materials. Journal of the Aerospace Sciences,1959

3. Description of Melting Ablation Model

■ Flowchart of solution:

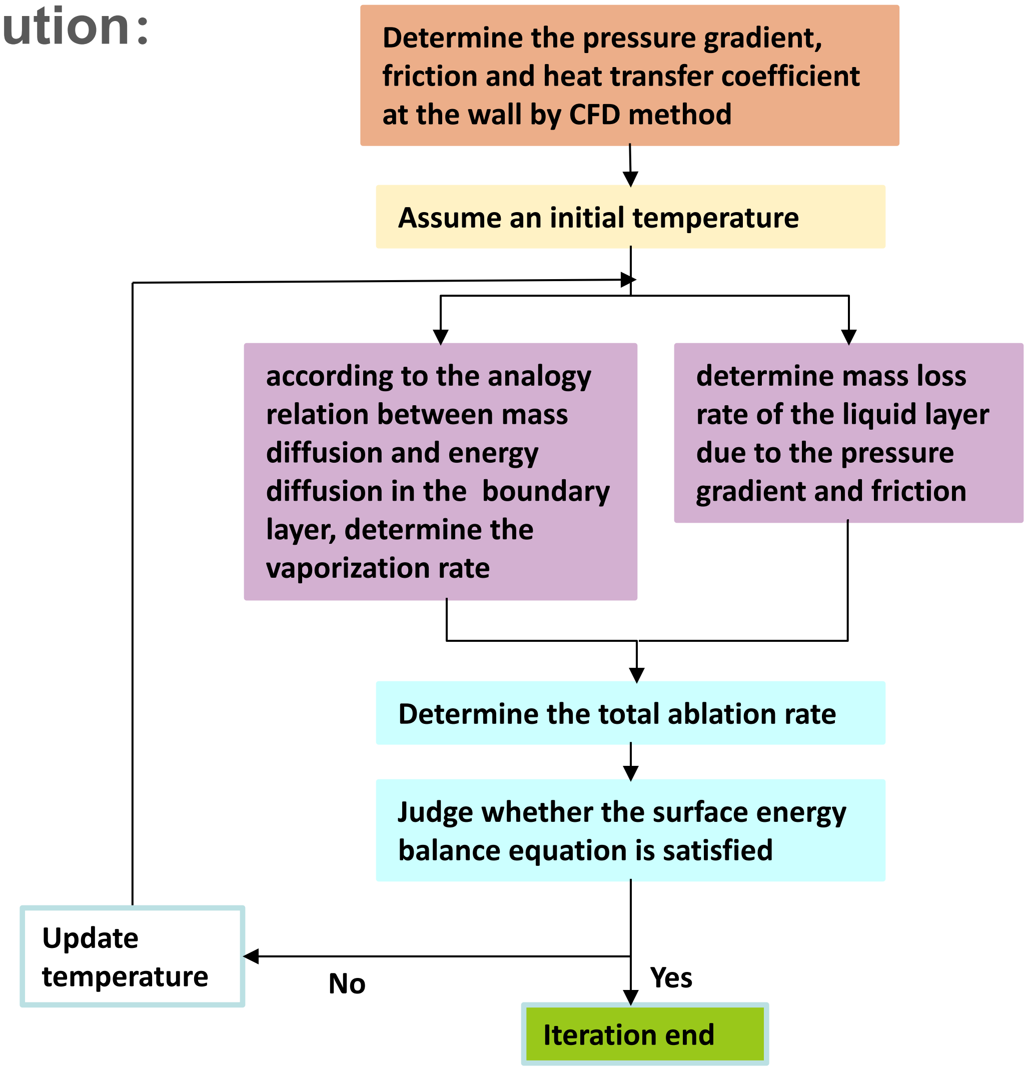

3. Description of Melting Ablation Model

Validation: Fused Silica at NASA Ames

- Fused Quartz test article
- 45 deg sphere cones
- 1.524 cm depth
- 0.635 cm nose radius
- 3.07 cm base diameter

- State
- stagnation pressure 126kPa
- stagnation heat flux 3350W/cm2
- Enthalpy 20.6MJ/kg
- exposure time 2.66s

Yih-Kang Chen, Eric C Stern, Parul Agrawal. Thermal Ablation Simulation of Quartz Materials. Journal of Spacecraft and Rockets, 2019

3. Description of Melting Ablation Model

■ Validation：CFD Result

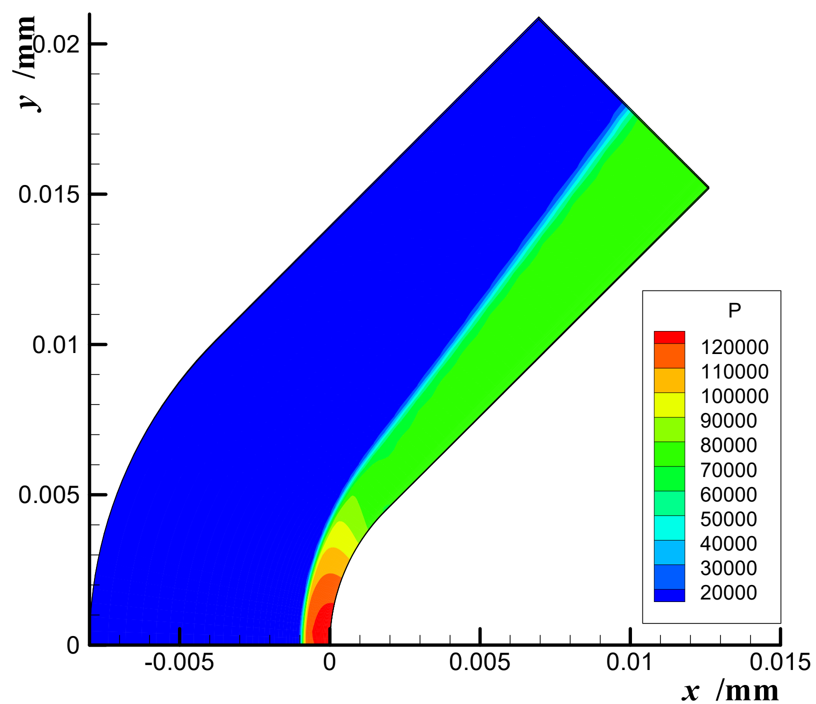

The pressure field

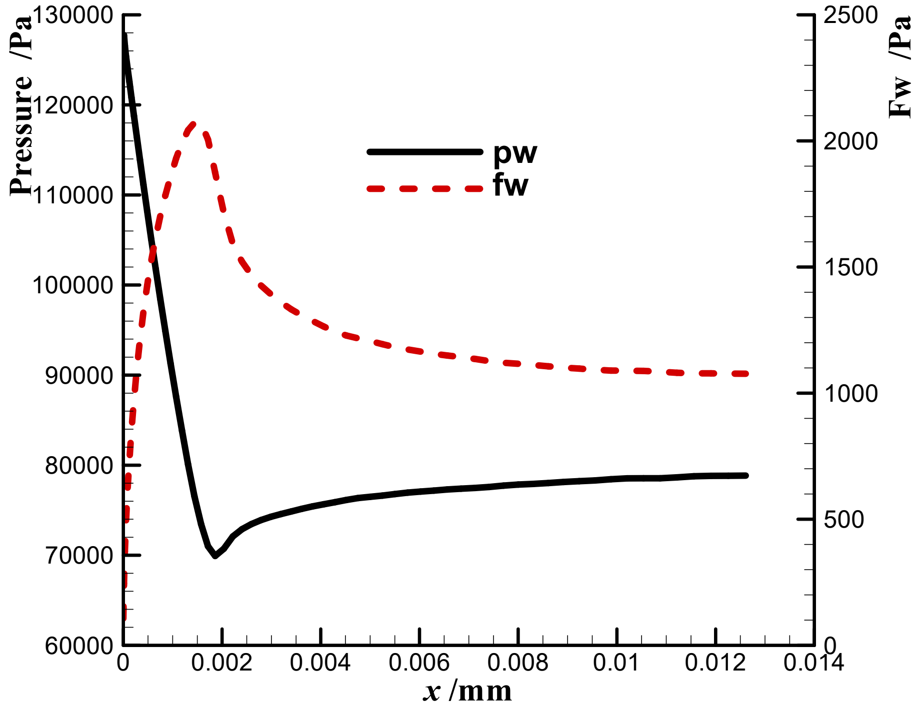

The pressure and wall friction distribution along the x-axis

■ Validation: Ablation Results

The ablation recession rate: 0.662mm/s

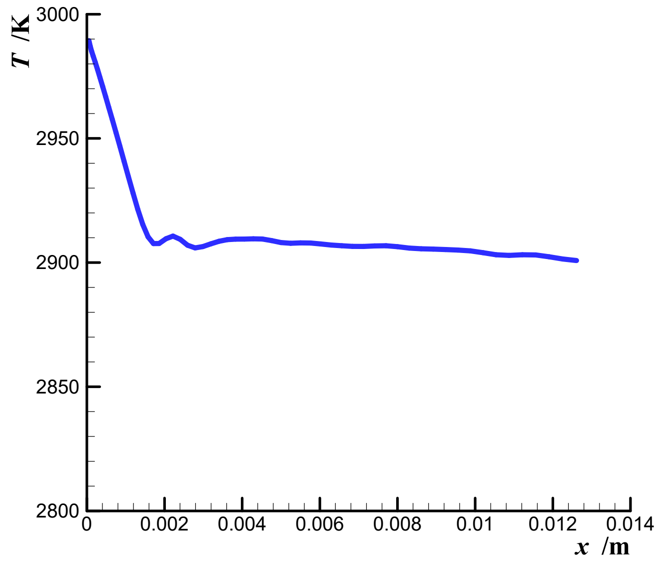

The surface temperature distribution

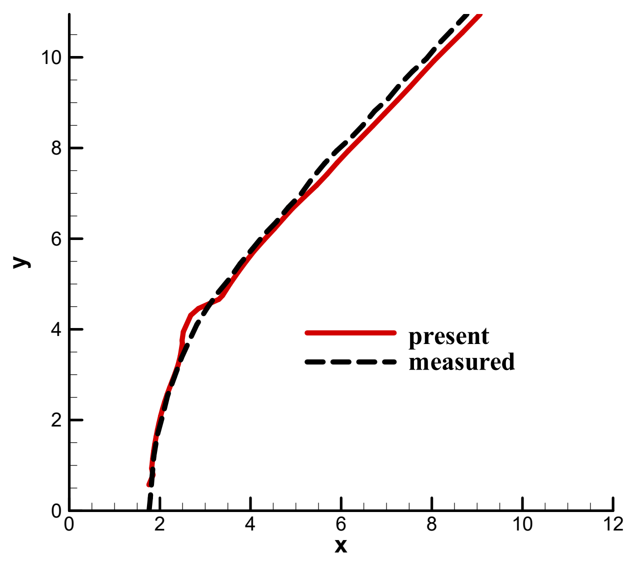

The posttest ablation shape at 2.66s

1. Background
2. Introduction to the Experiments at CARDC
3. Description of Melting Ablation Model
4. **Results and Conclusions**

The CFD Results

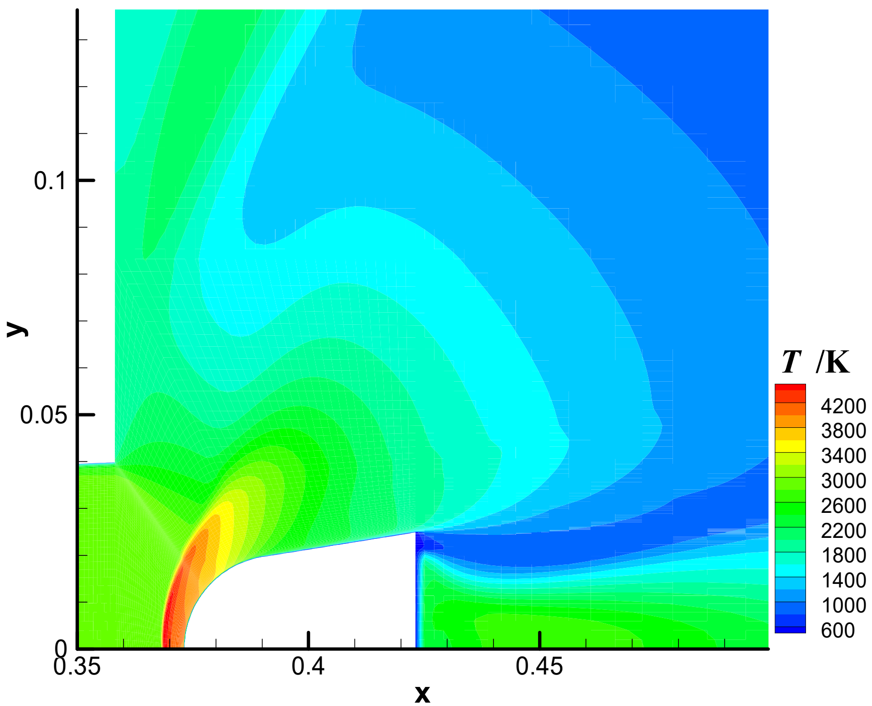

The temperature distribution

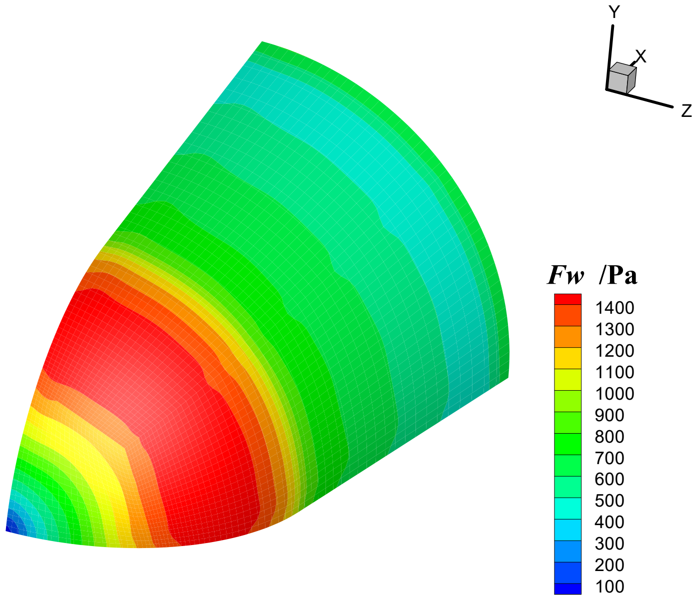

The wall friction distribution

The Ablation Results

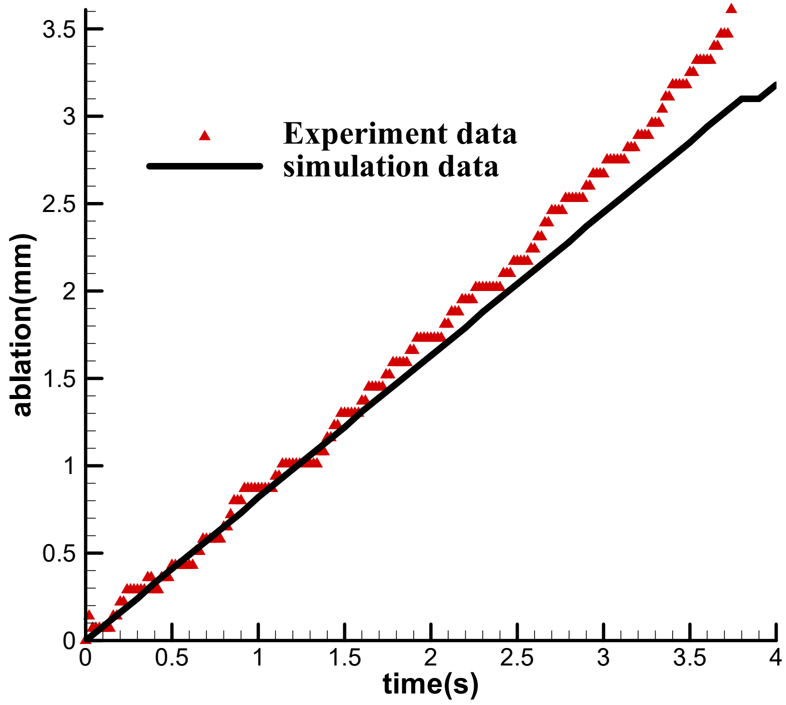

The ablation recession with time

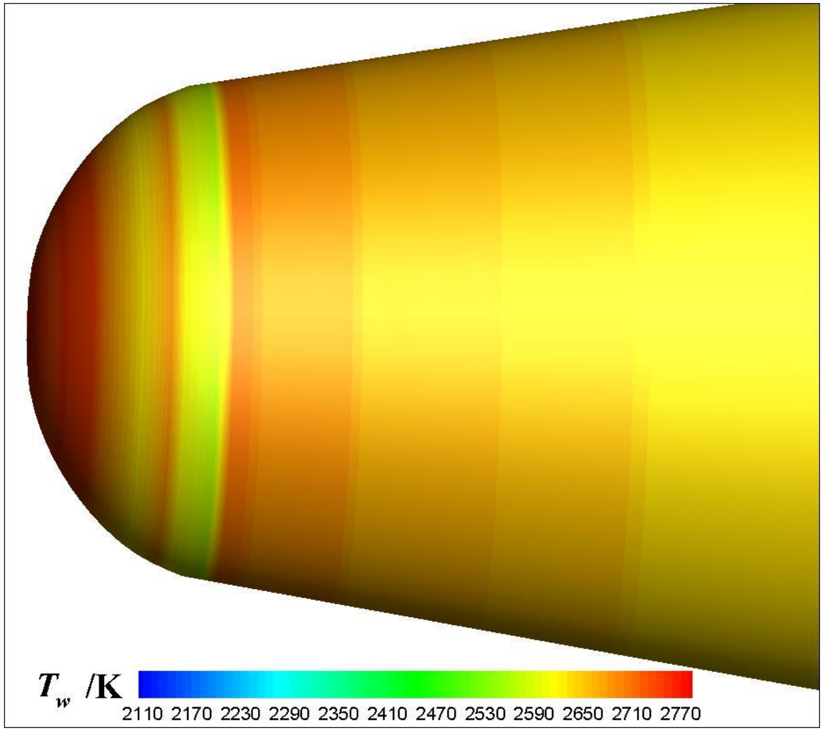

The surface temperature distrubtion

The Thermal stress analysis

The posttest shape (Model #1)

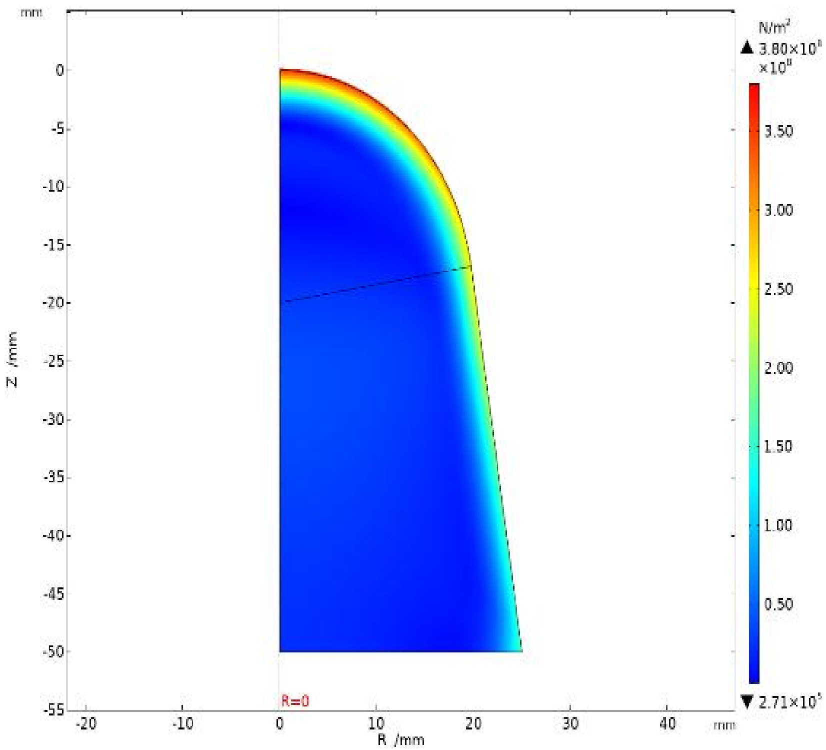

The von mises stress distribution at 4^{th} second (without ablation)

The brief concludsion:

1. The ablation recession rate and the final ablation shape is consistent with the experiment results.
2. Higher viscosity leads to the lower mass loss rate by the motion of melt layer, more energy are balanced by the evaporation. The surface temperature increases and the total mass loss rate decreases.
3. The thermal stress caused by the temperature gradient exceeds the material’s strength, which cause it to fragment.

The future work:

1. Employing the Numerical method to simulate the motion of melt layer is necessary to handle the asymmetric factors.
2. The theory model is helpful for us to comprehend what happened during the ablation and fragment process, while it is limited for the meteorite with some random structures.
3. The mass loss of the melt layer is sensitive to the viscosity and thermal conductivity of the molten compound, which should be measured precisely.

Thanks for your attention

Liu Sen, liusen@cardc.cn
Hypervelocity Aerodynamics Institute of China Aerodynamics Research and Development Center

Acknowledge to Wang Lei, Liu Jinbo for the experimental data.

Numerical Analysis of Aerodynamic Heating on Asteroid During Entry to Earth's Atmosphere

Su Siyao, Liu Sen, Dang Leiling, Zhang Zhigang

Hypervelocity Aerodynamics Institute
China Aerodynamics Research and Development Center

Outline

1、Background

2、Numerical method and physical-chemical model

3、Results and discussion

4、Summary

Outline

1、Background

2、Numerical method and physical-chemical model

3、Results and discussion

4、Summary

1. Background

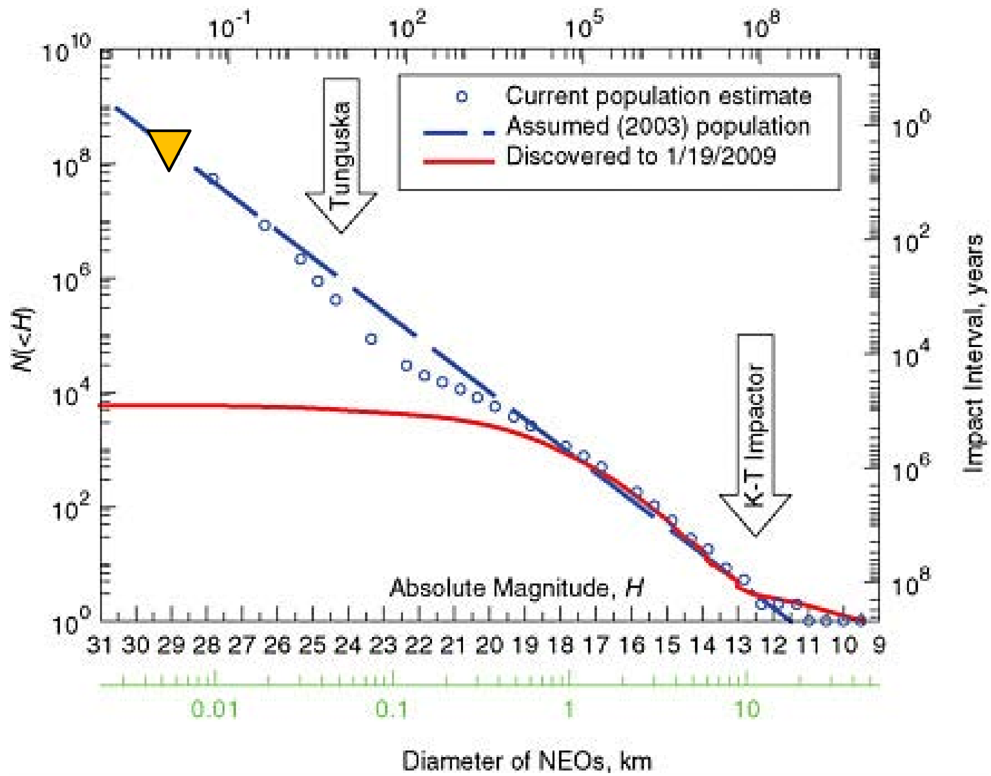

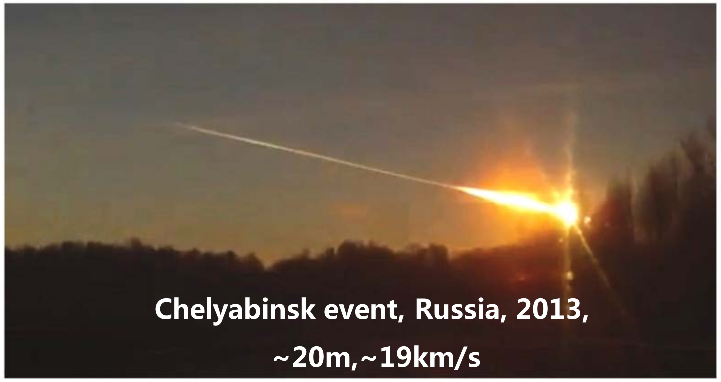

Chelyabinsk event, Russia, 2013, ~20m,~19km/s

K/T event, Chicxulub, Mexico, 65 millions years ago, ~10km,~14km/s

Meteorites in China

- **Jilin meteorites: 1976.3.8,** 3000 meteorites of total 2 ton mass have been recovered , one of the meteorites weighed as much as 1770kg.
- **Shangri-La, Yunnan: 2017.10.4 ,** many videos recorded.
- **Xishuangbanna, Yunnan: 2018.6.1 ,** many videos recorded.
- **Song Yuan, JiLin : 2019.10.11,** many videos recorded.

NO.1 meteor in Jilin meteorite event, 1976.3.8

Shangri-La Yunnan, 2017.10.4

1. Background

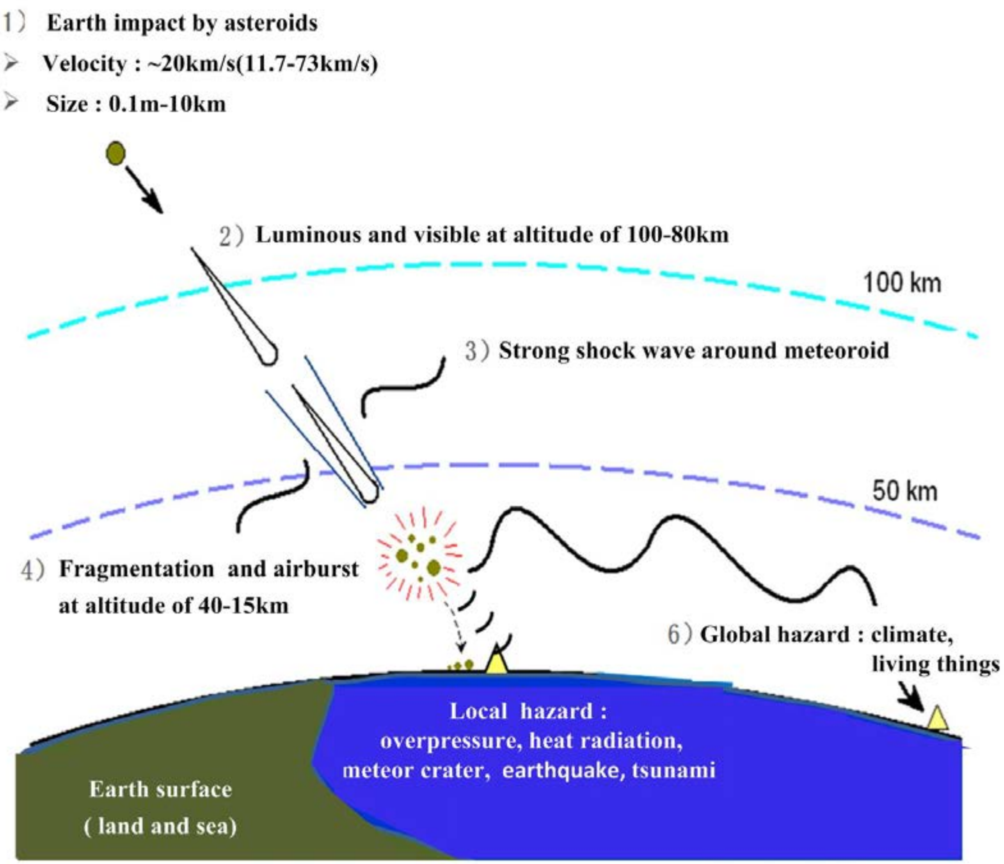

- aerodynamic forces and trajectory during ultra-high velocity entry
- aerodynamic heating during ultra-high velocity entry
- ablation and thermal response of asteroid structure
- physical characteristics of asteroid entry process

Earth entry issues in planetary defense

Outline

- **Could the numerical methods and physical-chemical models purposed for reentry vehicles be used in asteroid entry problems?**

	Reentry vehicle	Asteroids
Size	<6m	up to several km
Shape	regular , smooth	irregular , unsmooth
Surface Materials	TPS Materials C/H/O/N/Si	Depending on the type（S，M，X） O/S/Si/Fe/Mg/Ca/Na/Al
Interior structure	few defect	cracks, cavities, voids
Entry speed (km/s)	7.5~13	10~70
Peak temperature	≤20000K	~50000K

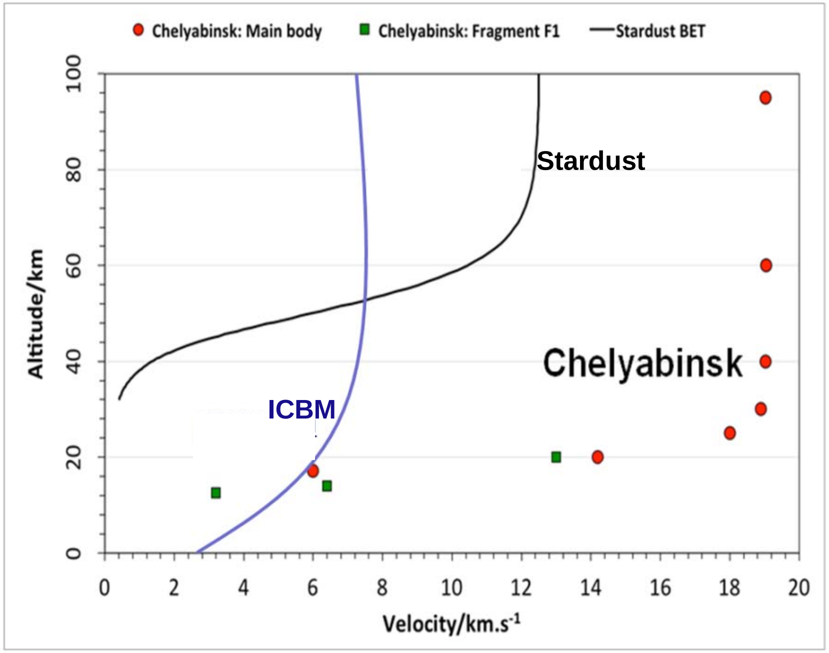

Comparison between the reentry vehicle and asteroid

2. Numerical method and physical-chemical model

- As the primary flow regime of asteroid's entry is continuum-near continuum, the CFD methods might be applicable for asteroid entry calculation;
- However, the physical-chemical models relevant to high temperature gas effects of traditional CFD should be confirmed and improved.

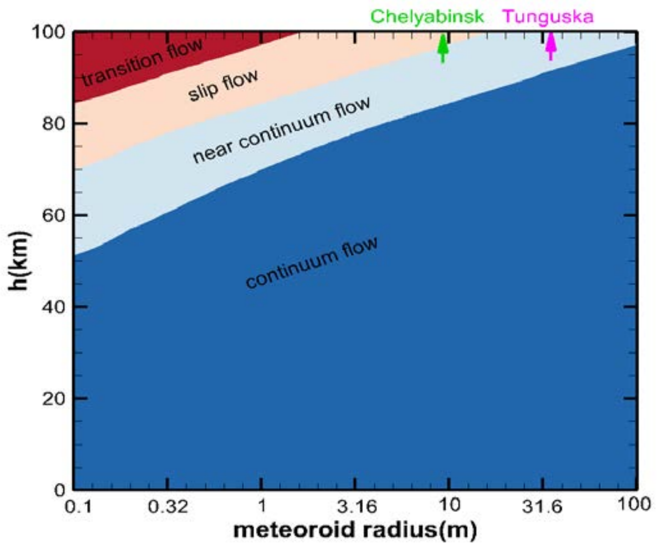

Flow regime of asteroid entry

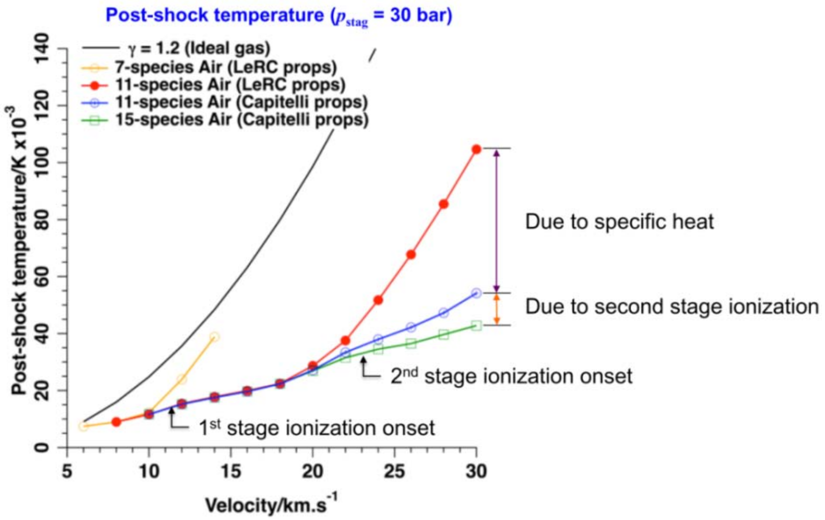

The effect of Air chemical model on post-shock temperature[1]

Ref 1: D.Prabhu.et.al. AIAA SCiTech 2016. Thermophysics Issues Relevant to High-Speed Earth Entry of Large Asteroids

Thermodynamic properties of ultra-high-temperature gas

- Thermodynamics properties of ultra-high-temperature gas are sensitive to the number of electronic states, high-lying level energies and cut-off criteria.
- Thermodynamics properties database valid up to 50,000 K should be constructed for both air species and ablation products.

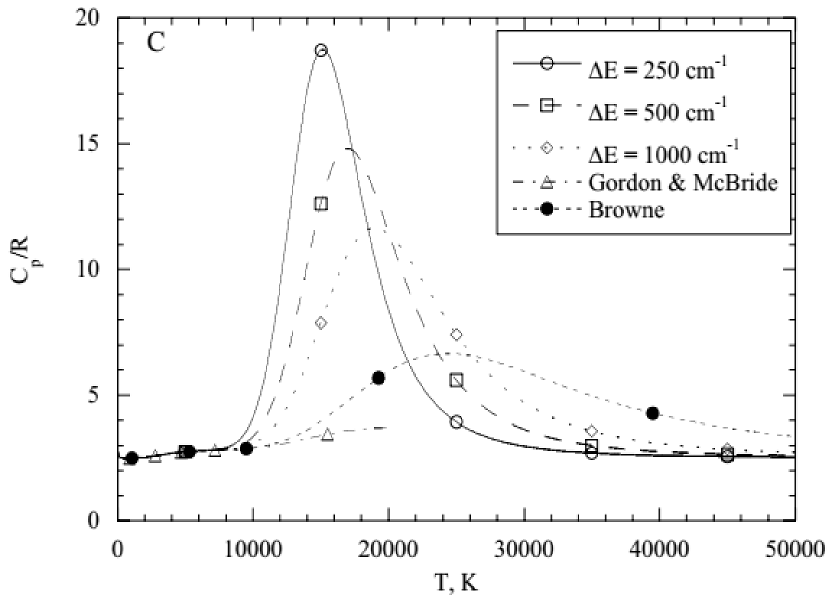

The influence of cut-off criteria on the Cp value of C[2]

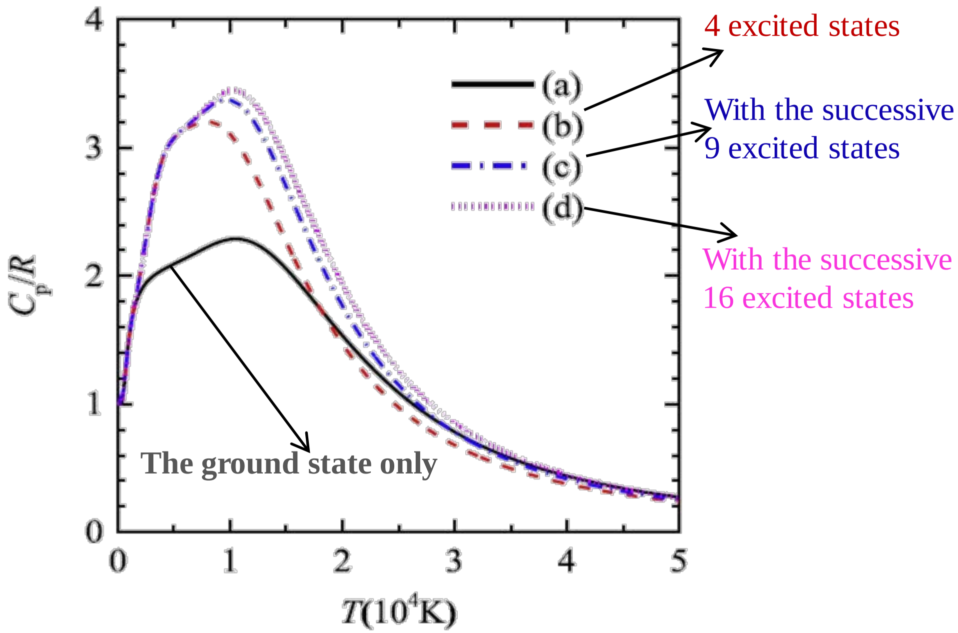

The influence of electronic states on the Cp value of CN[3]

Ref 2: Capitelli.et.al. ESA STR246. Tables of internal partition functions and thermodynamic properties of high-temperature Mars-atmosphere species from 50K to 50000K
Ref 3: Z. Qin .et.al. JQSRT 210 (2018) 1–18 . High-temperature partition functions, specific heats and spectral radiative properties of diatomic molecules with an improved calculation of energy levels

Transport properties of ultra-high-temperature gas

- Based on the Chapman-Enskog method, the collision cross section are needed for transport properties computation.
- high accuracy database of collision cross section up to 50,000 K are needed for both air species and ablation products.

Table 2 Viscosity collision integral $\Omega^{2,2}$ (Å^2) as a function of temperature for neutral–neutral and electron-neutral interactions in air

Interaction	T, K: 300	500	600	1000	2000	4000	5000	6000	8000	10,000	15,000	20,000	Acc.,%	Ref.
N_2–N_2	13.72	—	11.80	10.94	9.82	8.70	—	8.08	7.58	7.32	—	—	10	9
N_2–O_2	11.23	—	—	8.36	7.35	6.47	6.21	—	—	5.42	4.94	—	20	5
N_2–NO	13.44	11.87	11.44	10.48	9.32	8.04	7.61	7.27	6.74	6.33	5.62	—	25	24
N_2–N	11.21	—	9.68	8.81	7.76	6.73	—	6.18	5.74	5.36	—	—	10	8
N_2–O	8.99	—	—	6.72	5.91	5.22	5.01	—	—	4.36	3.95	—	20	5
N_2–Ar	11.97	10.50	—	9.28	8.38	7.53	7.25	7.02	6.63	6.32	5.73	—	20	5
O_2–O_2	12.62	11.06	10.65	9.72	8.70	7.70	7.38	7.12	6.73	6.42	5.89	—	20	24
O_2–NO	12.93	11.32	10.90	9.94	8.89	7.80	7.45	7.17	6.73	6.39	5.80	—	25	24
O_2–N	—	8.79	8.47	7.68	6.63	5.67	5.38	5.14	4.78	4.51	4.04	—	25	16
O_2–O	10.13	—	8.61	7.78	6.71	5.67	—	5.13	4.78	4.50	—	—	10	8
O_2–Ar	12.33	10.82	—	9.57	8.54	7.48	7.14	6.87	6.44	6.12	5.54	—	20	5
NO–NO	13.25	11.58	11.15	10.16	9.07	7.91	7.53	7.21	6.73	6.36	5.72	—	20	24
NO–N	—	9.65	9.26	8.29	7.07	5.94	5.60	5.33	4.91	4.60	4.06	—	25	16
NO–O	—	8.79	8.47	7.66	6.64	5.69	5.40	5.17	4.82	4.55	4.08	—	25	16
NO–Ar	13.03	11.33	10.89	9.90	8.85	7.79	7.44	7.15	6.71	6.37	5.77	—	25	24
N–N	9.11	7.94	—	6.72	5.82	4.98	4.70	4.48	4.14	3.88	3.43	3.11	5	15
N–O	9.08	8.15	—	7.09	6.06	5.14	4.88	4.67	4.34	4.07	3.56	3.21	5	15
N–Ar	—	9.31	8.96	8.03	6.84	5.75	5.42	5.17	4.77	4.47	3.95	—	20	16
O–O	9.46	8.22	—	6.76	5.58	4.67	4.41	4.20	3.88	3.64	3.21	2.91	5	15
O–Ar	11.11	10.13	—	8.87	7.69	6.60	6.26	6.00	5.59	5.28	4.74	4.37	20	5
Ar–Ar	12.88	11.12	—	9.66	8.60	7.57	7.23	6.96	6.53	6.20	5.60	5.17	5	24
e–N_2	—	1.46	—	2.07	2.96	3.88	4.09	4.15	4.04	3.85	3.41	3.12	25	28
e–O_2	—	—	—	1.30	1.73	2.10	2.18	2.23	2.29	2.31	2.32	2.31	20	28
e–NO	—	—	—	—	5.64	4.52	4.05	3.73	3.37	3.18	2.92	2.75	35	28
e–N	—	—	—	—	5.68	3.71	3.52	3.42	3.30	3.20	2.95	2.58	35	39, 40
e–O	—	—	—	0.82	1.05	1.34	1.44	1.52	1.65	1.73	1.85	1.90	30	27
e–Ar	—	—	—	0.17	0.30	0.79	1.05	1.31	1.81	2.25	3.07	3.48	15	26

The estimated accuracy of collision cross section data [4]

Ref 4: Wright.et.al. AIAA Journal 43 (2005) 12，2558–2564. Recommended Collision Integrals for Transport Property Computations Part 1:Air Species

Chemical kinetics of ultra-high-temperature gas

- Chemical kinetics models for vehicle entry should not be used directly for asteroid entry.
- New chemical kinetics such as multiple stage ionization、photochemical kinetics and chemical kinetics for asteroid ablation products should be developed.

  - Chemical kinetics for multiple stage ionization

$$N^{+} + e \Leftrightarrow N^{++} + e + e$$

$$O^{+} + e \Leftrightarrow O^{++} + e + e$$

  - Photochemical kinetics
  - Chemical kinetics for ablation products

[5]

Table 1: Photochemical processes applied in the present study.

#	Process		Spectral Range	Data Source
1	N_2 Photodissociation:	$N_2 + h\nu \leftrightarrow 2N$	9.8 eV $< h\nu$	Stanley and Carlson[30]
2	O_2 Photodissociation:	$O_2 + h\nu \leftrightarrow 2O$	7.1 eV $< h\nu$	Mnatsakanyan[31]
3	N_2 Photoionization:	$N_2 + h\nu \leftrightarrow N_2^+ + e^-$	12.4 eV $< h\nu$	Romanov et al.[32]
4	O_2 Photoionization:	$O_2 + h\nu \leftrightarrow O_2^+ + e^-$	9.7 eV $< h\nu$	Romanov et al.[32]
5	N Photoionization:	$N + h\nu \leftrightarrow N^+ + e^-$	12.4 eV $< h\nu$	TOPbase[33]
6	O Photoionization:	$O + h\nu \leftrightarrow O^+ + e^-$	9.7 eV $< h\nu$	TOPbase[33]

Table 2: Chemical kinetics for meteor ablation products.

i	Reaction	$A_{f,i}$	$n_{f,i}$	$D_{f,i}$	Ref.
1	$Si + e^- \leftrightarrow Si^+ + e^- + e^-$	2.5e+34	-3.82	9.46e+4	Based on N rate[17]
2	$Fe + e^- \leftrightarrow Fe^+ + e^- + e^-$	2.5e+34	-3.82	9.17e+4	Based on N rate[17]
3	$Mg + e^- \leftrightarrow Mg^+ + e^- + e^-$	2.5e+34	-3.82	8.87e+4	Based on N rate[17]
4	$Si + NO \leftrightarrow SiO + N$	3.2e+13	0.0	1775.0	Mick et al.[38]
5	$Si + O_2 \leftrightarrow SiO + O$	2.1e+15	-0.53	16.83	Le Picard et al.[39]
6	$SiO + M \leftrightarrow Si + O + M$	4.0e+14	0.0	9.56e+4	Estimate
7	$SiO_2 + M \leftrightarrow SiO + O + M$	4.0e+14	0.0	9.56e+4	Estimate
8	$Fe + O_2 \leftrightarrow FeO + O$	1.3e+14	0.0	1.02e+4	Akhmadov et al.[40]
9	$Mg + O_2 \leftrightarrow MgO + O$	5.1e+10	0.0	0.0	Hodgson and Mackie[41]
10	$SO + O \leftrightarrow S + O_2$	2.4e+07	1.51	2.53e+3	Lu et al.[42]
11	$SO_2 + S \leftrightarrow SO + SO$	4.8e+14	0.0	1.08e+4	Murakami[43]
12	$O_2 + SO \leftrightarrow SO_2 + O$	2.3e+12	0.0	3.70e+3	Garland[44]
13	$Al + O_2 \leftrightarrow AlO + O$	2.0e+13	0.0	0.0	Cohen and Westberg[45]
14	$Al + SO_2 \leftrightarrow SO + AlO$	9.6e+13	0.0	2.00e+3	Fontijn and Felder[46]
15	$Al + e\text{-} \leftrightarrow Al^+ + e\text{-} + e\text{-}$	2.5e+19	-0.82	6.94e+4	Based on N rate[17]
16	$NaO + O \leftrightarrow Na + O_2$	2.2e+14	0.0	0.0	Plane and Husain[47]
17	$Na + e\text{-} \leftrightarrow Na^+ + e\text{-} + e\text{-}$	2.5e+19	-0.82	5.96e+4	Based on N rate[17]
18	$Ca + O_2 \leftrightarrow CaO + O$	2.5e+14	0	7.25e+3	Kashireninov et al.[48]
17	$Ca + e\text{-} \leftrightarrow Ca^+ + e\text{-} + e\text{-}$	2.5e+19	-0.82	7.09e+4	Based on N rate[17]

Ref 5: Johnston.et.al. AIAA 2017-4533. Impact of Coupled Radiation and Ablation on the Aerothermodynamics of Meteor Entries

Internal degree relaxation model of ultra-high-temperature gas

- **Park’s two-temperature model （Ttr-Tve）, Multi-temperature model（Tt-Tr-Tvi-Tel）, State-To-State model.**

- **model parameter such as vibrational relaxation time need to be validated at ultra-high-temperature.**

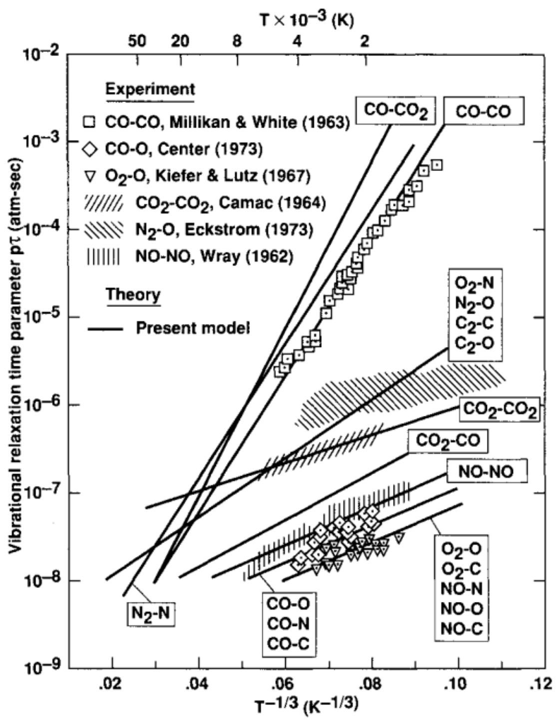

Fig. 2 Comparison between the measured vibrational relaxation times[7,8,51–53] and the present model for carbon-containing species. [6]

Ref 6: Chul, Park.et.al. JTHT 8(1),1994. Review of chemical-kinetic problems of future NASA missions. II - Mars entries.

Radiation model of ultra-high-temperature gas

- Radiation computation: line-by-line method，e.g. NEQAIR.
- Radiation database：TOPbase 、HITEMP. Radiation band of asteroid ablation products should be developed.

Table 3: Summary of molecular band modeling for meteor ablation products[5]

Specie	Transition	Spectral Range (eV)	Data Source
SiO	A-X	4.54-5.79	Franck-Condon factors and energy levels from Geier et al.,[51] and band oscillator strength from Park and Arnold.[52]
SiO	E-X	5.74-7.55	Franck-Condon factors and band oscillator strength taken from Naidu et al.[53] and Drira,[54] and energy levels from Lagerqvist.[55]
FeO	Orange	1.68-2.38	Oscillator strengths and energy levels taken from Michels.[56]
MgO	B-A	1.72-2.45	Oscillator strengths and energy levels taken from Daily[57] and Bell et al.[58]
MgO	D-A	1.72-2.45	Oscillator strengths and energy levels taken from Naulin et al.[59] and Bell et al.[58]
MgO	B-X	2.38-2.69	Oscillator strengths and energy levels taken from Daily[57] and Bell et al.[58]
CaO	A-X	1.1-2.0	Oscillator strengths and energy levels taken from Doherty[60] and Liszt.[61]
CaO	B-X	2.6-3.7	Oscillator strengths and energy levels taken from Pasternack[62] and Liszt.[61]
CaO	Orange	1.7-2.2	Oscillator strengths and energy levels taken from Pasternack[62] and Liszt.[61]
CaO	Green	1.7-2.2	Oscillator strengths and energy levels taken from Pasternack,[62] Liszt,[61] and Baldwin.[63]
SO	A-X	3.8-5.0	Franck-Condon factors and band oscillator strength taken from Borin[64] and energy levels from Rosen.[65]
AlO	B-X	2.2-3.0	Oscillator strengths and energy levels taken from Borovicka.[66]

Ref 5: Johnston.et.al. AIAA 2017-4533. Impact of Coupled Radiation and Ablation on the Aerothermodynamics of Meteor Entries

AHENS

- The CFD code AHENS , developed at our institute for aerothermal environment simulation, solves the NS equations on structured grids.

Numerical Method

- The finite-volume method is used to discretize the governing equations.
- Hybrid Steger-Warming and Godunov flux scheme with second-order spatial accuracy.
- LU-SGS implicit algorithm for time step iteration.
- MPI based parallelism.

High-temperature Gas Model

- **1T / 2T /3T Multi-species gas mixture model.**
- **Finite-rate chemistry model.**
- **Polynomial fitting method for thermodynamic properties.**
- **Gupta's model with collision cross section data for transport coefficients.**
- **Modified Fick's model for mass diffusion.**

$$J_{s\neq e} = -\rho D_s \nabla Y_s - Y_s \sum_{r\neq e} -\rho D_r \nabla Y_r \qquad J_e = -\frac{1}{q_e}\sum_{s\neq e} q_s J_s$$

It ensures that the sum of mass fluxes is zero.

Boundary condition

- Freestream inflow, extrapolation outflow, symmetry.
- RCS jet boundary condition, stagnation boundary condition.
- Unslip or slip boundary condition.
- Isothermal wall or radiative equilibrium wall condition.
- Quasi steady ablation with finite-rate surface chemistry .
- Catalytic wall conditon: non-catalytic , super-catalytic, specified catalytic coefficients.

Radiation model

- **Non-Boltzmann models for diatomic molecules and atomic species electronic state populations**
- **Line information and cross-sections following the work of Johnston.**[7]

Molec.	Transition	Name	Spectral Range (eV)
N_2	$B^3\Pi_g$ - $A^3\Sigma_u^+$	1^+ (1^{st}-positive)	0.2 - 2.5
N_2	$C^3\Pi_u$ - $B^3\Pi_g$	2^+ (2^{nd}-positive)	2.7 - 4.7
N_2	$c_4{}'\Sigma_u^+$ - $X^1\Sigma_g^+$	Carroll-Yoshino	11.5 - 14.0
N_2	$c_3{}'\Pi_u$ - $X^1\Sigma_g^+$	Worley-Jenkins	11.5 - 14.0
N_2	$b^1\Pi_u$ - $X^1\Sigma_g^+$	Birge-Hopfield I	7.0 - 13.1
N_2	$b'^1\Sigma_u^+$ - $X^1\Sigma_g^+$	Birge-Hopfield II	7.6 - 14.0
N_2	$o_3{}^1\Pi_u$ - $X^1\Sigma_g^+$	Worley	10.4 - 14.0
N_2^+	$B^2\Sigma_u^+$ - $X^2\Sigma_g^+$	1^- (1^{st}-negative)	1.2 - 4.6
NO	$B^2\Pi_r$ - $X^2\Pi_r$	β (beta)	2.1 - 6.9
NO	$A^2\Sigma^+$ - $X^2\Pi_r$	γ (gamma)	3.2 - 7.5
NO	$C^2\Pi_r$ - $X^2\Pi_r$	δ (delta)	3.7 - 7.6
NO	$D^2\Sigma^+$ - $X^2\Pi_r$	ε (epsilon)	3.4 - 8.0
NO	$B'^2\Delta$ - $X^2\Pi_r$	β' (beta-prime)	3.9 - 8.4
NO	$E^2\Sigma^+$ - $X^2\Pi_r$	γ' (gamma-prime)	4.6 - 8.9
O_2	$B^3\Sigma_u^-$ - $X^3\Sigma_g^-$	Schumann-Runge	2.6 - 7.0

molecular band systems

Ref 7: Johnston. Nonequilibrium shock-layer radiative heating for Earth and Titan entry[D].PhD Thesis.

Radiation Transfer

- **Radiative Transfer Equation:**

$$\frac{dI_\nu(s,\Omega)}{ds} = j_\nu(s) - \kappa_\nu'(s) I_\nu(s,\Omega)$$

- **Tangent Slab approximation:**

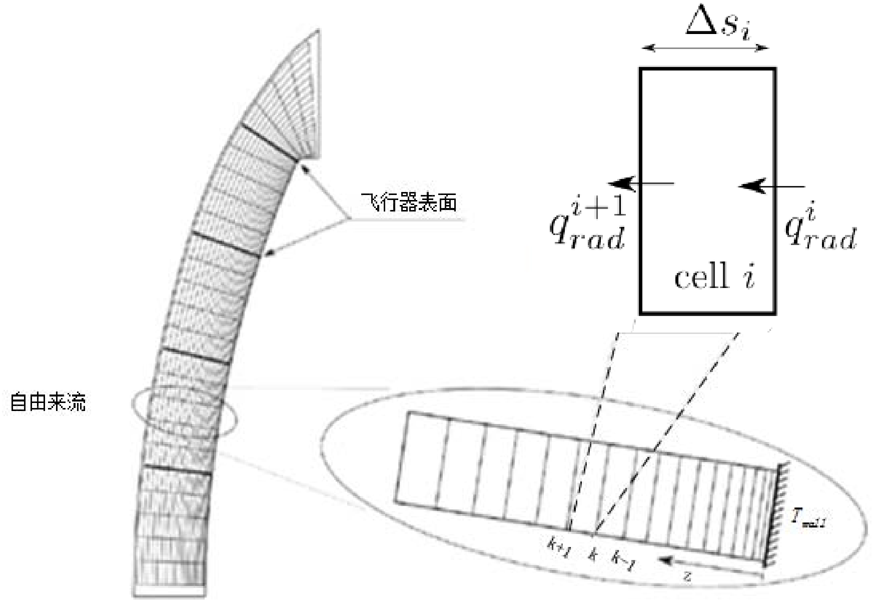

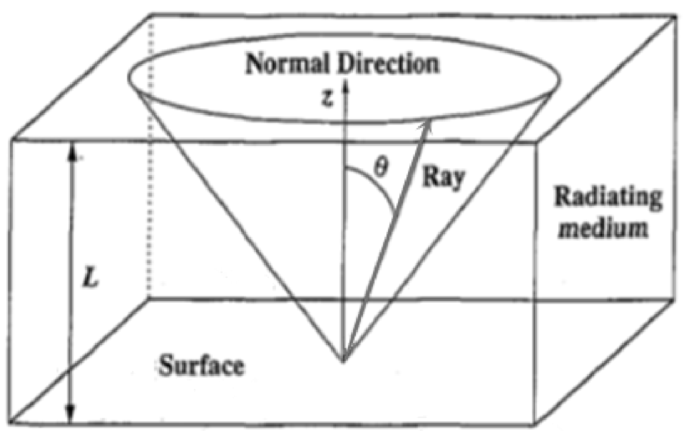

$$-(\nabla \cdot \vec{q}_{\mathrm{rad}})_i = -\left(\frac{\partial q_{\mathrm{rad}}}{\partial s}\right)_i \approx \frac{-\left(q_{\mathrm{rad}}^{(i+1)} - q_{\mathrm{rad}}^{(i)}\right)}{\Delta s_i}$$

Loosely coupled approach

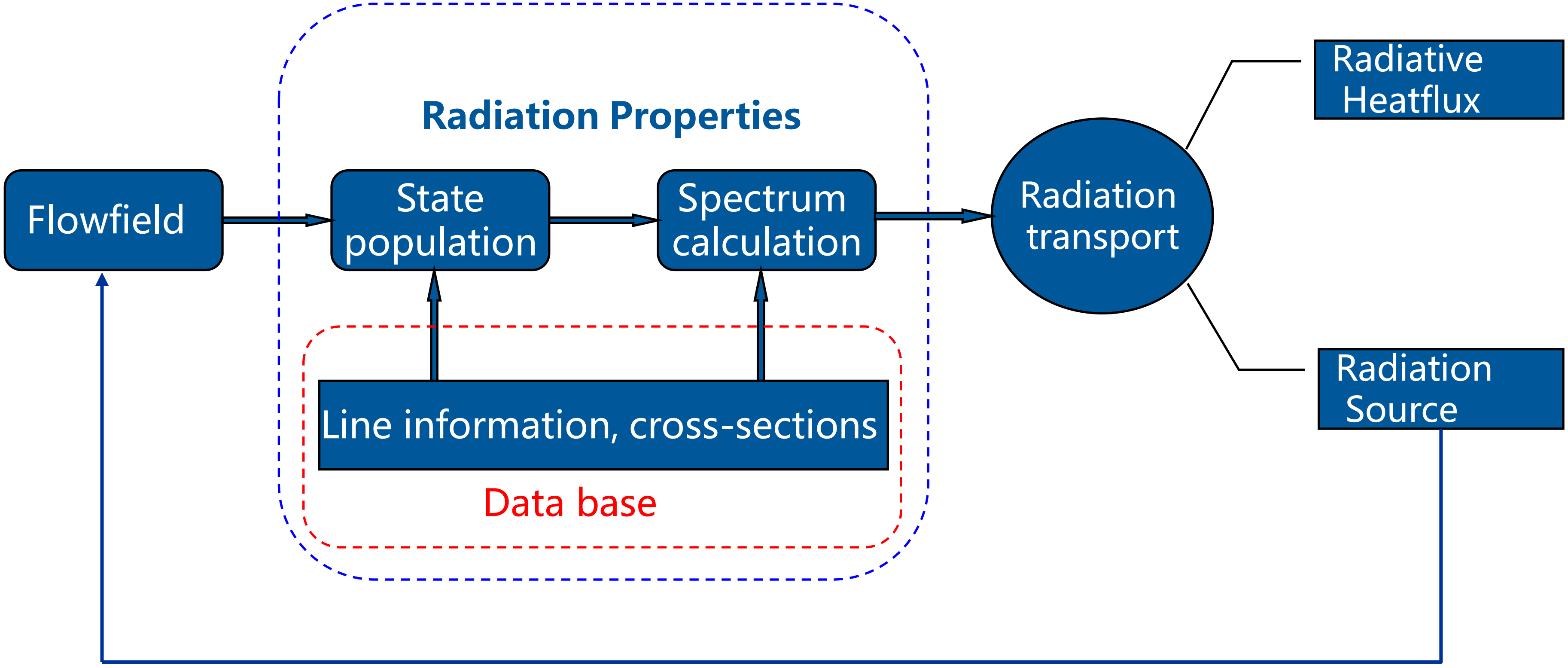

Coupled simulation of flow and radiation

Outline

Stardust vehicle reentry

- **The radiation-flow coupling effect is relatively small to the flowfield of the reentry vehicle.**

case	H(km)	Voo(m/s)	AoA(°)	Wall conditon
1	59.77	11136.7	0	super-catalytic

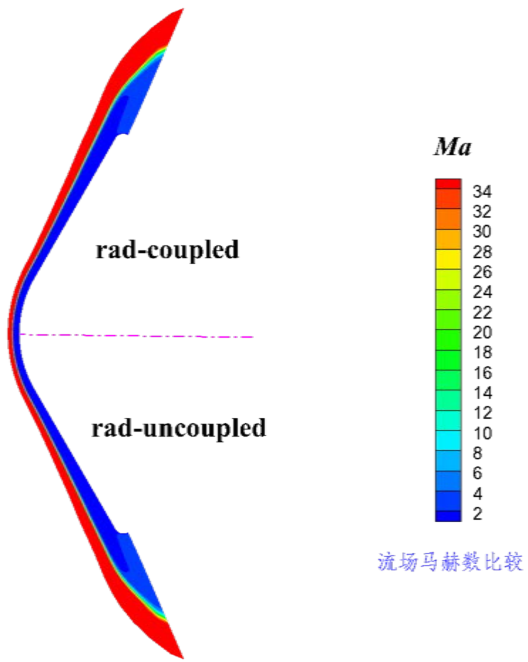

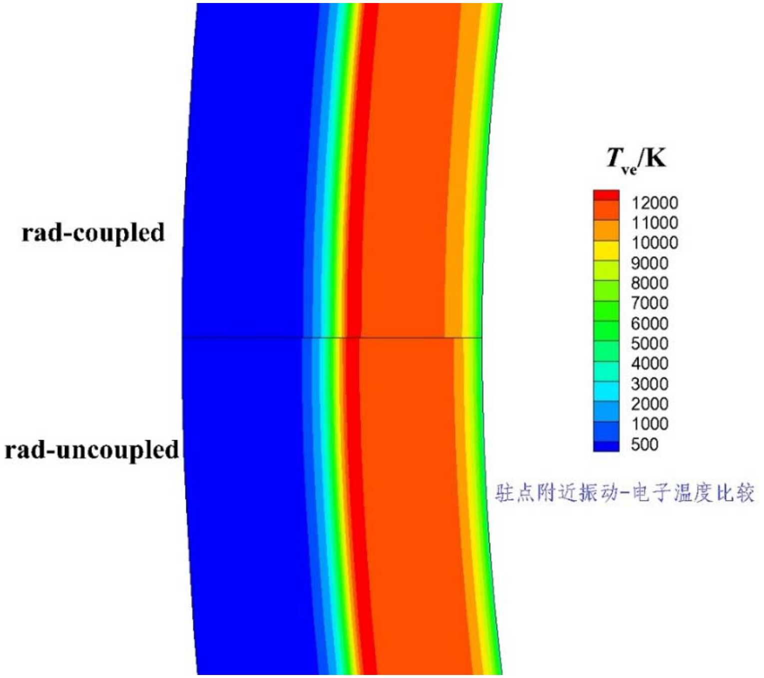

Comparison of the predicted flow properties

Stardust Capsule reentry

- **The convective is the dominated mechanism of aerodynamic heating for reentry vehicles, un-coupled radiation simulation can be adopted.**

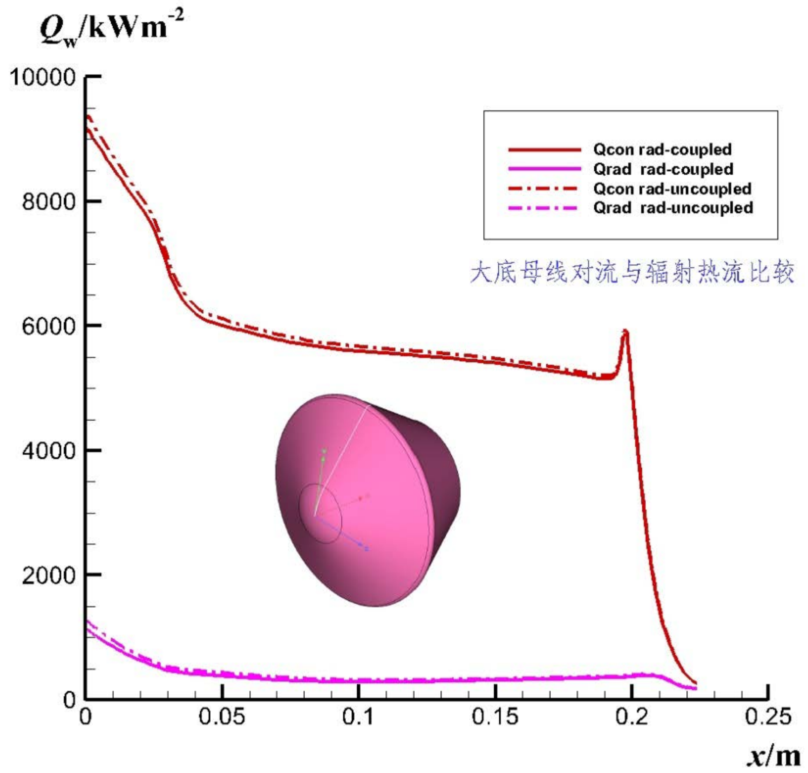

Comparison of the predicted heat flux

Asteroid entry

- Coupled and uncoupled radiation simulations are carried out for typical asteroid entry condition to investigate the influence mechanism radiation-flow coupling on aerodynamic heating.

- A 13 species (N2,O2,N,O,NO,NO+,N2+,N+,N++,O2+,O+,O++,e-) ionized air model is incorporated. [8]

case	H(km)	Voo(km/s)	Wall conditon	D(m)
1	50	15、20	super-catalytic	20
2	50	15、20	super-catalytic	50
3	50	15、20	super-catalytic	100
4	50	15、20	super-catalytic	140

Ref 8: Johnston.et.al. Aerothermodynamic Characteristics of 16-22 km/s Earth Entry[R]. AIAA 2015-3110, 2015.

□Asteroid entry

- Radiation-flow coupling effect plays a significant role in flow structure of asteroid entry.
- Compared with uncoupled case, the temperature and thickness of shock layer are much smaller.

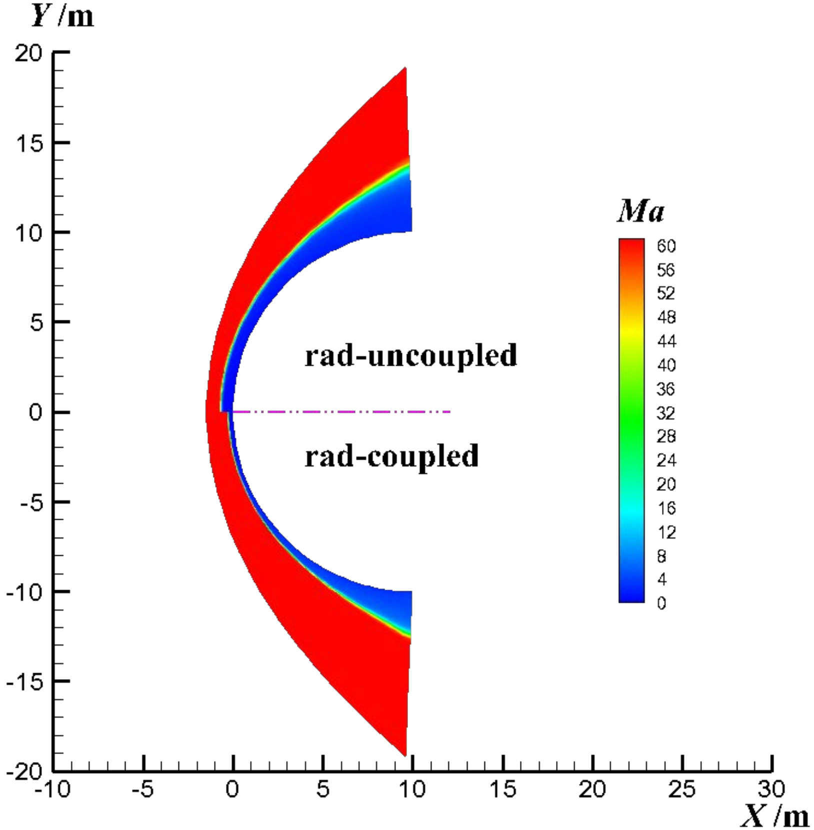

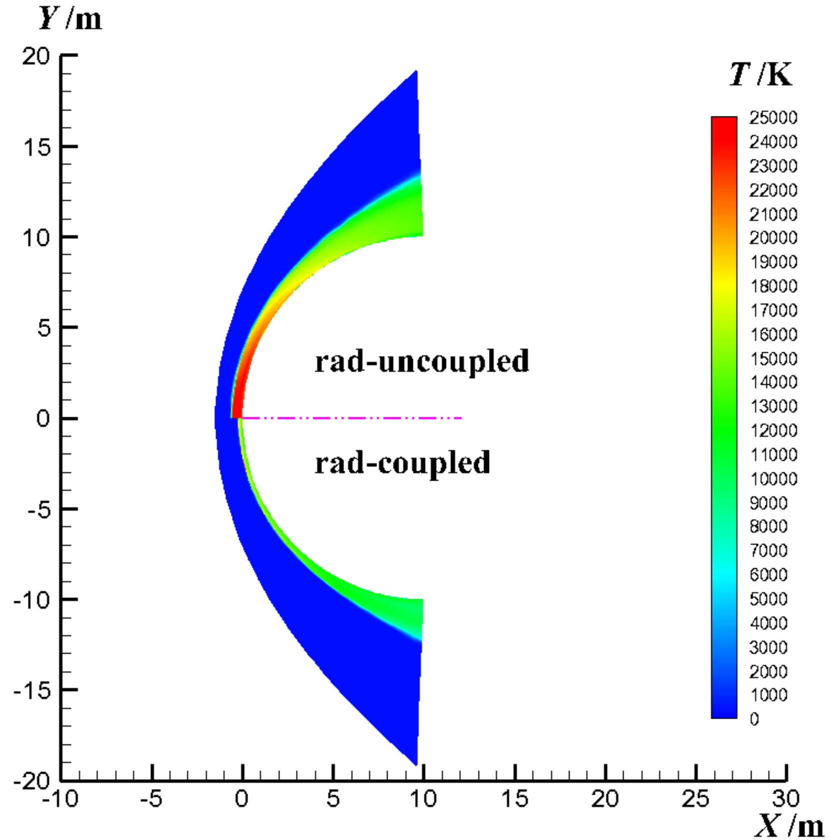

D=20m,V=20km/s

□Asteroid entry

- **With the increase of entry velocity, the coupling effects on flowfield is enhanced, and the variations of shock standoff distance and peak temperature are enlarged.**

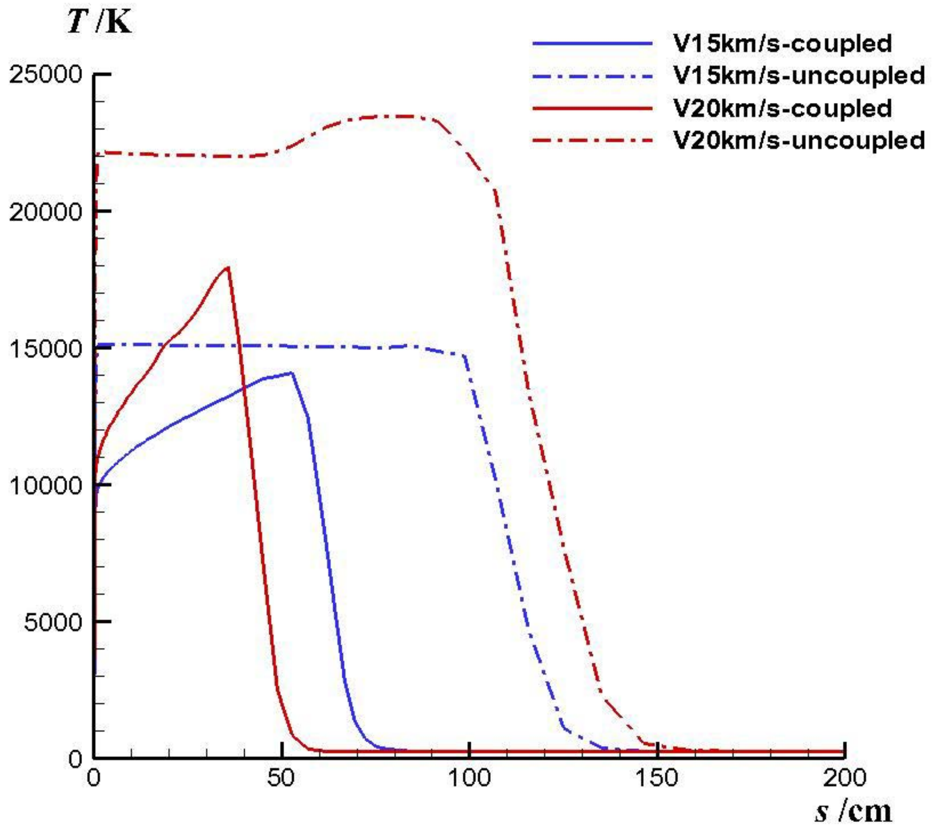

Flow temperature along stagnation line(D=50m)

□Asteroid entry

- The radiative cooling and thin shock layer are the physical mechanism that radiation-flow coupling will ease aero-heating.

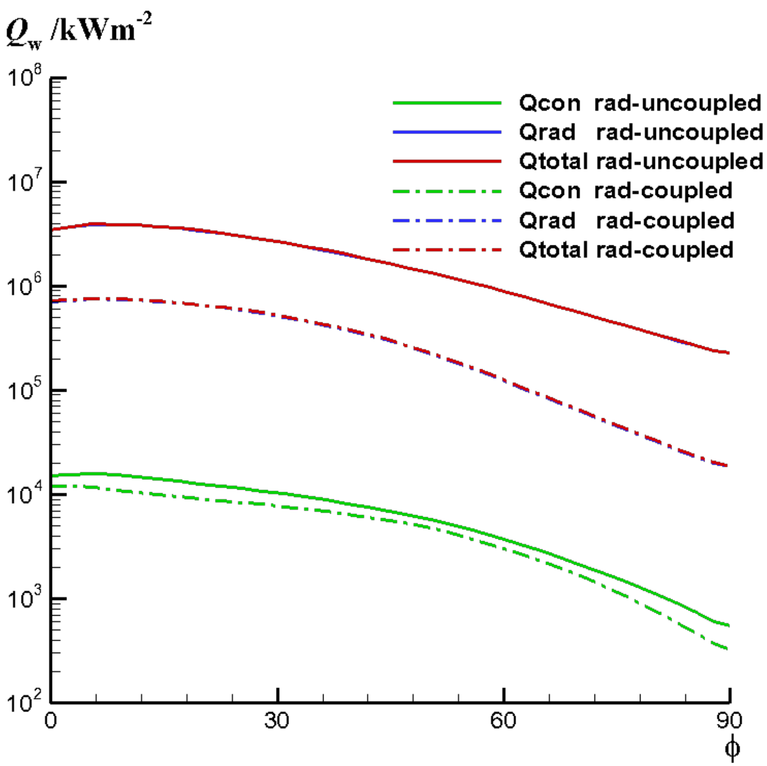

D=20m,V=20km/s

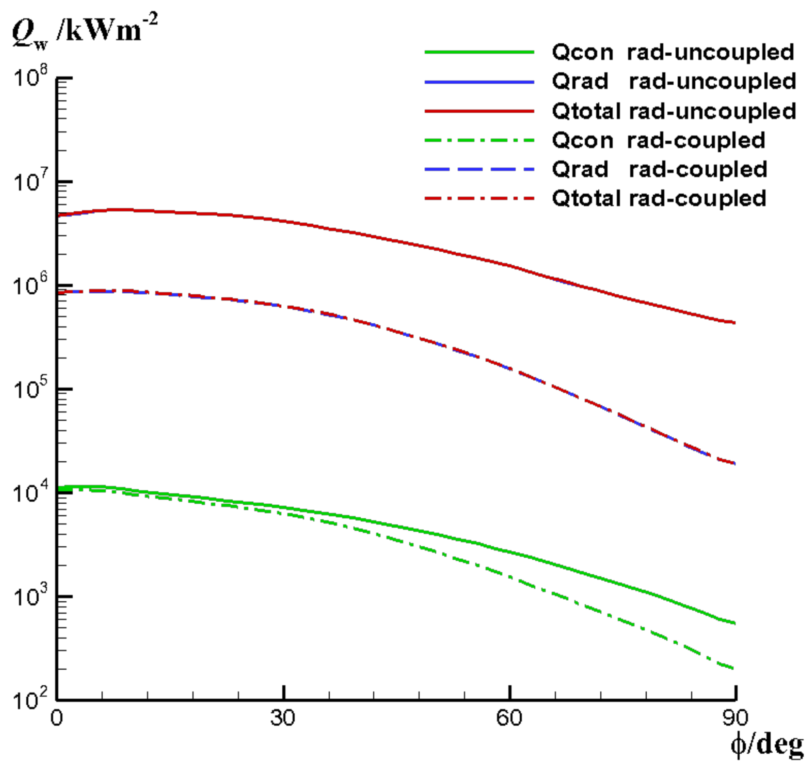

D50m,V=20km/s

Heatflux along surface

☐Asteroid entry

- There are obvious differences of heating character between asteroid entry and hypersonic vehicle reentry:
- The radiative heating is dominant for asteroid entry and the convective heating is negligible.
- Total heat flux at stagnation point increases with diameter.

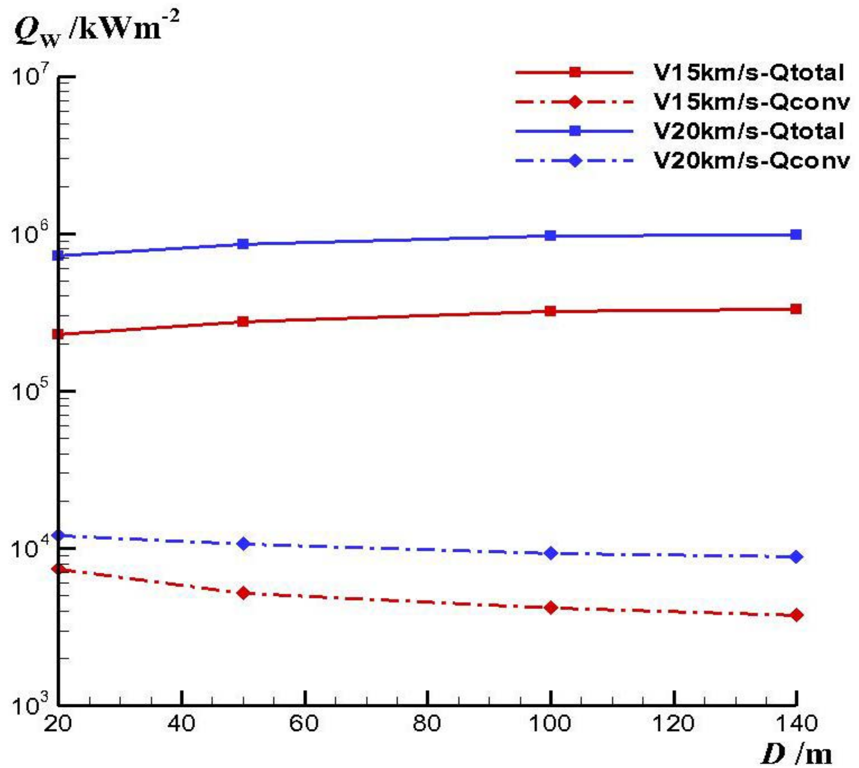

Stagnation point Heatflux

Outline

(1) Hypervelocity aerothermodynamics plays an important role in the analysis of asteroid impacting the Earth.

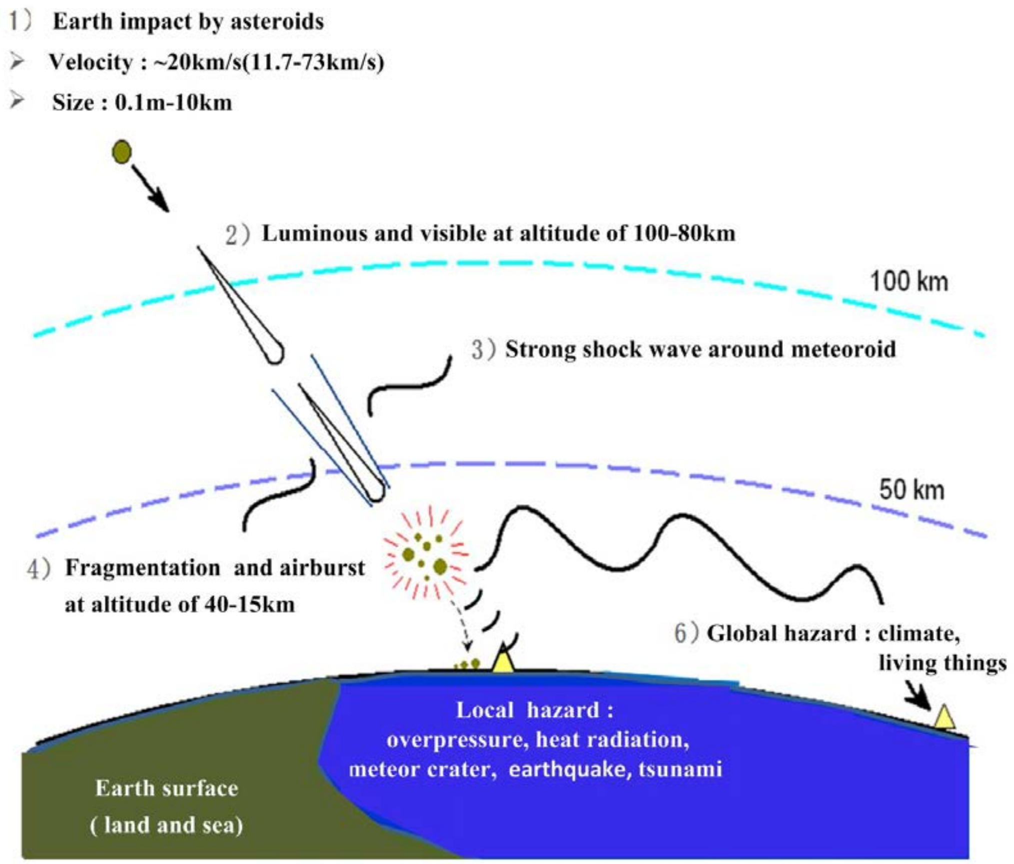

- aerodynamic forces and trajectory during ultra-high velocity entry
- aerodynamic heating during ultra-high velocity entry
- ablation and thermal response of asteroid structure
- physical characteristics of asteroid entry process

4. Summary

(2) In order to investigate the aerothermodynamic problems in asteroid entry to Earth, the high temperature gas models, such as thermo-chemical models and radiation data, need to be extend to greater than 20000K.

(3) Since there are strong coupling effects among flow-field, radiation and ablation in Earth entry problem of asteroid, both the coupling mechanism and numerical methods are needed to be further explored.

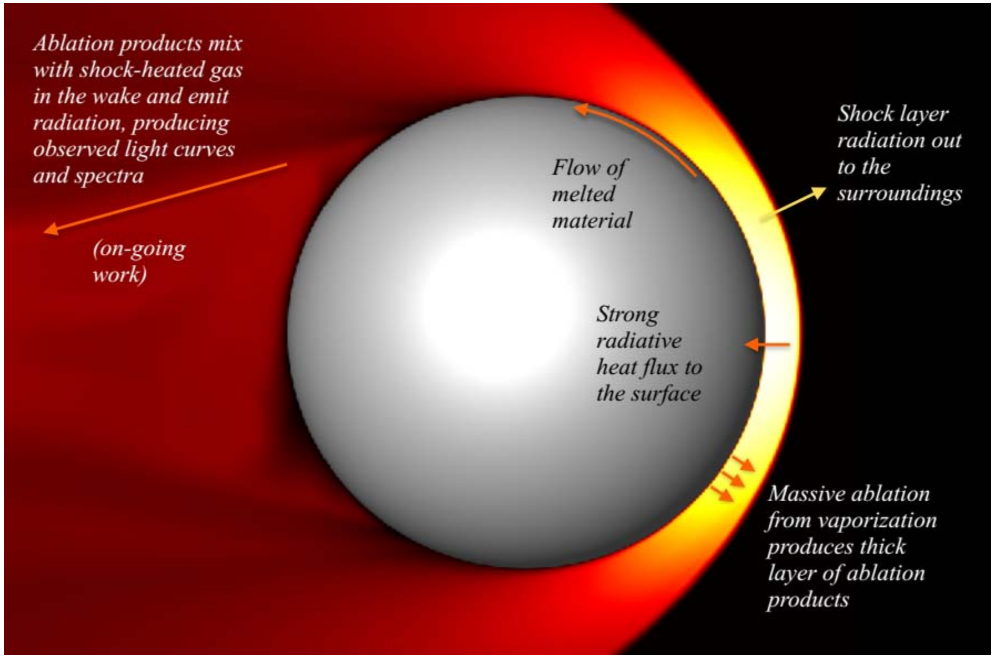

The coupling between asteroid entry flow, radiation and ablation [7]

Ref 9: Eric Stern.et.al. Entry Modeling for Asteroid Threat Assessment

Thanks for your attention

Hypervelocity Aerodynamics Institute of China Aerodynamics Research and Development Center

IMPACT EFFECTS CALCULATOR

http://AsteroidHazard.pro

SHOCK WAVE EFFECTS FROM IMPACTS OF COSMIC OBJECTS WITH DIAMETER FROM A FEW METERS TO 3KM

IAA PLANETARY DEFENSE CONFERENCE 2021

26-30 APRIL 2021

IDG RAS

D.O. Glazachev,
O.P. Popova,
V.V. Svetsov,
V.V. Shuvalov,
N.A.Artemieva,
and E.D.Podobnaya

Motivation

Physical process

impossible for a full – scale laboratory experiment

Modeling

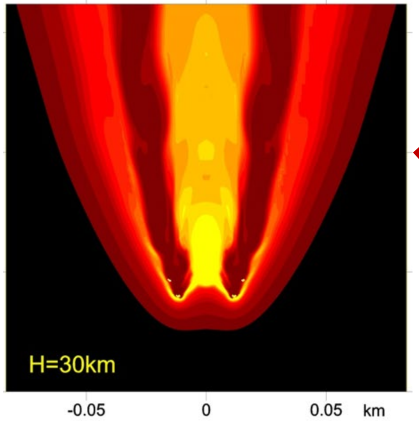

slow calc

Scaling relations

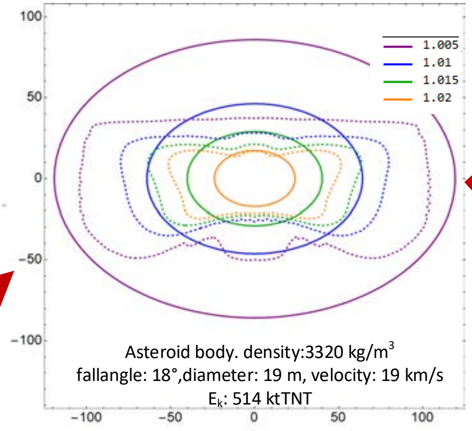

quick calc

online calculator

easy to use

***

The main motivation is to create a quick and accurate tool for assessing the consequences of the impact of a cosmic body.

Quasi-liquid meteoroid model

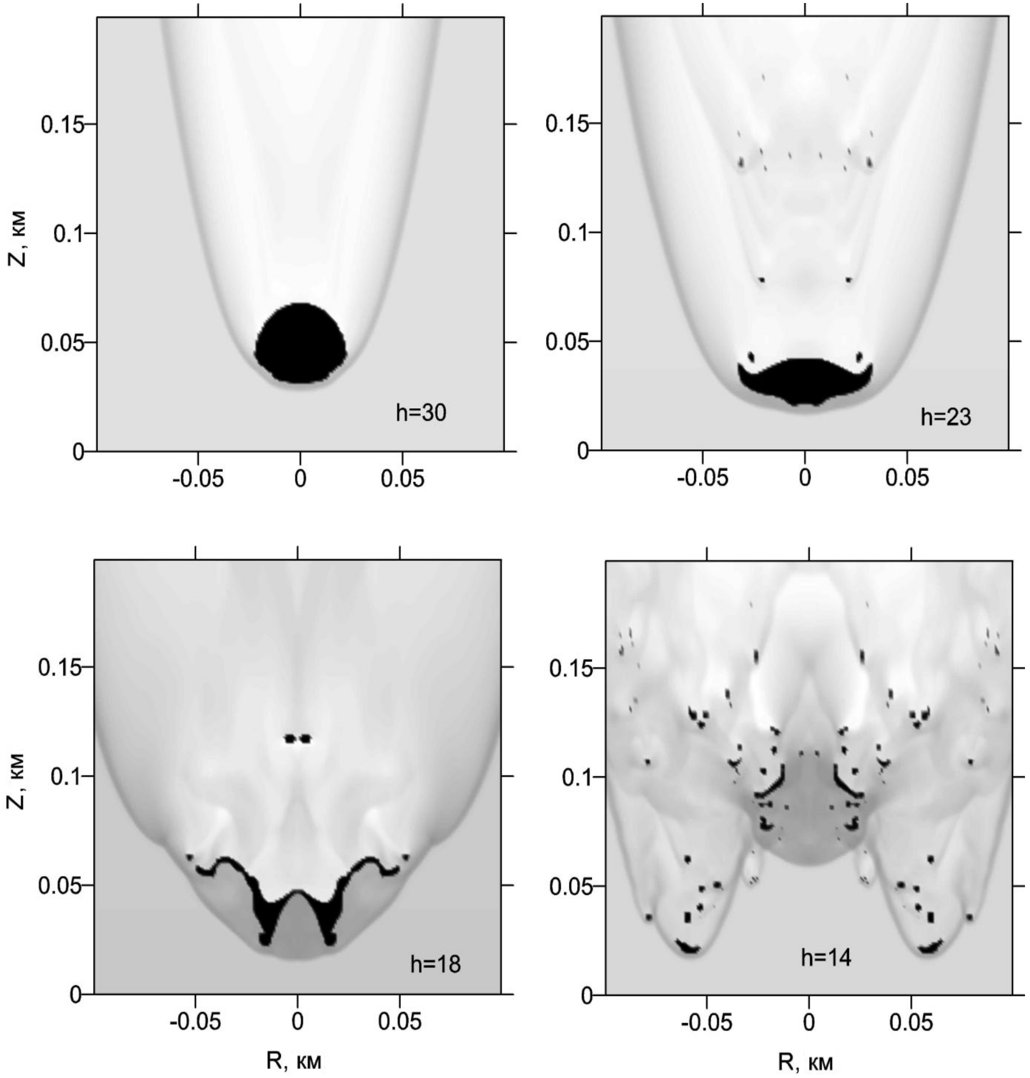

Relative density distribution along trajectory at different altitudes h
D=40 m, V=18 km/s; chondritic material (2650 kg/m^3), α=90^0
Black – solid meteoroid material

Basis:

large meteoroid deformation begins at h, where aerodynamical loading>>strength

Main assumptions

- Zero strength
- Ablation as evaporation
- Radiation transfer in thermal conductivity approximation

Formal range

D>30-50 m; h<40 km (Svettsov et al. 1993)

Restrictions:

quasi-liquid assumption

Quasi-liquid model= QL model

D-30-45-20

density: 3320 kg/m^3
diameter: 30 m

entry angle: 45°
velocity: 20 km/s

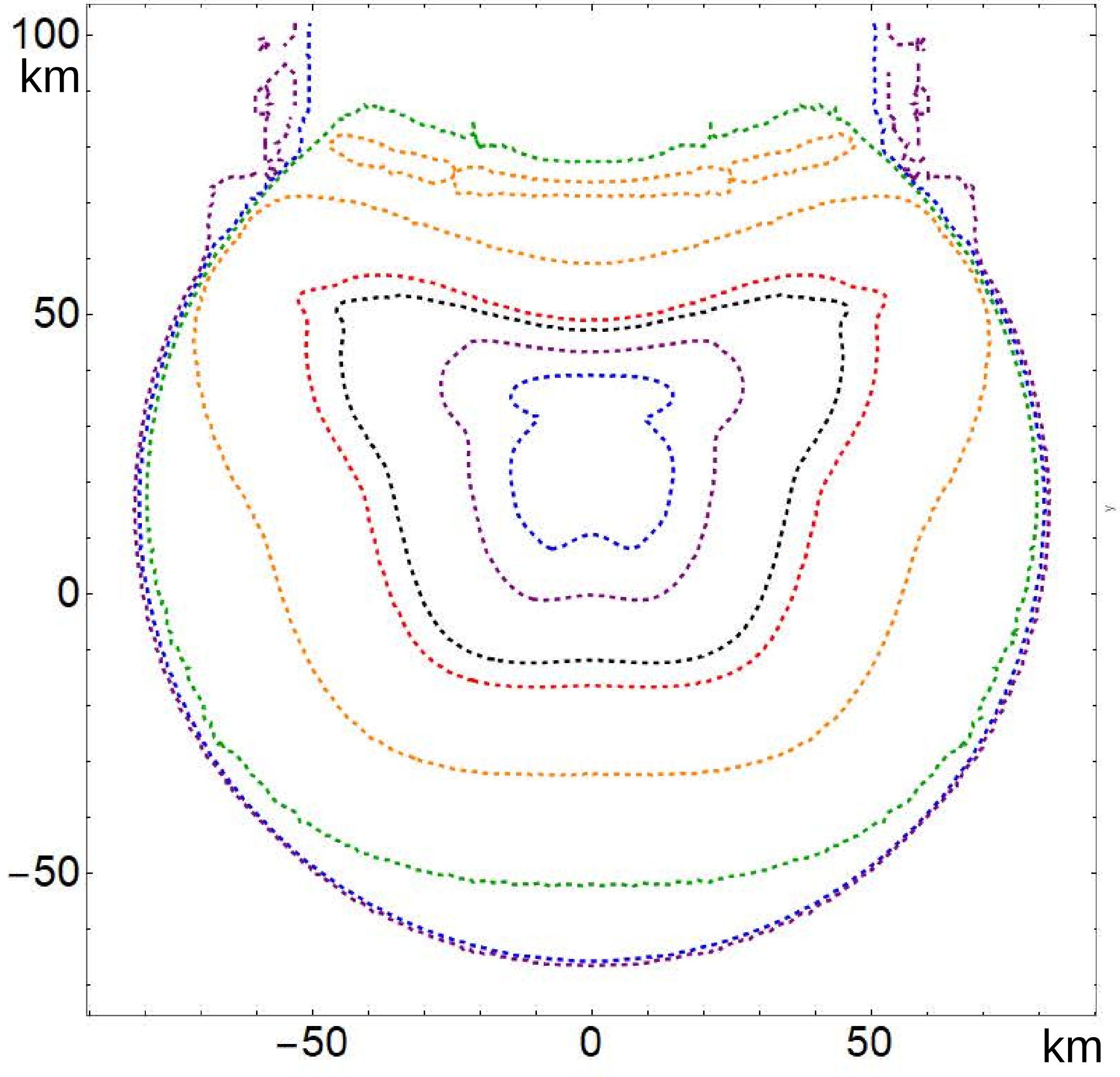

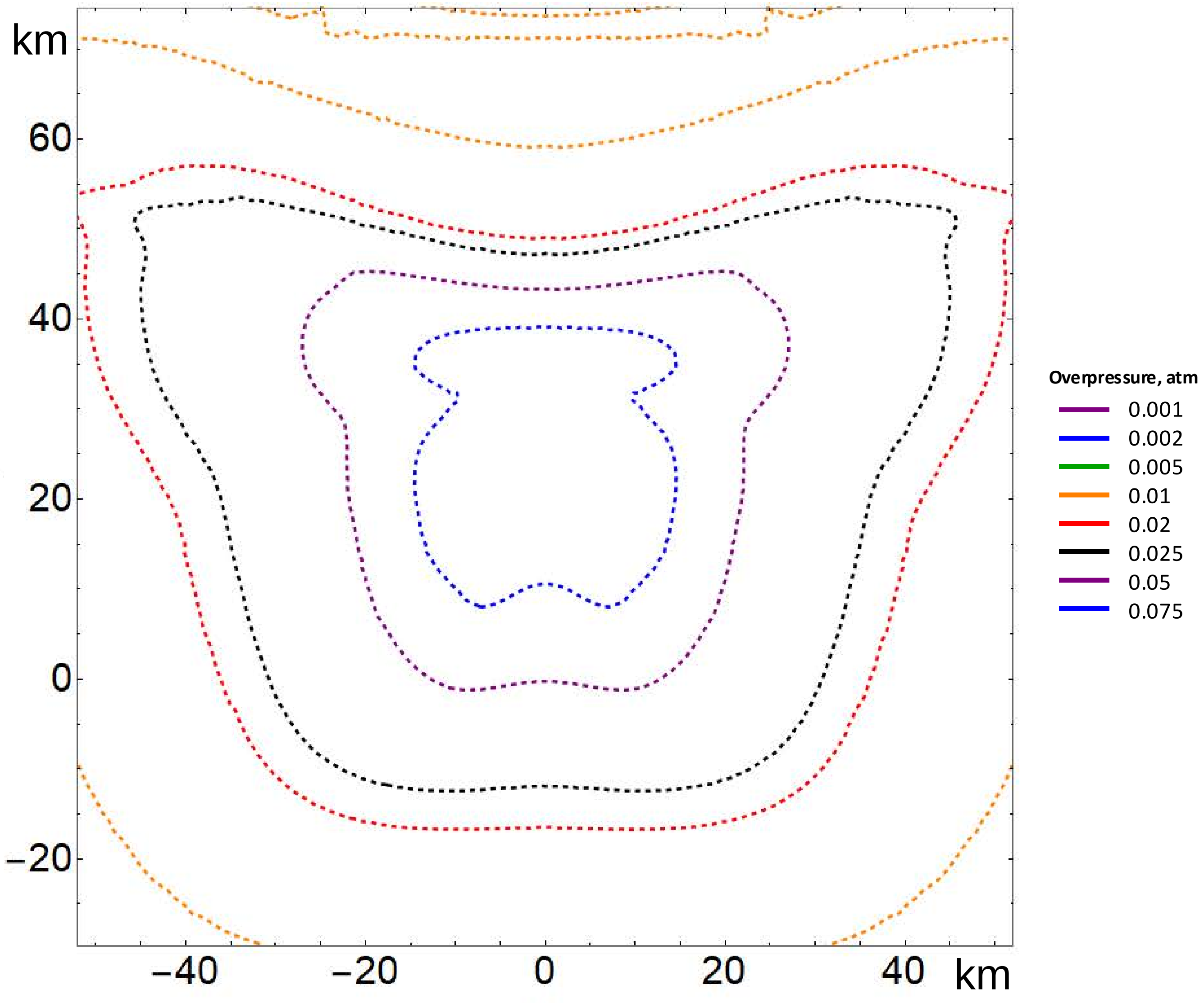

Central zone

Overpressure distribution obtained for one variant

Modeled variants

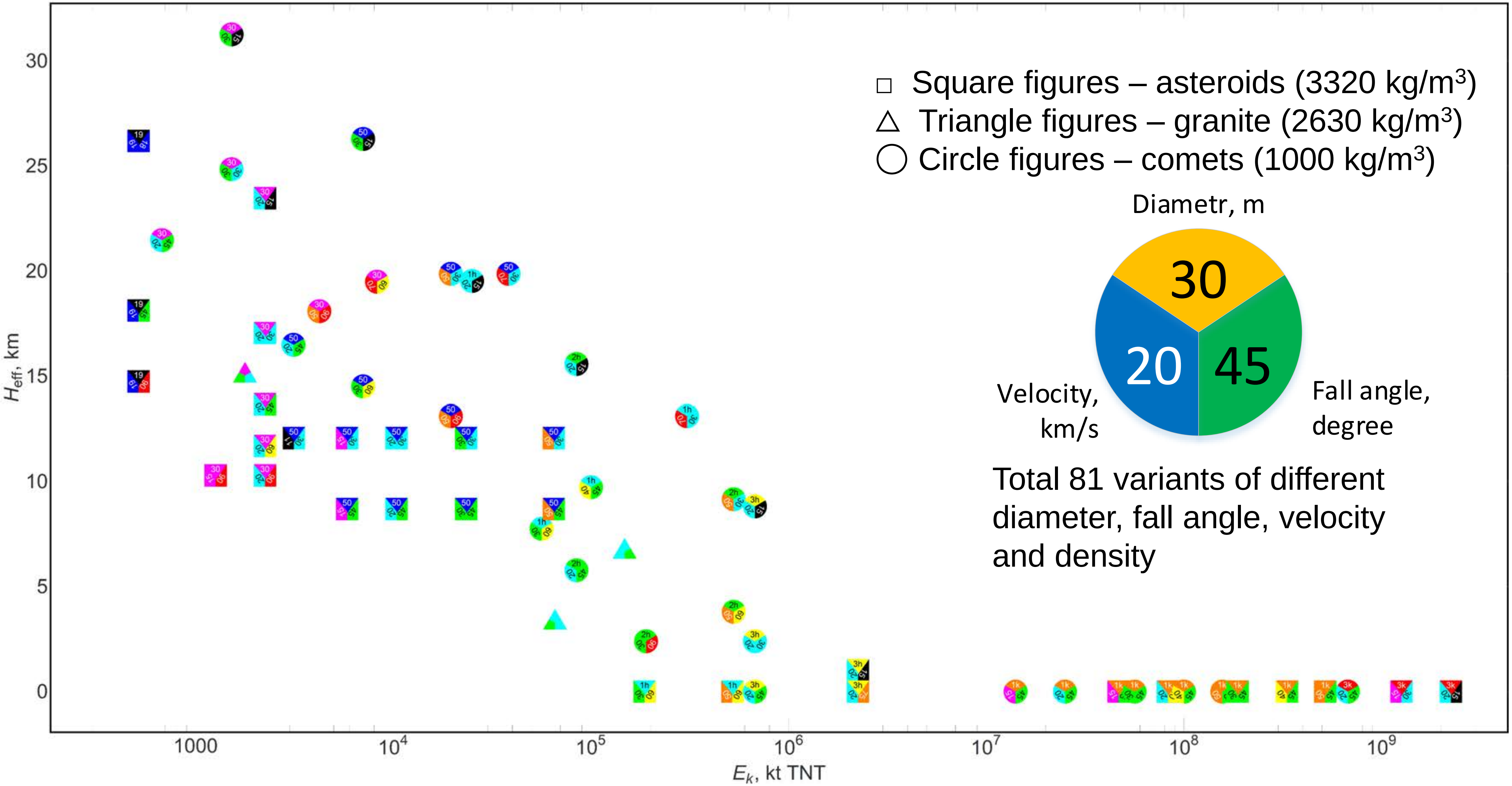

Effective airburst altitude

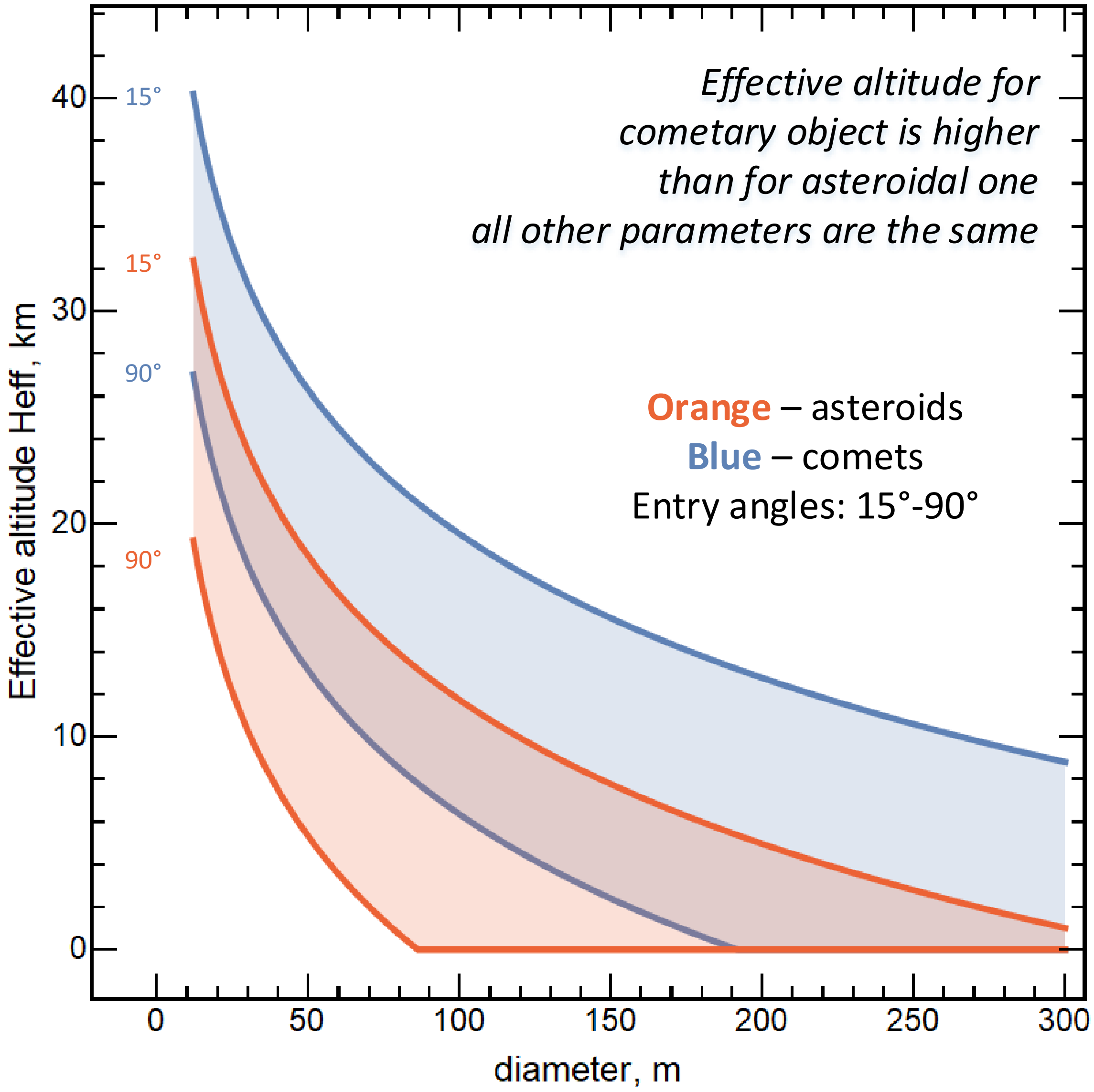

Effective altitude dependence on meteoroid size

$$H_{eff} = (-1.3 * H * \mathrm{Ln}(D * (\mathrm{Sin}[\alpha]/H) * (\rho/\rho 0)^{2/3}) + H)/1000$$

For quick rough evaluation of the impact consequences (levels of damage, area of the damage, etc) at large distances from the ground zero spherical source - reasonable SW evaluation if the altitude Heff of E-equivalent point explosion is correctly determined

QL model was used to determine Heff =f(D,density,α) (Shuvalov et al. 2016)

This approach:

-Precision of estimates - 2-3 km (random character of disruption)

-Is applicable for D>10-30 m

- for D~10-30 m the uncertainty in effective altitude may reach 10-15 km (Chelyabinsk, $TC_3$2008 and other cases)
-(strength, fragmentation features etc)

Determination of the height of the "meteoric explosion"
Shuvalov et al. Solar System Research 2016, V.50, I.1, pp 1-12

Effective airburst altitude – uncertainty area

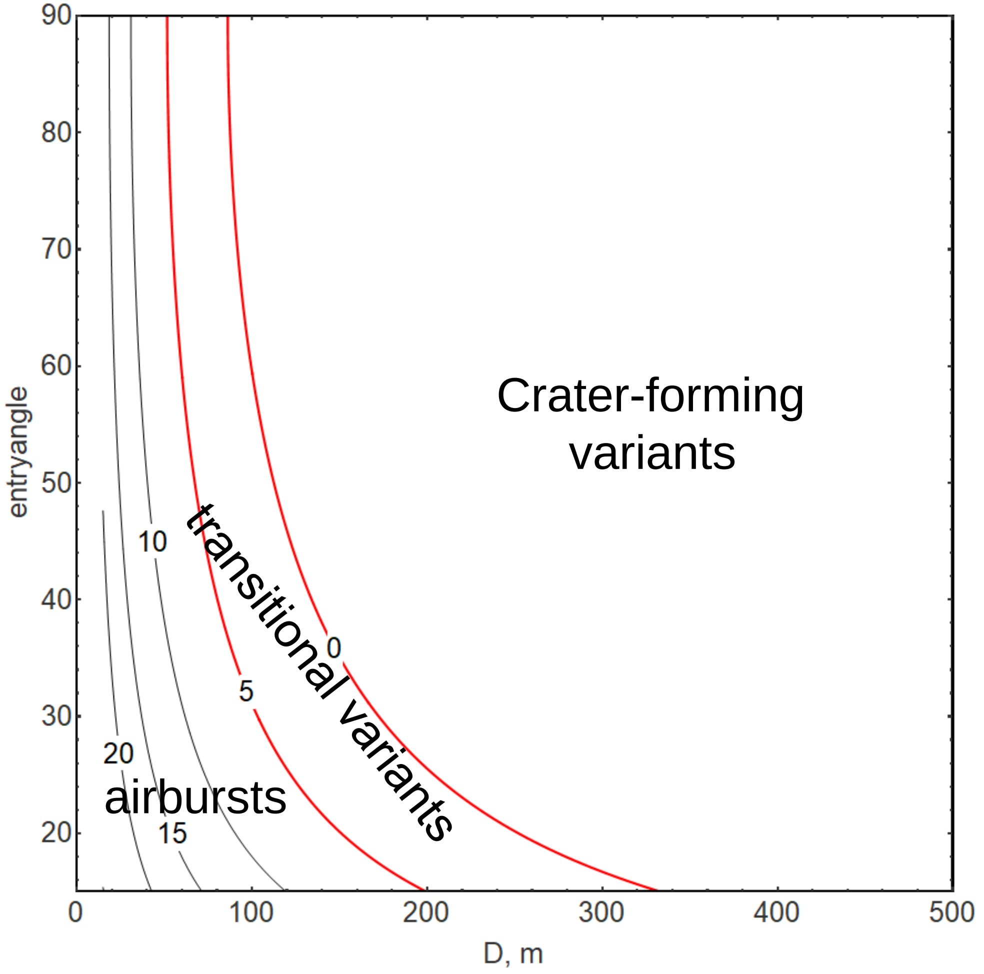

Asteroids

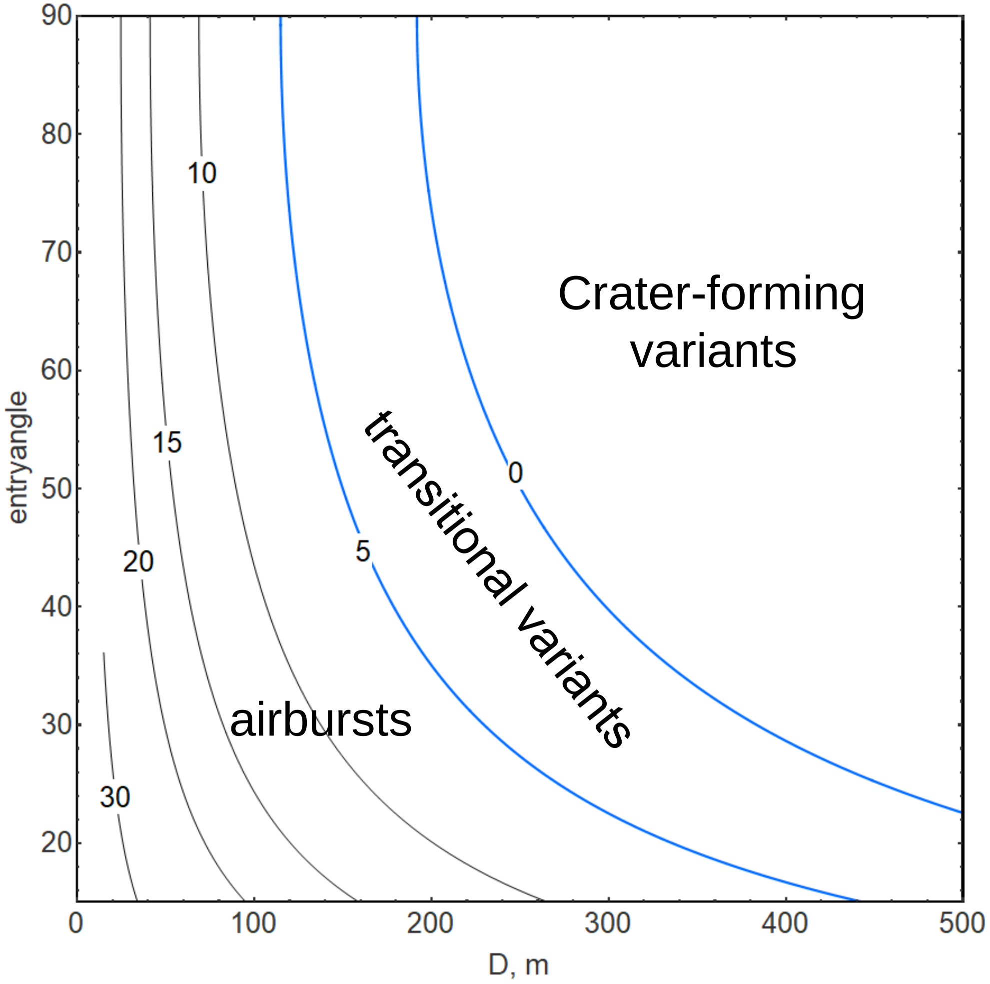

Comets

$$H_{eff} = (-1.3 * H * \mathrm{Ln}(D * (\mathrm{Sin}[\alpha]/H) * (\rho/\rho 0)^{2/3}) + H)/1000$$

Scaling relation for overpressure

$$\Delta p = el * m * \left(\frac{{E_k}^{1/3}}{{H_{eff}}^2 + x^2 + y^2} \right)^{pow}$$

x, y – spatial coordinates
el– ellipticity parameter,
E_k – kinetic energy of the impactor in kt TNT,
H_{eff}- effective height of point source,
ϕ – arctan(y/x).

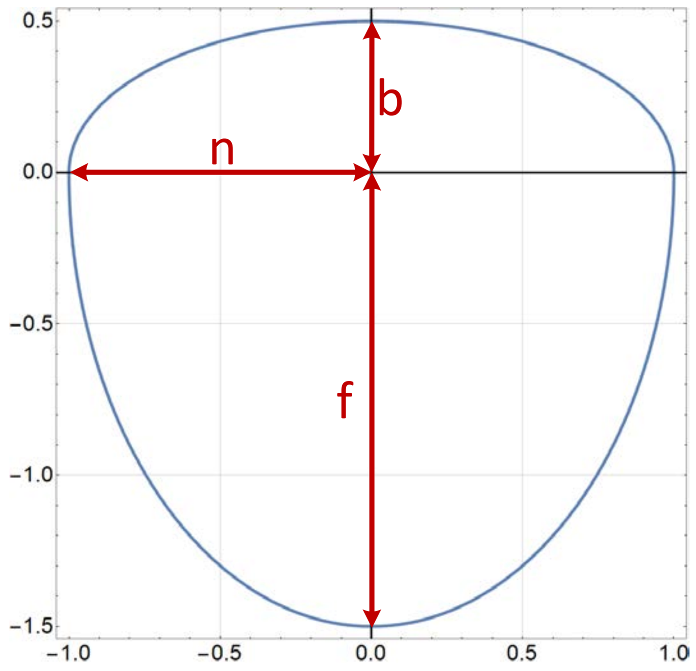

the spatial heterogeneity

$$el(\phi, \dots) = \begin{cases} \frac{n * \mathrm{b}}{\sqrt{n^2 \mathrm{Sin}[\phi]^2 + \mathrm{b}^2 \mathrm{Cos}[\phi]^2}}, 0 \le \phi < \pi \\ \frac{n * \mathrm{f}}{\sqrt{n^2 \mathrm{Sin}[\phi]^2 + f^2 \mathrm{Cos}[\phi]^2}}, -\pi \le \phi < 0 \end{cases}$$

Airburst

$$pow = 1.5$$
$$m = const$$
$$H_{eff} = function(\rho, D, \alpha)$$
$$el = el(\phi, n_{ab}, b_{ab}, f_{ab})$$
$$n_{ab} = fucntion(\rho, D, \alpha, V)$$
$$b_{ab} = fucntion(\rho, D, \alpha, V)$$
$$f_{ab} = fucntion(\rho, D, \alpha, V)$$

Crater-forming

$$pow = 1.4$$
$$m = function(E_k)$$
$$H_{eff} = 0$$
$$el = el(\phi, n_{cf}, b_{cf}, f_{cf})$$
$$n_{cf} = fucntion(\rho, D, \alpha, V)$$
$$b_{cf} = fucntion(\rho, D, \alpha, V)$$
$$f_{cf} = fucntion(\rho, D, \alpha, V)$$

Wind speed:

$$Vmax = \frac{330}{\gamma} * (p/p0 - 1) * \left(1 + \frac{\gamma + 1}{2 * \gamma} * (p/p0 - 1)\right)^{-1/2}$$

γ - adiabatic index

$$vmax = \begin{cases} \frac{67.1 * {E_k}^{0.38}}{{H_{eff}}^{1.53}}, \rho = 1000\ kg/m^3 \\ \frac{40.51 * {E_k}^{0.39}}{{H_{eff}}^{1.45}}, \rho = 3320\ kg/m^3 \end{cases}$$

Overpressure field with model and errors

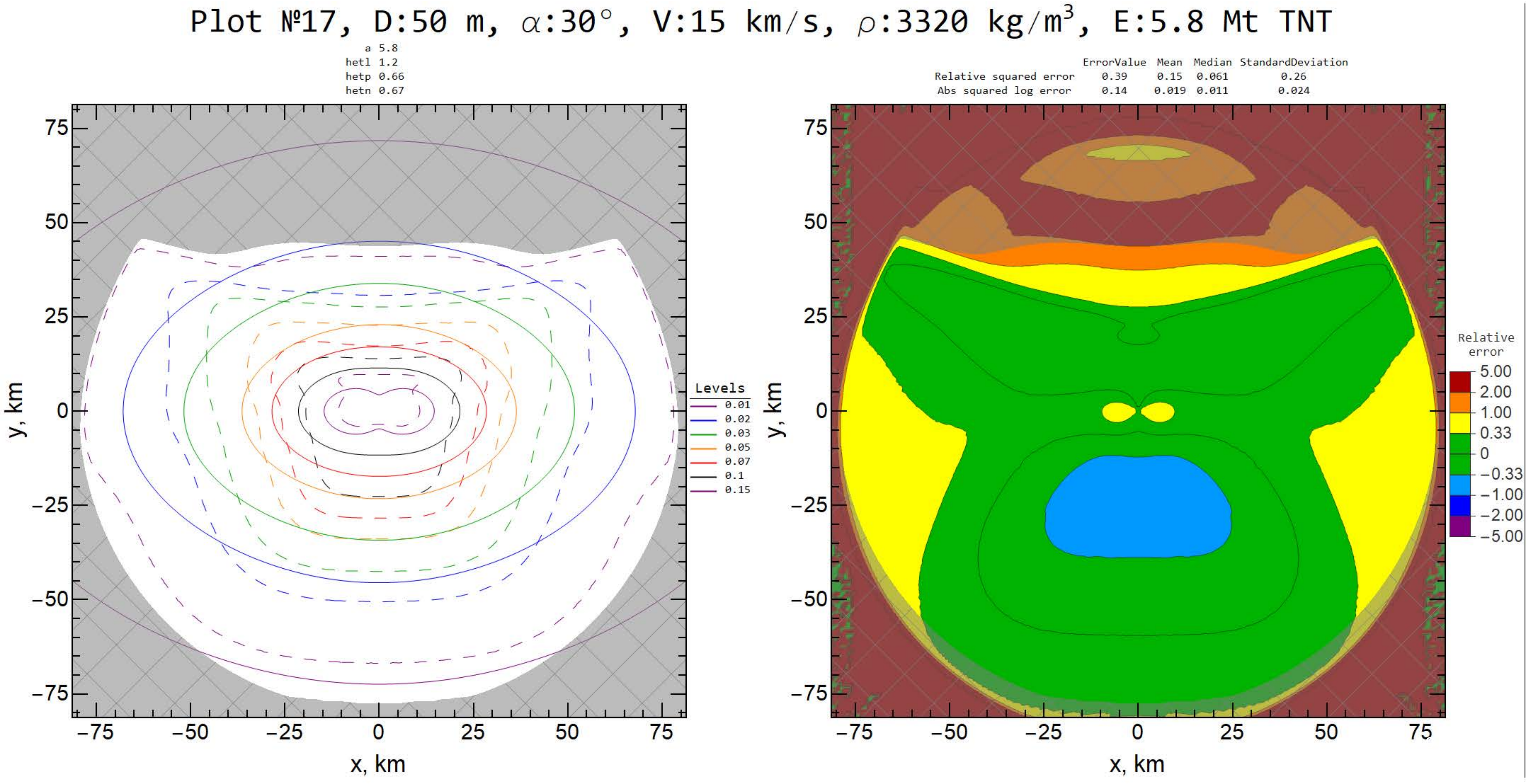

Results comparison

Our scaling relations
http://AsteroidHazard.pro

D-50-30-15

density: 3320 kg/m³
diameter: 50 m
fall angle: 30°
velocity: 15 km/s

Scalings-solid

Numerical modeling data - dashed

Collins et al. 2017

$$p(r) = 3.14 \times 10^{11}(r^2 + z_b^2)^{-2.6/2} + 1.8 \times 10^{7}(r^2 + z_b^2)^{-1.13/2} \quad (7)$$

$$z_{b,50\%} = 25.7 - 7.83\log_{10}E_{Mt} - 0.31(\log_{10}E_{Mt})^2 \quad (6b)$$

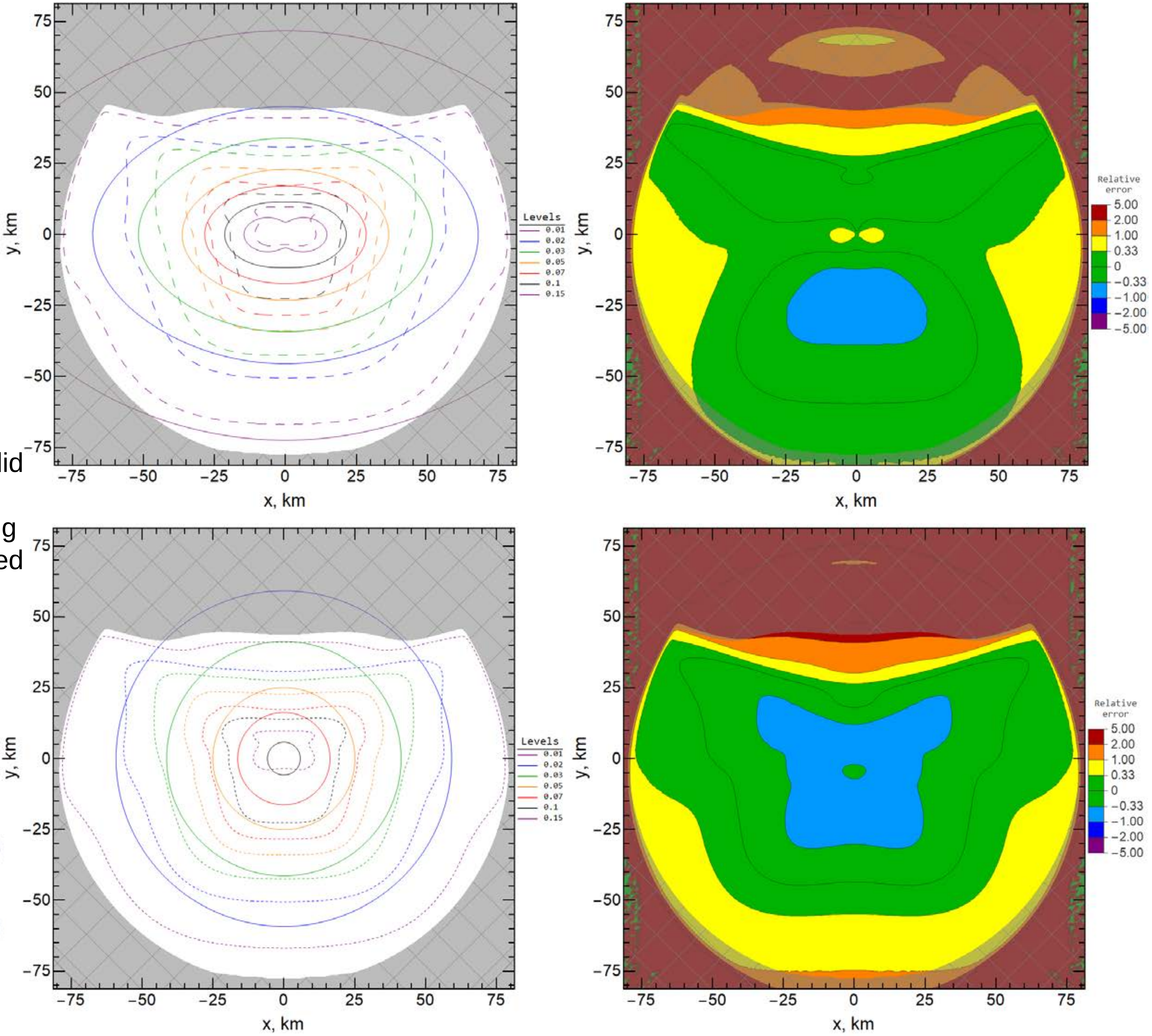

Modeled variants in 2021 PDC excercise

«As mentioned previously, the size of 2021 PDC is highly uncertain, ranging from as small as 35 meters to as large as 700 meters. This estimate is based on the asteroid's brightness, its estimated distance, and the wide range of possible albedos (reflectivities).

Little is known about other properties of the object, such as composition and density. As a result, the potential impact damage and population risk is also highly uncertain. Based on these estimates, the possible energy released on impact could range from 1.2 Mt to 13 Gt (TNT equivalent).

Velocity from 15.12 to 15.87 km/s
Entry angle from 0 to 90°

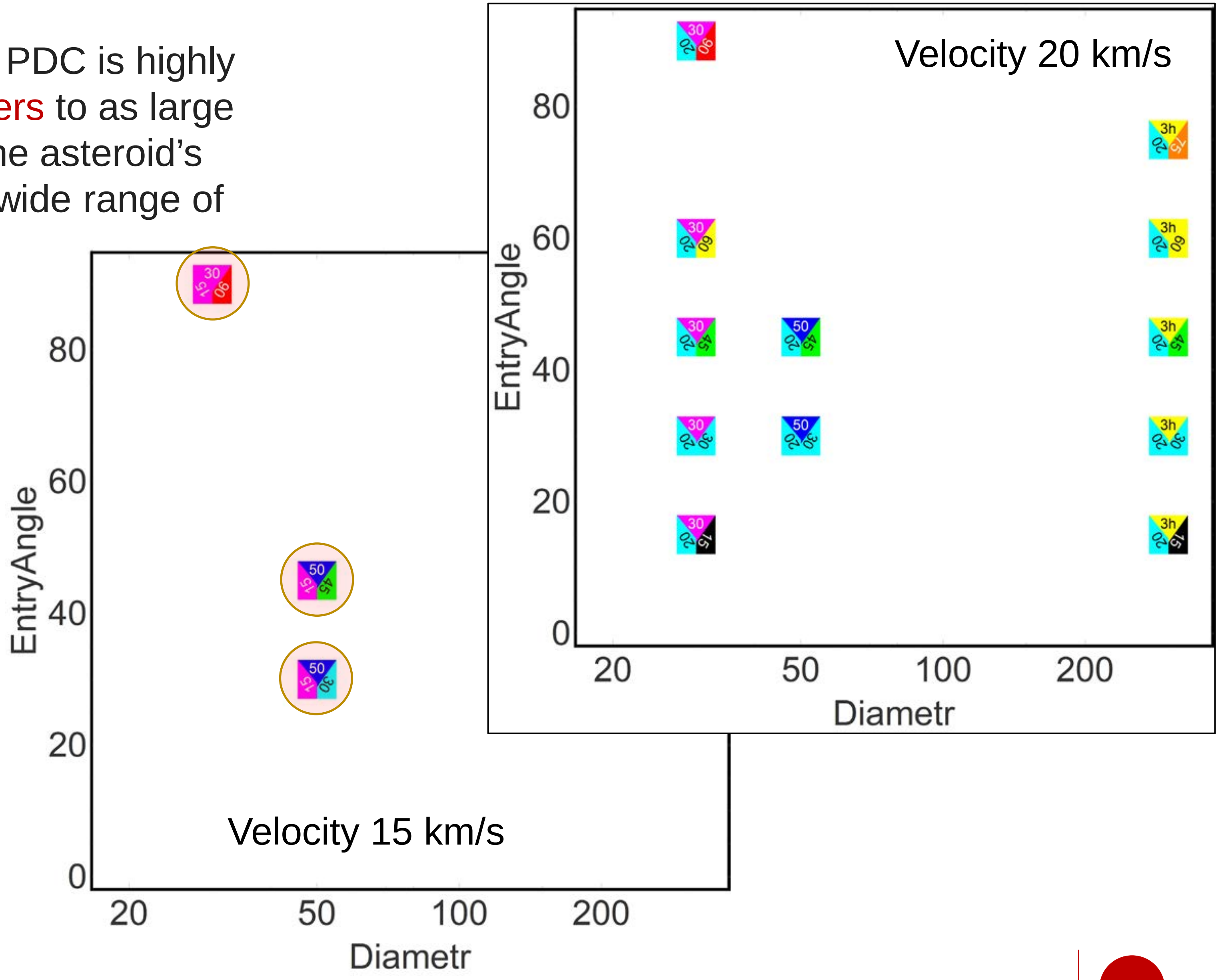

Scaling relation for different diameters

density: 3320 kg/m^3
diameter: various
fall angle: 60°
velocity: 15 km/s

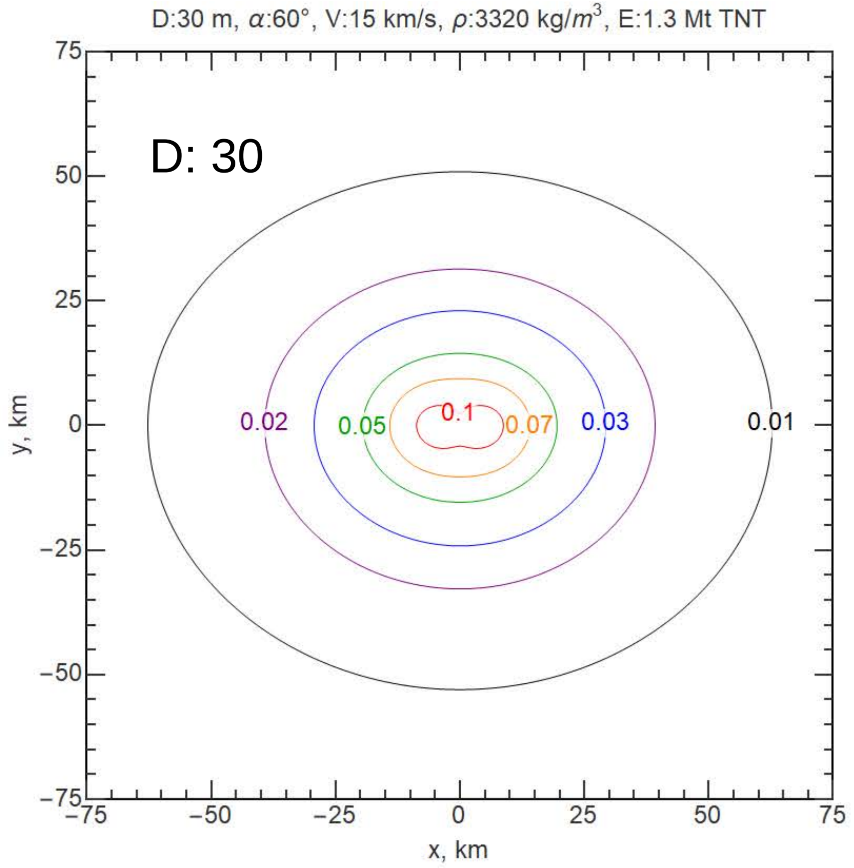

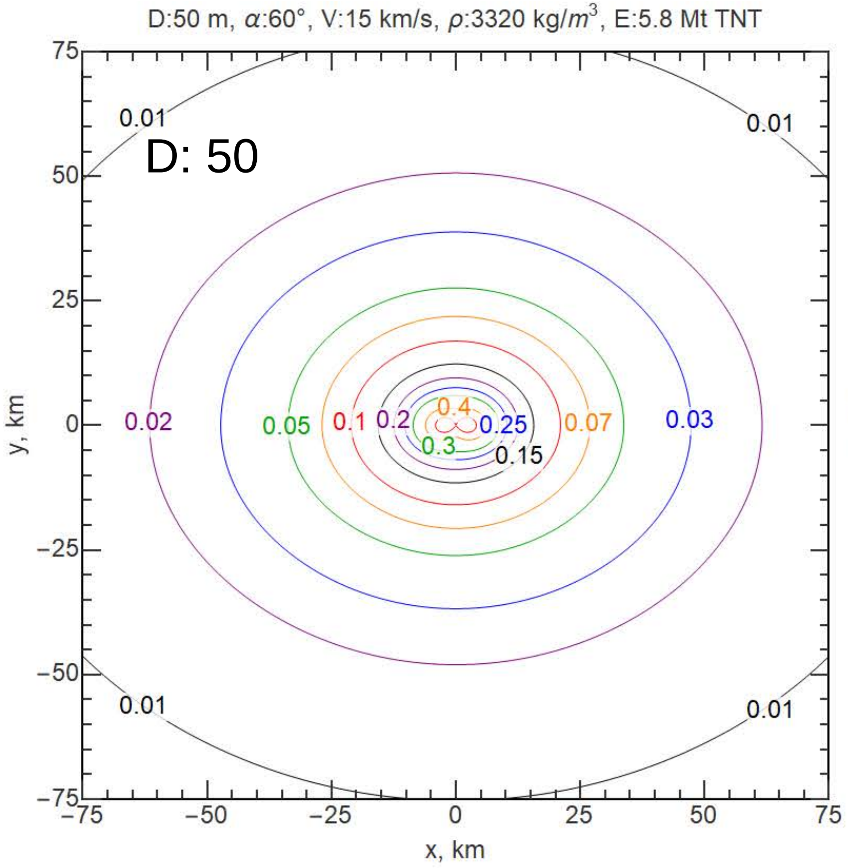

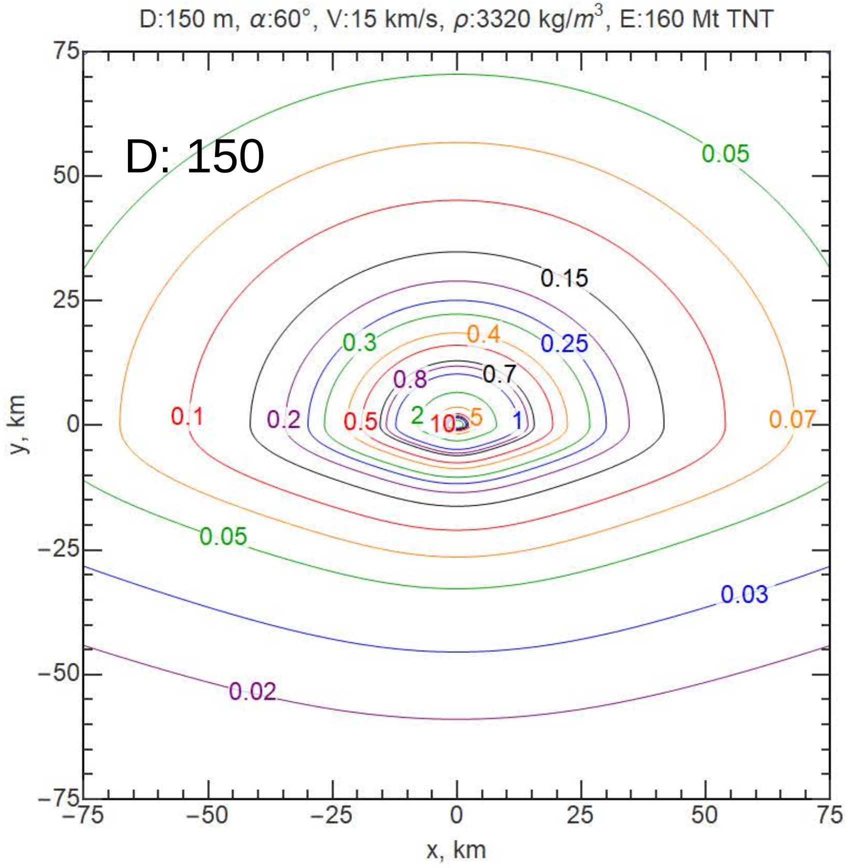

Scaling relation for different diameters

density: 3320 kg/m^3
diameter: various
fall angle: 60°
velocity: 15 km/s

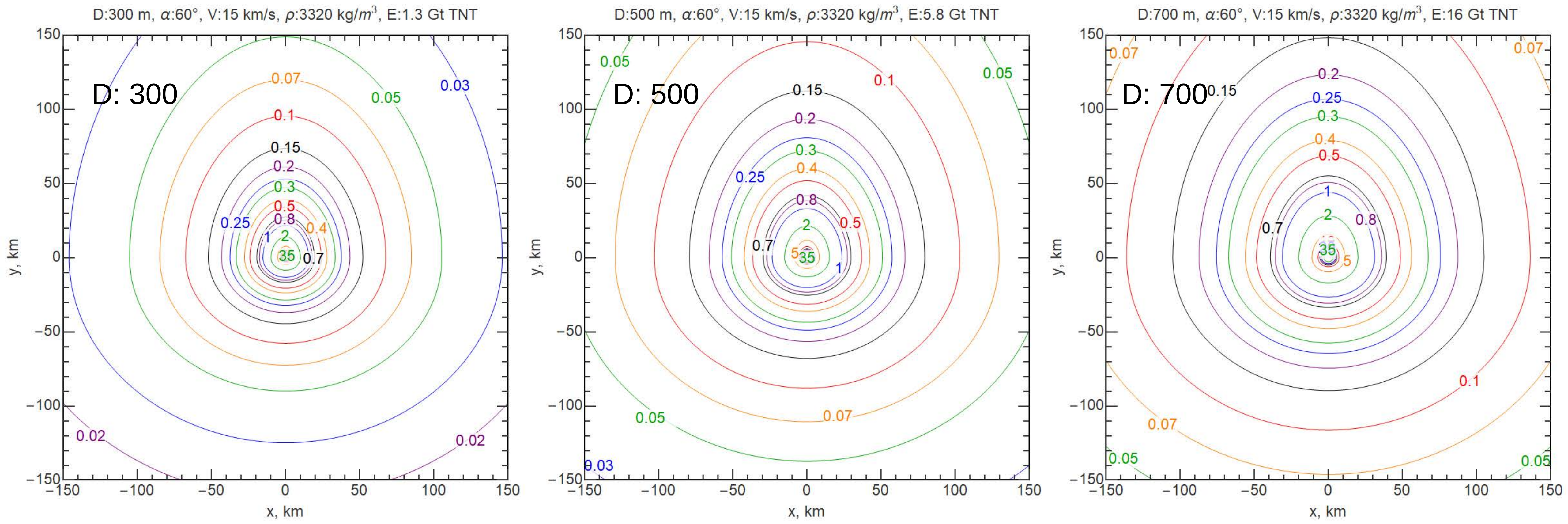

Scaling relation for different entry angles

density: 3320 kg/m^3
diameter: 300 m
fall angle: various
velocity: 15 km/s

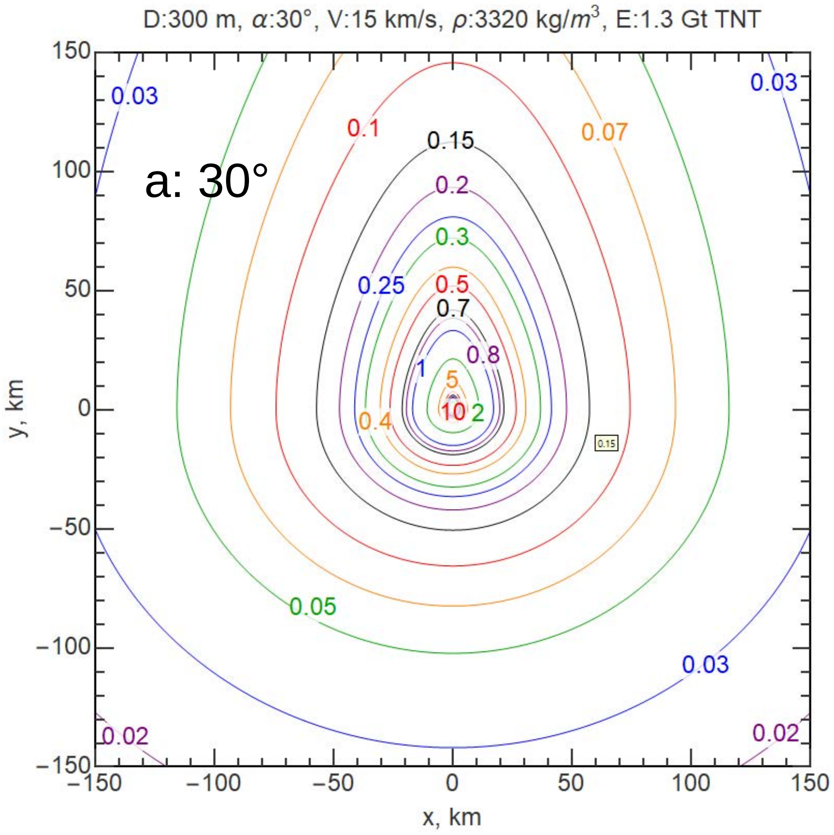

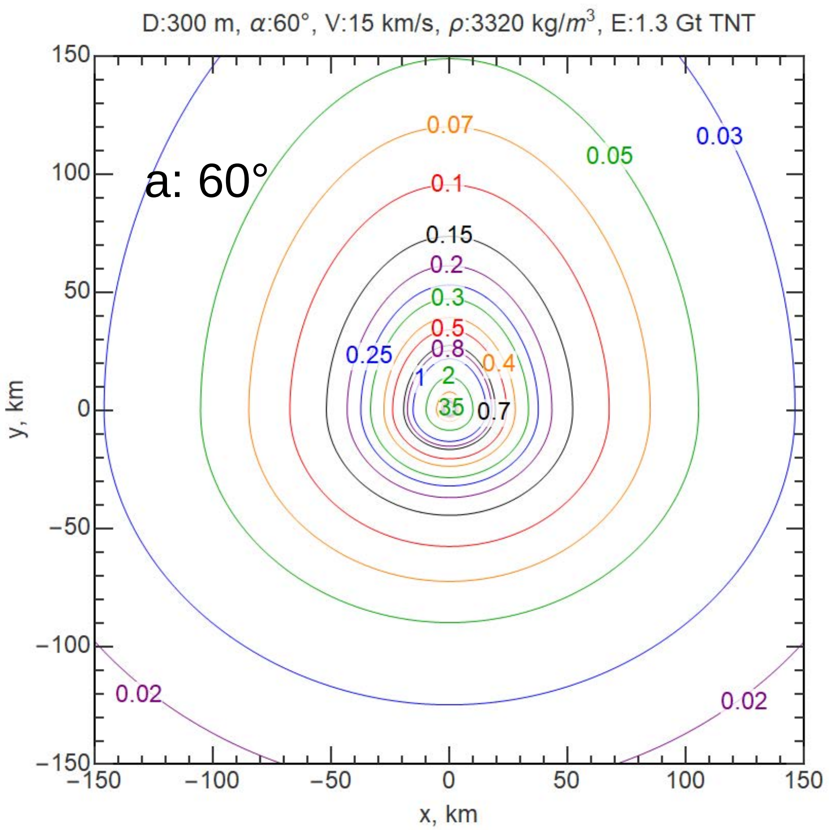

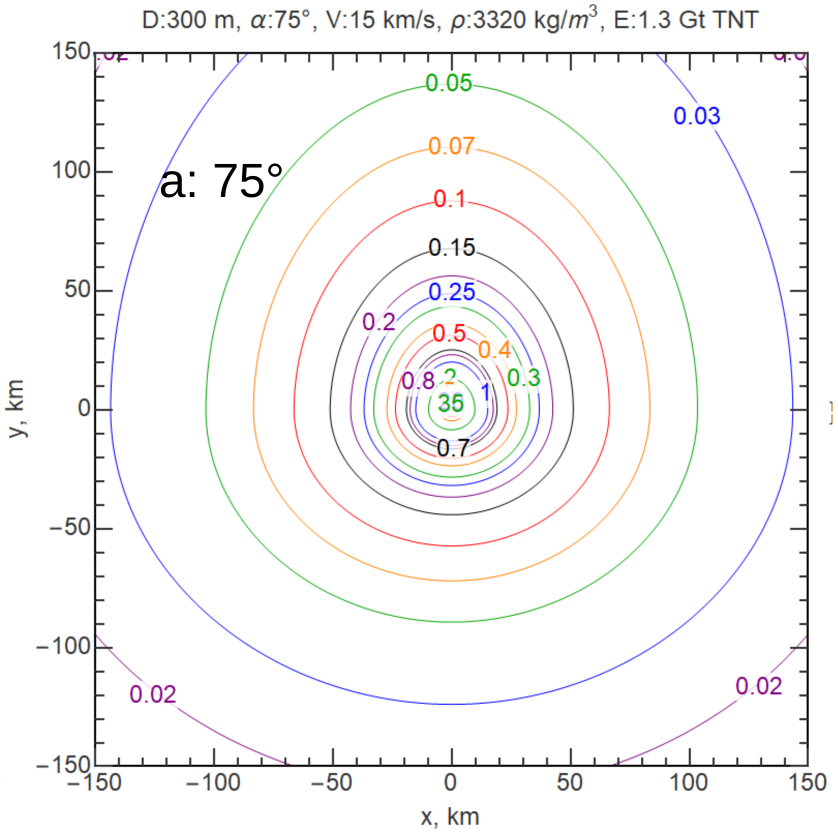

Tunguska and Chelyabinsk events

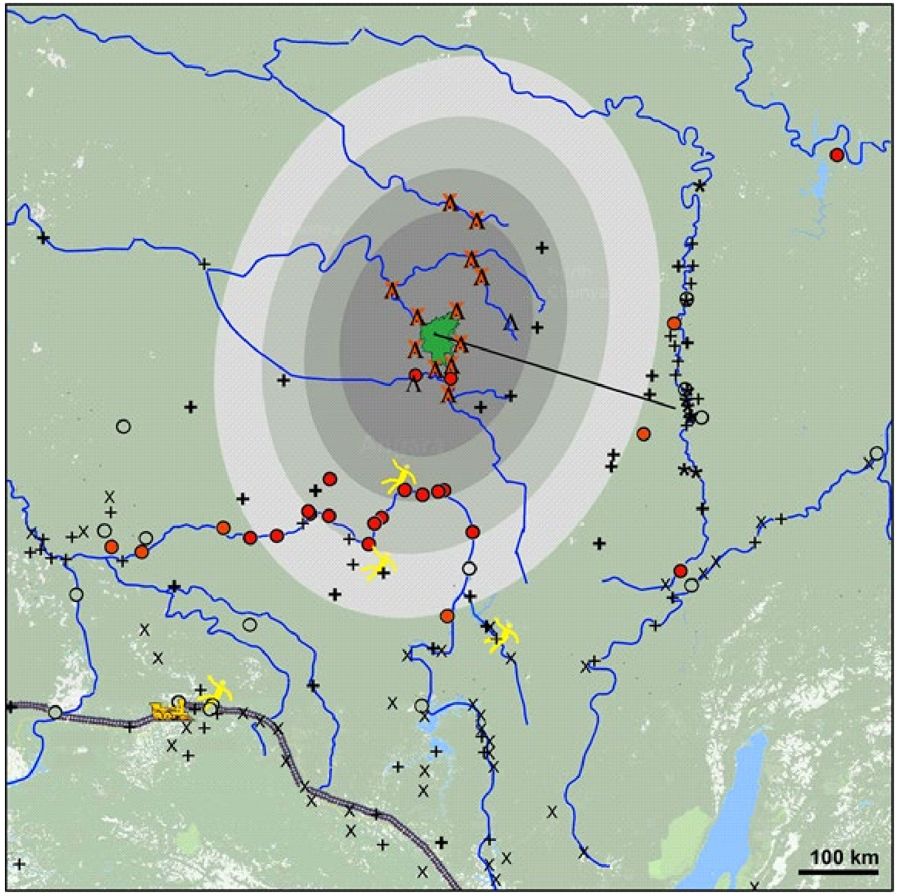

Location map of eyewitness reports. .
Glass damage (filled red circle); glass rattled, not broken (o); chum destruction (Λ); heat and unconsciousness (orange X); people falling (person symbol).
Gray areas - ΔP based on scaling relations (12 Mt, 2000 kg/m3, 25°, 27 km/s).
Contours (from dark to light): ΔP ~1500, 1000, 700 and 500 Pa
(Jenniskens et al. 2019)

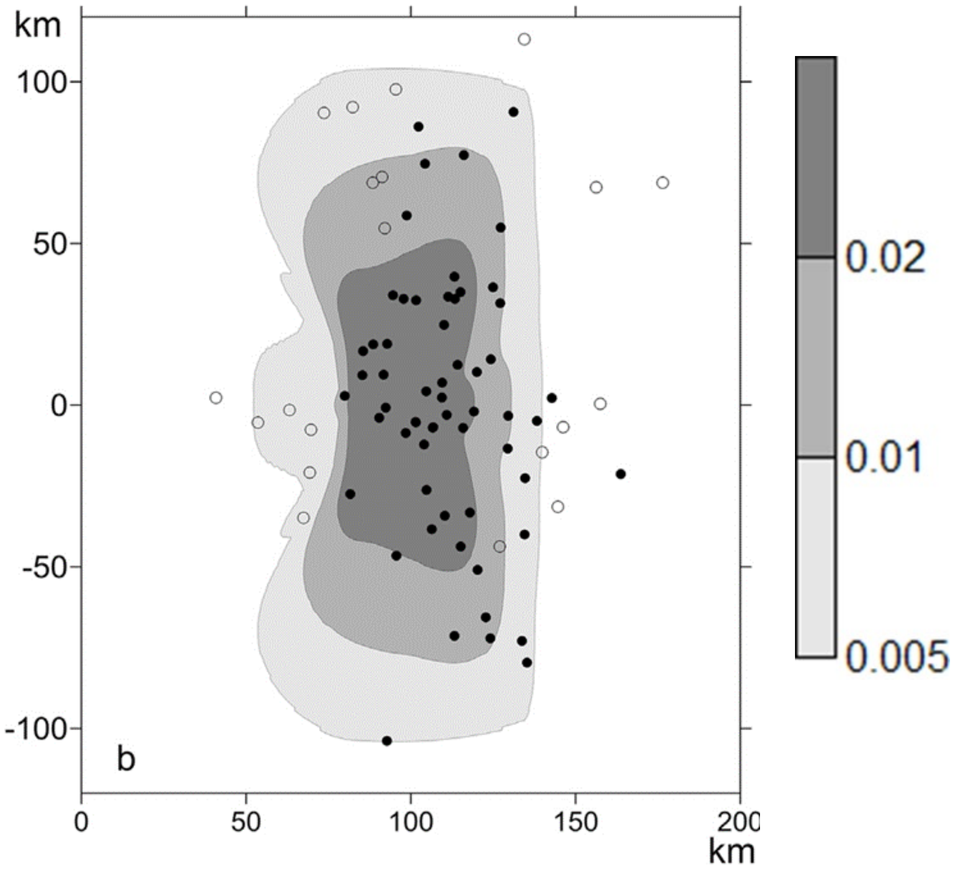

ΔP obtained in the frame of QL model *(Shuvalov et al.2017),*
black circles - reported damage, open circles – no damage.
Main characteristics of ΔP zones (>1 kPa) - satisfactory agreement
Scaling relations (not given) are also in agreement.

Impact Effects http://www.AsteroidHazard.pro Home Русский

Projectile Parameters

Diameter: *19 m*
Density: *3320 kg/m³*

Impact Parameters

Velocity: *19.2 km/s*
Entry Angle: *18.3 °*

Point of Effect

Distance to the point of intersection of the trajectory with the Earth's surface: *100.05 km*

BASIC ADVANCED

Projectile Parameters

Diameter, m
19
15 m 150 m

Density, kg/m³
3320
500 kg/m³ comet asteroid 3320 kg/m³

Impact Parameters

Velocity, km/s
19.2
10 km/s 72 km/s

Entry Angle, °
18.3
15 ° 90 °

Point of Effect

Distance to the point of intersection of the trajectory with the Earth's surface, km
100.05
0 km 500 km

Angle to Trajectory Projection, °
89.95
0 ° 360 °

RUN CALCULATIONS

Projectile Parameters

Diameter: *19 m*
Density: *3320 kg/m^3*
Energy: *2.19 * 10^{15} J*
Energy (kt TNT): *5.23 * 10^2 kt TNT*

Entry Parameters

Velocity: *19.16 km/s*
Entry Angle: *18°*
Latitude: *54.45°*
Longitude: *64.56°*
Azimuth: *103°*

Observation Point

Zero Point: *The point of intersection of the trajectory with the Earth's surface*
Angle to Trajectory Projection, ψ: *92°*
Distance to the Zero Point, L: *107 km*
Distance Across the Trajectory Projection, L_y: *107 km*
Distance Along the Trajectory Projection, L_x: *3 km*
Latitude, ϕ: *54.04°*
Longitude, λ: *59.62°*

ALTER PARAMETERS

RESULTS

Airblast Wave	Overpressure: 0.0016 atm (0.16 kPa)	more...
Irradiation	Thermal exposure: 0.14 J/cm^2	more...
Crater	No crater	more...
Ejecta	No ejecta	more...
Seismic effect	Magnitude: 3.4	more...
Atmospheric disturbances	Peak amplitude of relative density oscillations at an altitude of 300 km: 0.52	more...

Projectile Parameters
Diameter: *30 m*
Density: *3320 kg/m^3*
Energy: *5.28 * 10^{15} J*
Energy (kt TNT): *1.26 * 10^3 kt TNT*

Entry Parameters
Velocity: *15.00 km/s*
Entry Angle: *60°*
Latitude: *54.45°*
Longitude: *64.56°*
Azimuth: *103°*

Observation Point
Zero Point: *The point of intersection of the trajectory with the Earth's surface*
Angle to Trajectory Projection, ψ: *180°*
Distance to the Zero Point, L: *50 km*
Distance Across the Trajectory Projection, L_y: *0 km*
Distance Along the Trajectory Projection, L_x: *-50 km*
Latitude, ϕ: *54.46°*
Longitude, λ: *64.45°*

ALTER PARAMETERS

RESULTS

Airblast Wave
Overpressure: 0.013 atm (1.3 kPa) ...less

Numerical simulations of a shock wave from the cosmic object impact provide possibility to suggest scaling relations for a value of maximal overpressure and its distribution on the surface, for maximal wind velocity behind the front and for a squares, where overpressure is larger than a fixed levelall values are determined based only on the properties of the impactor

Effective Altitude: 12 km
Maximal overpressure: 0.12 atm (12 kPa)
Distance to the center of a overpressure field from the point of intersection of the trajectory with the Earth`s surface: 5.6 km
Areas, at which chosen levels of overpressure exceed:
- at 0.02 atm: 0.42 km^2
- at 0.05 atm: 0.07 km^2
- at 0.1 atm: 0.04 km^2
- at 0.2 atm: 0.04 km^2

The value of the overpressure in the point of observation: 0.013 atm (1.3 kPa)
Maximum wind speed behind the shock front in the point of observation: 3 m/s

Irradiation
Thermal exposure: 1.0 J/cm^2 more...

API (application programming interface)

HTTP post request

```
retrievedF[d_] := Import[URLRead[HTTPRequest["http://asteroidhazard.pro/en/api", <|"Method" → "POST", "ContentType" → "application/json" , "Body" → ExportString[
        <|
         "effects" → {"shockwave"},
         "impactor" → <|"diameter" → d, "density" → 3320|>,
         "entry" → <|"angle" → 18.3, "velocity" → 19|>,
         "point_of_effect" → <|
           "distance_across_trajectory" → 20,
            "distance_along_trajectory" → 5|>
         |>
        , "RawJSON", "Compact" → True] |>]],
    "RawJSON"]["shockwave"]["overpressure"]["value"];

In[•]:= data = Table[{d, retrievedF[d]}, {d, 20, 200, 5}];
```

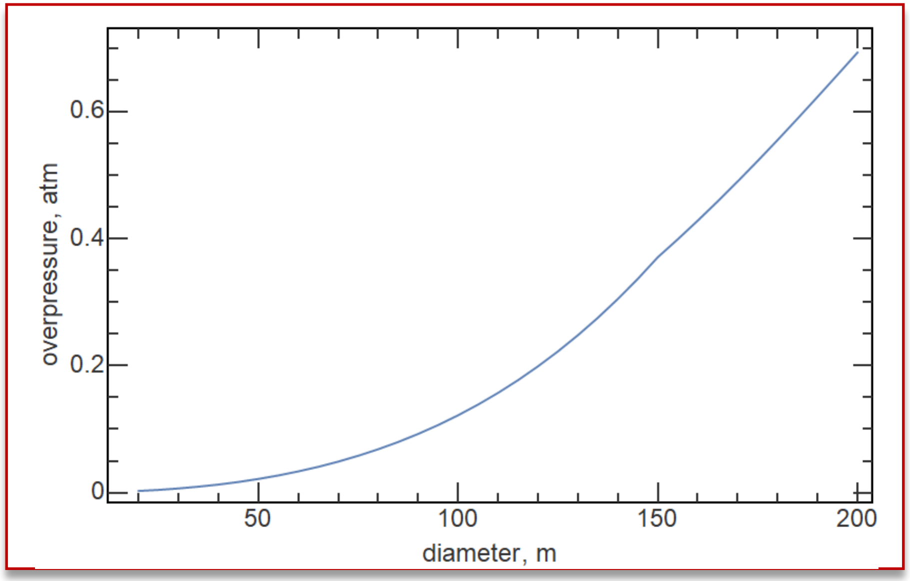

Summary

- The scaling relations for shock wave effects for 20 – 3000 m objects impact are presented. Scaling relations for overpressure, wind and some other characteristics are constructed.

- For the first time this scaling relations take into account spatial asymmetry induced by impact angle.

- Suggested scaling relations were compared with modelling results and existing observational data and demonstrated reasonable agreement

- Described scaling relations are implemented into web-based calculator

- PDC probable impactor parameters are very uncertain and its impact may result in consequences of different scale.

Thank you for attention

follow the updates on the site
AsteroidHazard.pro

ФГБУН
ИДГ РАН
Институт динамики геосфер РАН
Intra et Extra

Olga Popova
Vladimir Svetsov
Valery Shuvalov
Dmitry Glazachev
Elena Podobnaya
Valery Khazins
Natalia Artemieva

IAA PLANETARY DEFENSE CONFERENCE 2021
26-30 APRIL 2021

TYPE OF IMPACT

Asteroids and cometary objects from 20 m to 3 km in diameter were considered

Entry angles - from 15° to 90°;
Entry velocity - from 15 to 70 km/s

Total 122 cases:
56 airbursts, 66 crater-forming (including transitional)

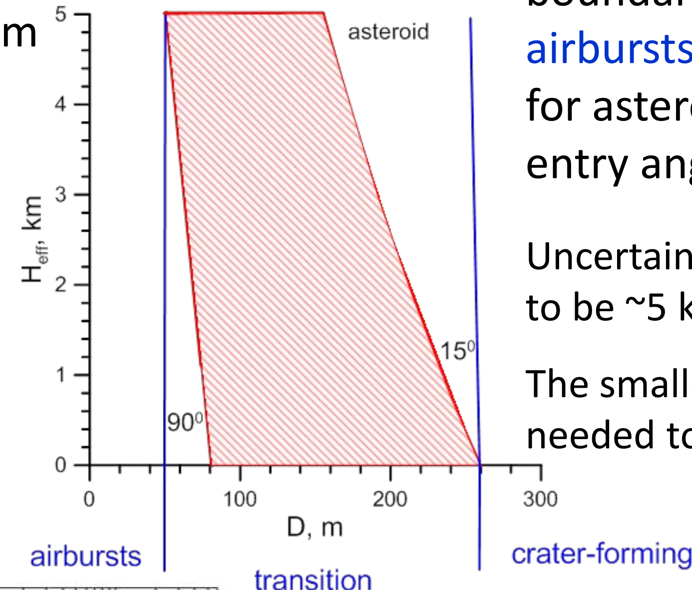

boundaries
airbursts - crater-formings
for asteroids with uncertain entry angle ~15-90^0

Uncertainty in Heff is assumed to be ~5 km

The smaller α the larger D is needed to create a crater

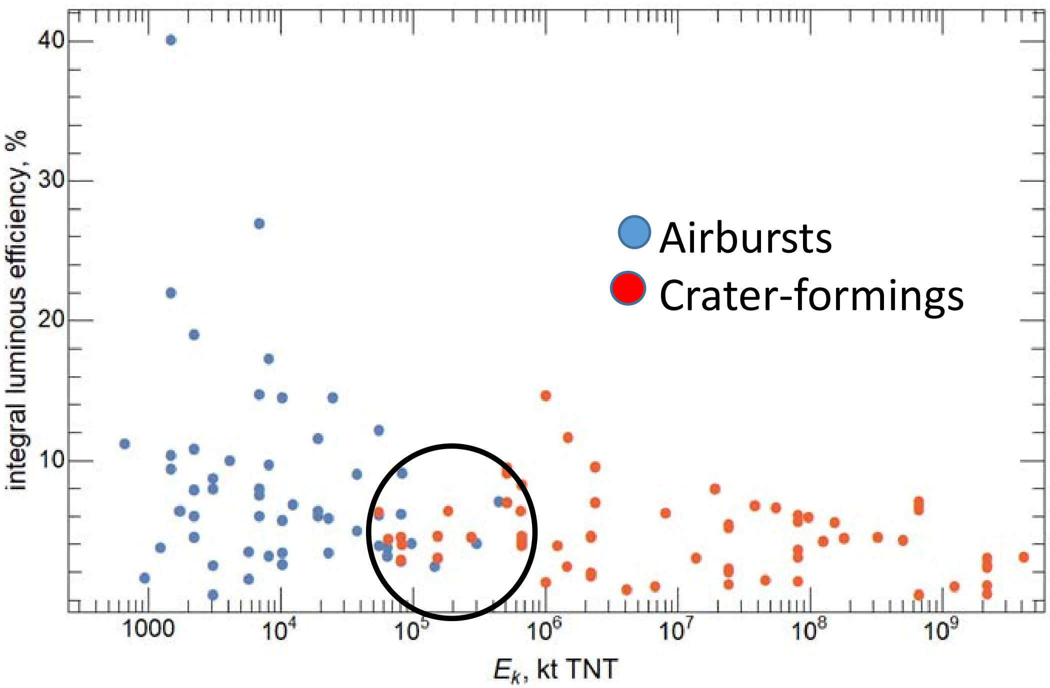

Transition sizes for asteroids:
~60 – 250 m
based on Heff ~ f(α)

Kinetic energy range
~3 10^4 – 5 10^5 kt TNT
based on serial simulations

2021 PDC probable impactor: asteroid, V~15 km/s D~35 - 700 m, α~3-90^0

Can be both an airbust and crater-forming

RADIATION FLUXES AND THERMAL EXPOSURE ON THE GROUND

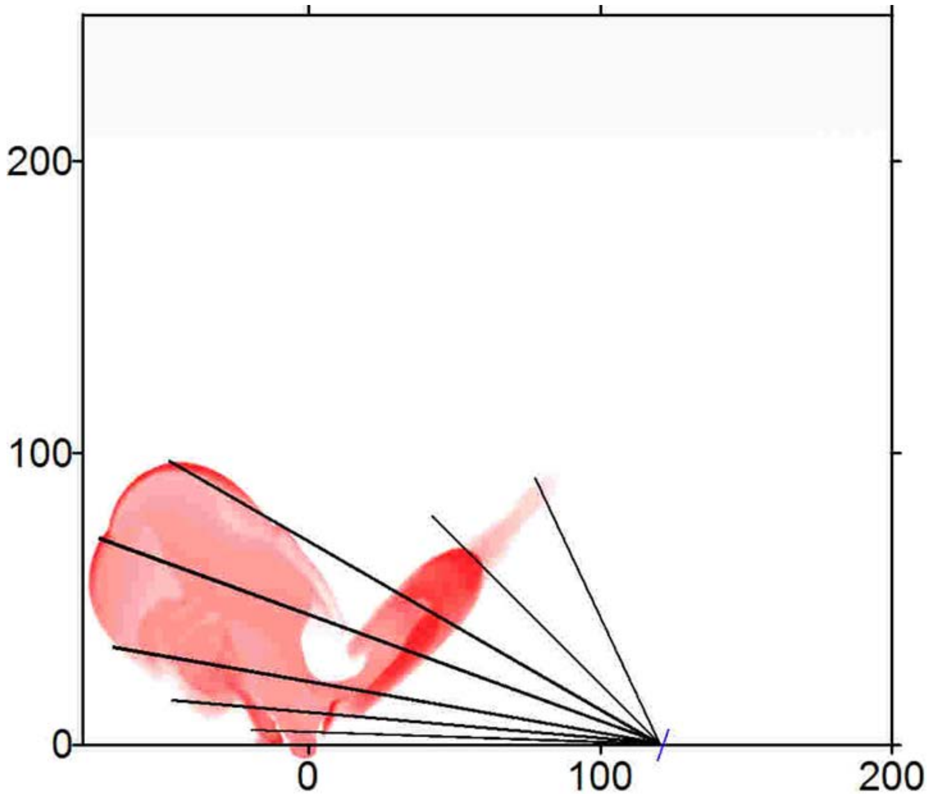

The equation of radiative transfer

$$\frac{dI_\varepsilon}{ds} + k_\varepsilon I_\varepsilon = k_\varepsilon B_\varepsilon$$

is solved along rays crossing the heated volume of air and vapor.

The total radiation intensity on the surface for a given angle of a ray is obtained by summing the intensities of radiation over photon energies.

Radiative flux density in a given point on the Earth's surface is calculated by integrating the radiation intensity, multiplied by the cosine of the angle between the ray and the normal to the irradiated surface, over all angles.

The integration of the flux over time allows us to determine radiant exposure (radiation energy received by a surface per unit area).

Thermal radiation – one of the main dangerous consequences of cosmic object impacts.

Direct thermal radiation from fireballs and impact plumes poses a great danger to people, animals, plants, and economic objects.

THERMAL EXPOSURE ON THE GROUND

Airburst - bolide radiation

50 m, asteroid, 20 km/s, 45^0, *Svetsov&Shuvalov 2018*

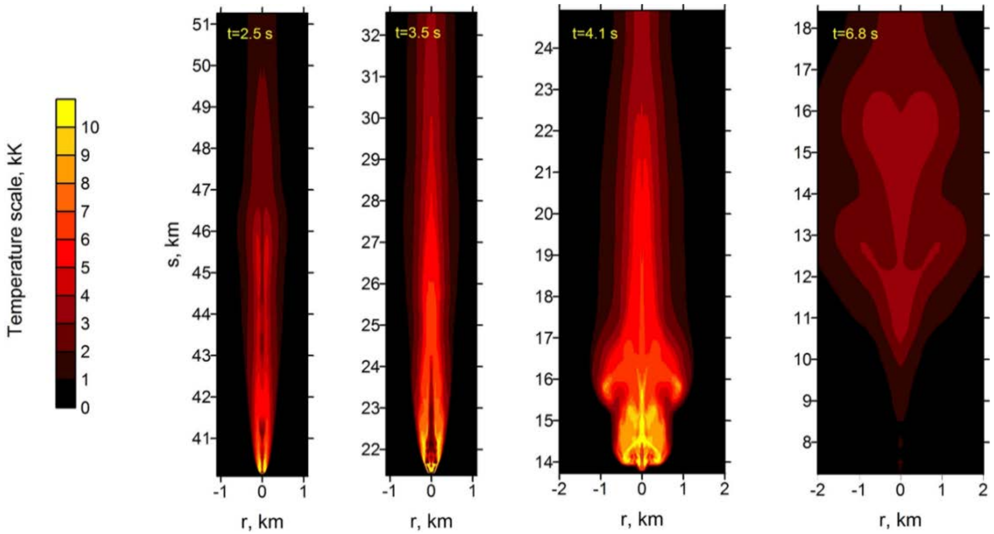

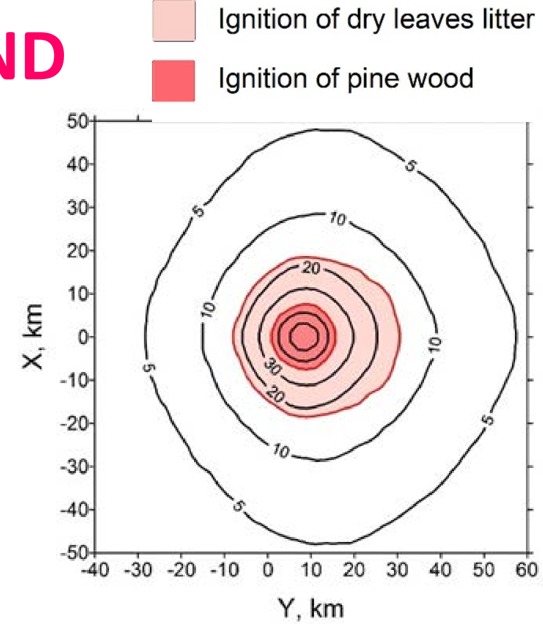

Thermal exposure, J/cm^2

Crater-forming - plume radiation

1 km, asteroid, 20 km/s, 45^0

Svetsov&Shuvalov 2018

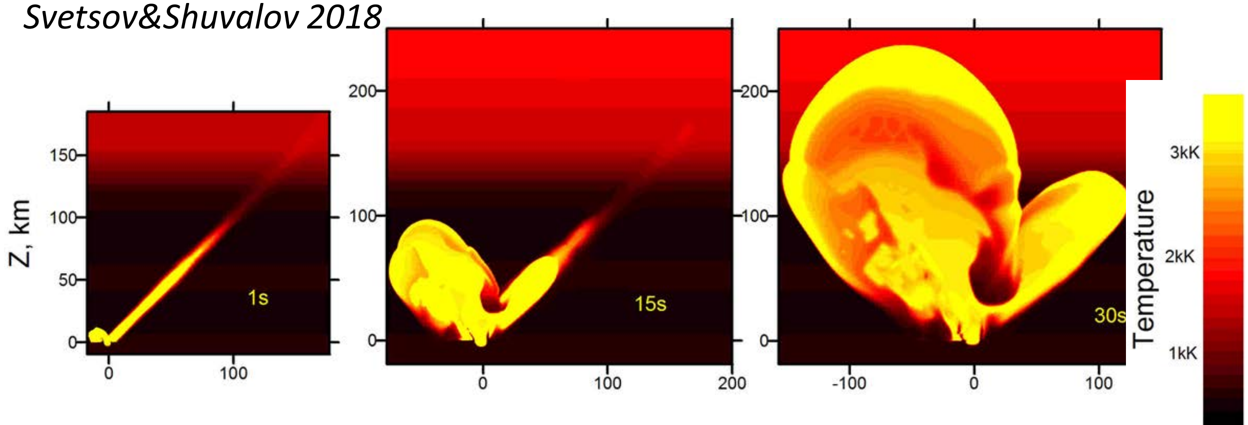

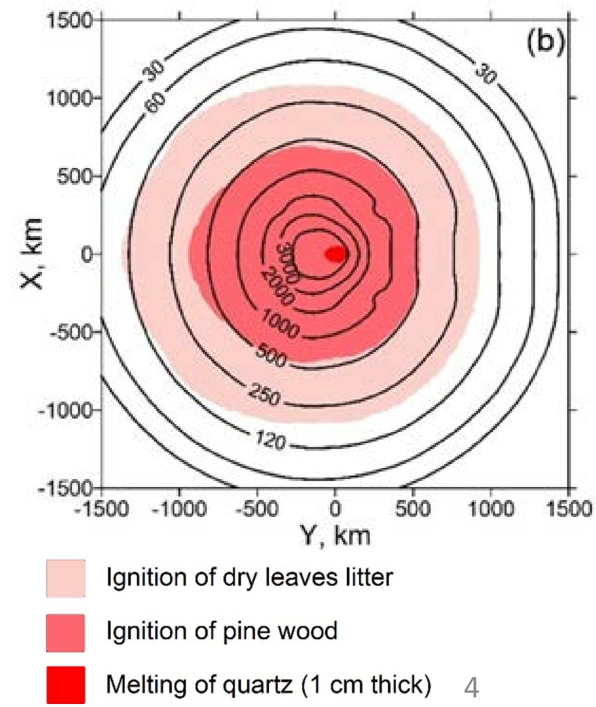

In dependence on impact scenario the thermal radiation is produced by fireball or/and impact plumes.

SCALING RELATION FOR THERMAL EXPOSURE

Analyzes of serial simulations permit to suggest **scaling relations (SC)**,
- allow us to estimate radiation field on the surface based only on impactor properties (D,V,α, ρ)

To describe the thermal exposure Q [J/cm^2] the point source approximation, corrected on spatial heterogeneity is suggested:

$$Q = 4.184 \cdot 10^{12} \cdot \frac{1}{4\pi} \cdot \frac{\eta}{100} \cdot \frac{E_{kt}}{10^{10}\left(H_{rad}^2 + x^2 + el \cdot y^2\right)}$$

x,y – spatial coordinates (km) (point of origin is under point of maximal thermal effect) ,
H_{rad}- radiative altitude (km), el - ellipticity parameter, E_{kt} – kinetic energy of impactor in kt TNT
η – integral luminous efficiency in %

The thermal exposure value of 10 J/cm^2 roughly corresponds to the first degree burn.
The value of about 500 J/cm^2 essentially exceeds the amount needed to ignite most materials
(Glasstone&Dolan 1977)

Scaling relation (SC) for Q was aimed to be applicable in the range 10-500 J/cm^2

INTEGRAL LUMINOUS EFFICIENCY

η – the fraction of the impactor kinetic energy, which is converted into the radiation

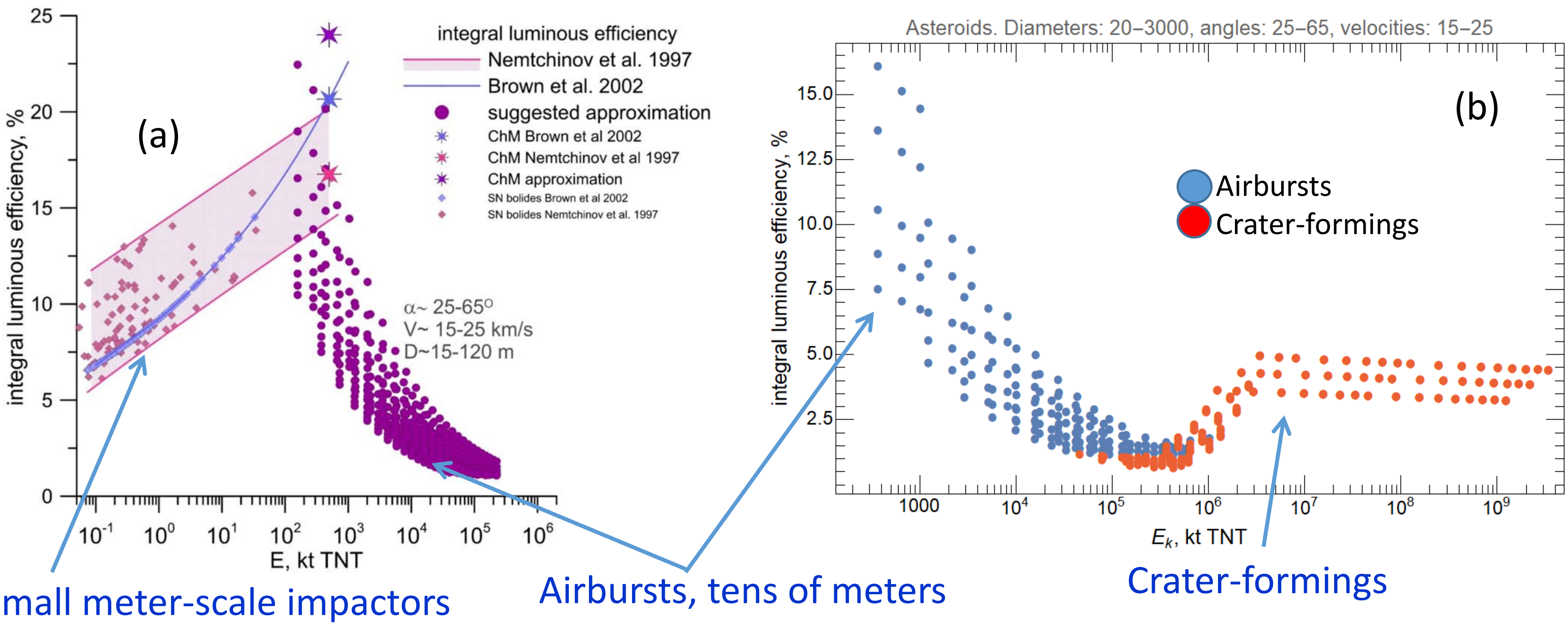

η for asteroids of different sizes entering at α~25-65° with V~15-25 km/s obtained based on SC
(a) is compared with η for meter-scale meteoroids (b); is extended to larger energies

(a) η is increasing with size up to ~20% at E~500 -1000 kt and is decreasing for large objects. This decrease is probably connected with an increase of the optical thickness of the emitting region, which leads to radiation losses mainly from its surface.
(b) Minimal efficiency is obtained for transition between airbusts-crater-formings, probably connected with change of the main input from bolide to the rarefied plume. Need to be clarified further.

SCALING RELATION FOR INTEGRAL LUMINOUS EFFICIENCY

η – the fraction of the impactor kinetic energy, which is converted into the radiation

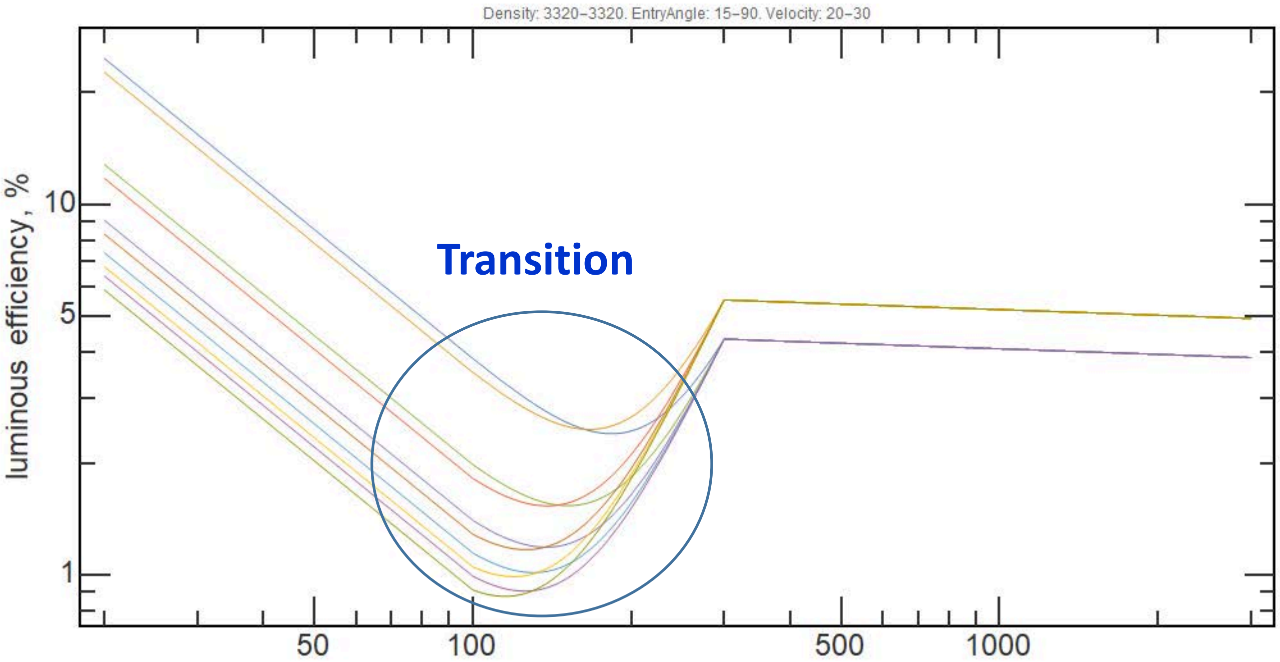

Integral luminous efficiency for asteroids V~20-30 km/s α~15-90^0 based on SC

Crater-formings:

$$\eta_{crater} = \frac{0.021 \cdot D^{1.3} \cdot v^{1.5}}{E_{kt}^{0.45}}$$

Airbusts:

$$\eta_{airbust} = \begin{cases} 100 \cdot \frac{10939 \cdot v^{0.56}}{E_{kt} \cdot Sin\alpha}, \rho = 3320\ kg/m^3 \\ 100 \cdot \frac{1225 \cdot v^{0.39}}{E_{kt}^{0.3} \cdot Sin\alpha}, \rho = 1000\ kg/m^3 \end{cases}$$

for any other density of the impactor - line interpolation by density is working well

Transition : conventional division by impactor diameter, if D ≤ 100-150 m AB values are used, if D ≥ 300 m CF values are applied, inbetween the linear interpolation by E_{kt} is used

Real dependence of η on V, α etc is quite complicated, but nevertheless suggested SC provides satisfactory agreement with modeling results with precision about 2 times.

RADIATIVE ALTITUDE AND TIME

$$H_{rad} = \begin{cases} 3.85 + 1.05 * H_{eff}, density = 3320\ kg/m^3 \\ 4.09 + 0.95 * H_{eff}, density = 1000\ kg/m^3 \end{cases}$$

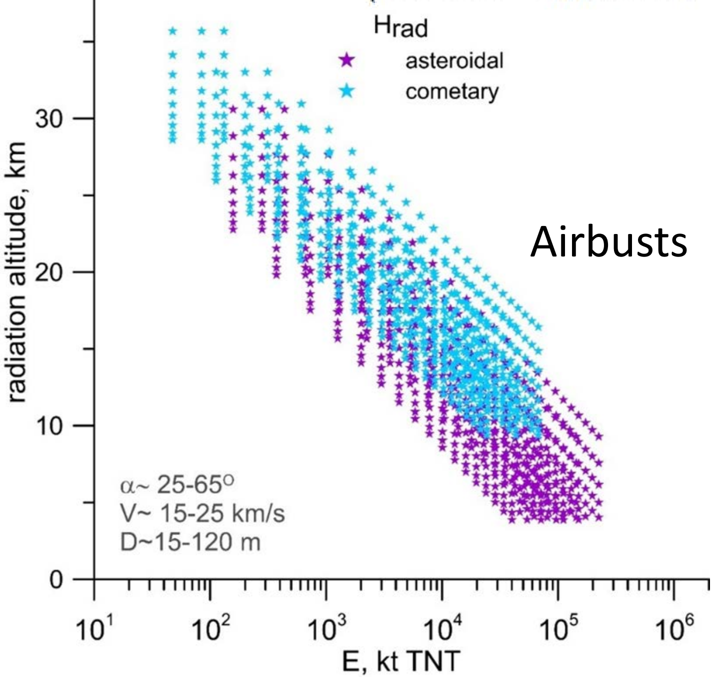

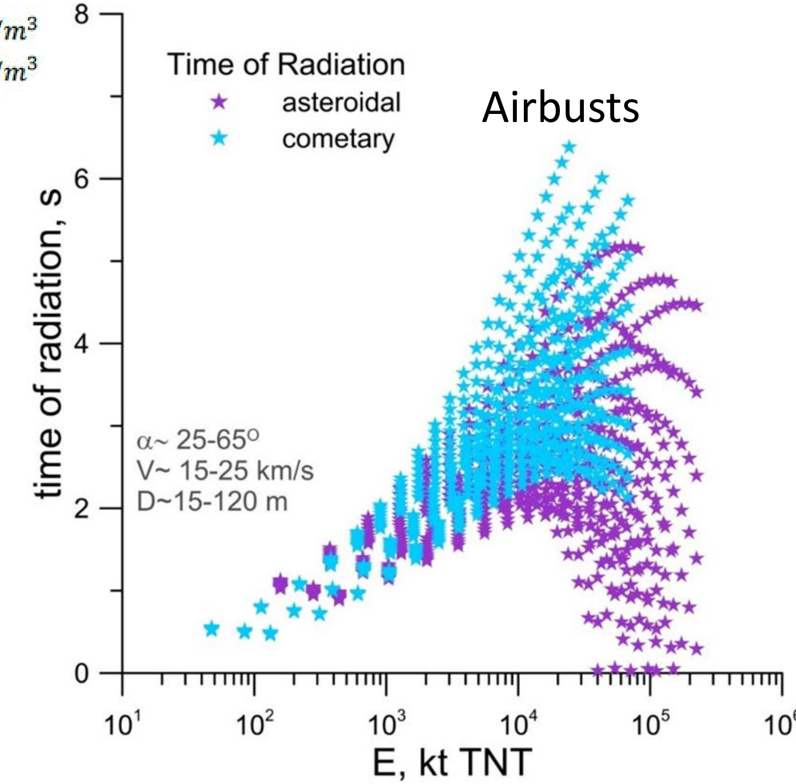

(a) H_{rad} in dependence on E_{kt} based on SC (b) The characteristic time of radiation (80% of total thermal exposure is irradiated)

Airbursts radiation can be represented as radiation of the source at H_{rad} (from 20–30 to several km) with spatial heterogeneity and duration ~1-4 s.

H_{rad} >H_{eff} and maximal thermal effect is shifted relatively the overpressure maximum.

H_{rad} for **crater-formings** is an adjustable parameter, is not the effective source height, affects Q only in the central zone, where Q has a complex structure (due to the complex nature of the flow, propagation, interaction and mixing of emissions from the crater with the atmosphere).

H_{rad} is fixed as 100 km for large impacts.

AIRBURST THERMAL EXPOSURE BASED ON SC

comet, D=30 m, $\alpha=45^0$, V=20 km/s

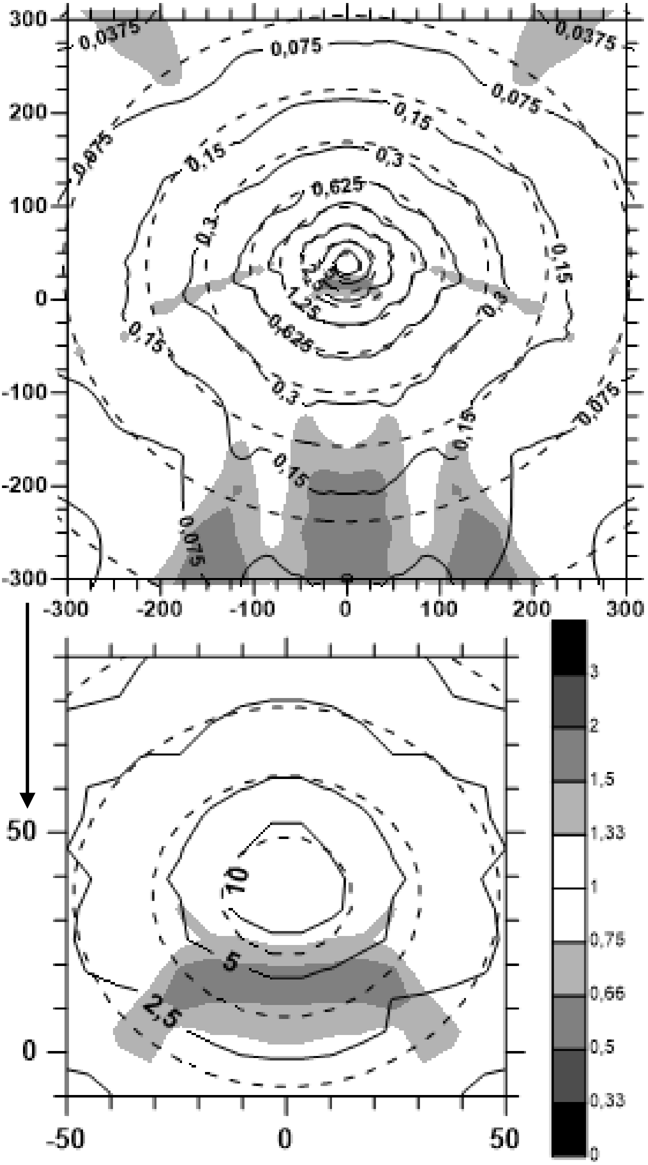

Ellipticity ***el*** allows to take into account the spatial inhomogeneity of the radiation field; ***el***=f(E_{kt}, α, H_{eff}).

Ingomogenity is more evident forward along the trajectory (after the epicenter)

Q (values are shown on contours, J/cm^2) obtained in the numerical simulations – solid lines.
Dashed – Q based on SC, Q_sc
Gray - the ratio of Q_sc/Q
Bottom panel - central part on a larger scale.

Suggested scaling relations allow us to estimate thermal exposure and radiative flux distributions based on the impactor parameters with uncertainty of about two times.

Trajectory is top – bottom
Axes origin – trajectory intersection with ground (no deceleration)

TUNGUSKA THERMAL RADIATION

Data to fit – area of burn trees, visible charring - at 40 J/cm^2 (Svetsov 1996)
Impactor parameters uncertain, numerical simulations results : **50 m, 20 km/s, 3300 kg/cm^3**

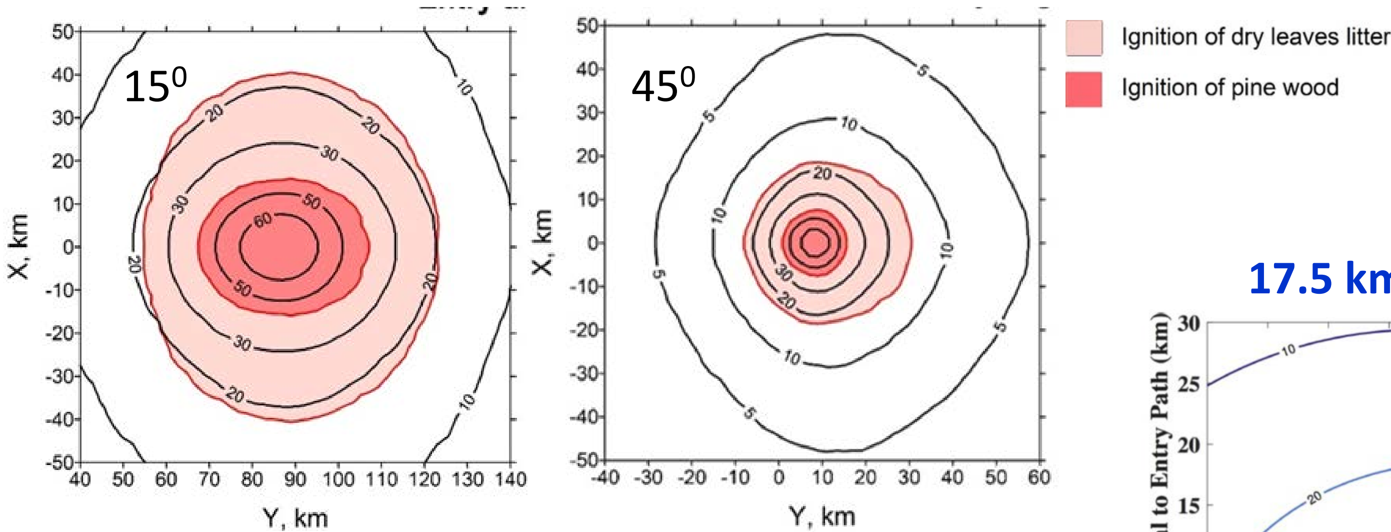

Model by Johnston&Stern 2019
Carbonaceous chondrite 3000 kg/m^3
D~50-400 m, V~6-18 km/s, H~10-30 km,
pancake fragmentation model

17.5 km/s, 72 m, 30°

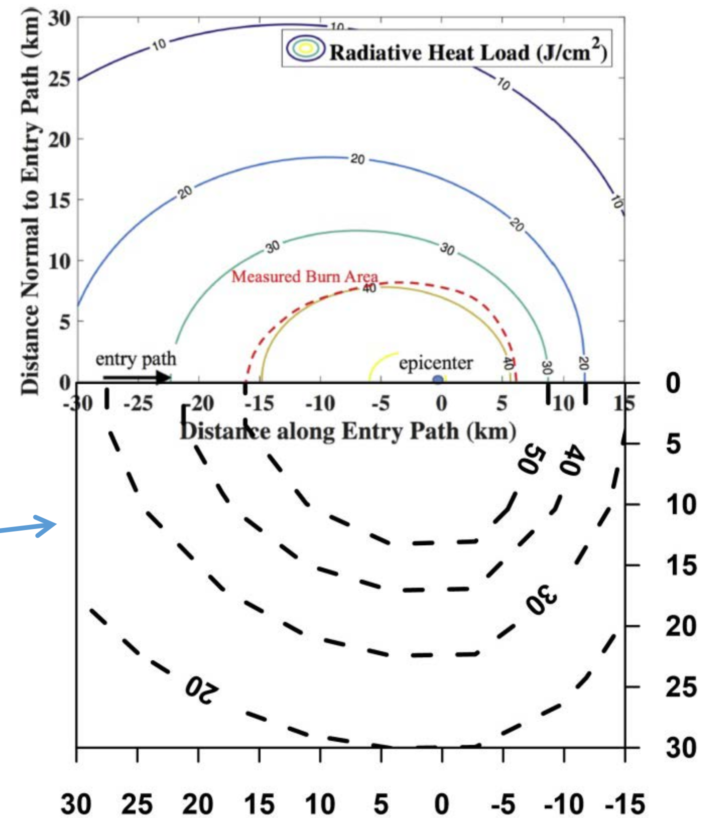

20 km/s, 68 m, 15°

Scaling relation distribution Q_sc example

Despite a range of impactor parameters allows to describe burn area,
different model results are quit close,
our modeling suggested more oblique impact.

THERMAL EXPOSURE BASED ON SC FOR CRATER-FORMINGS

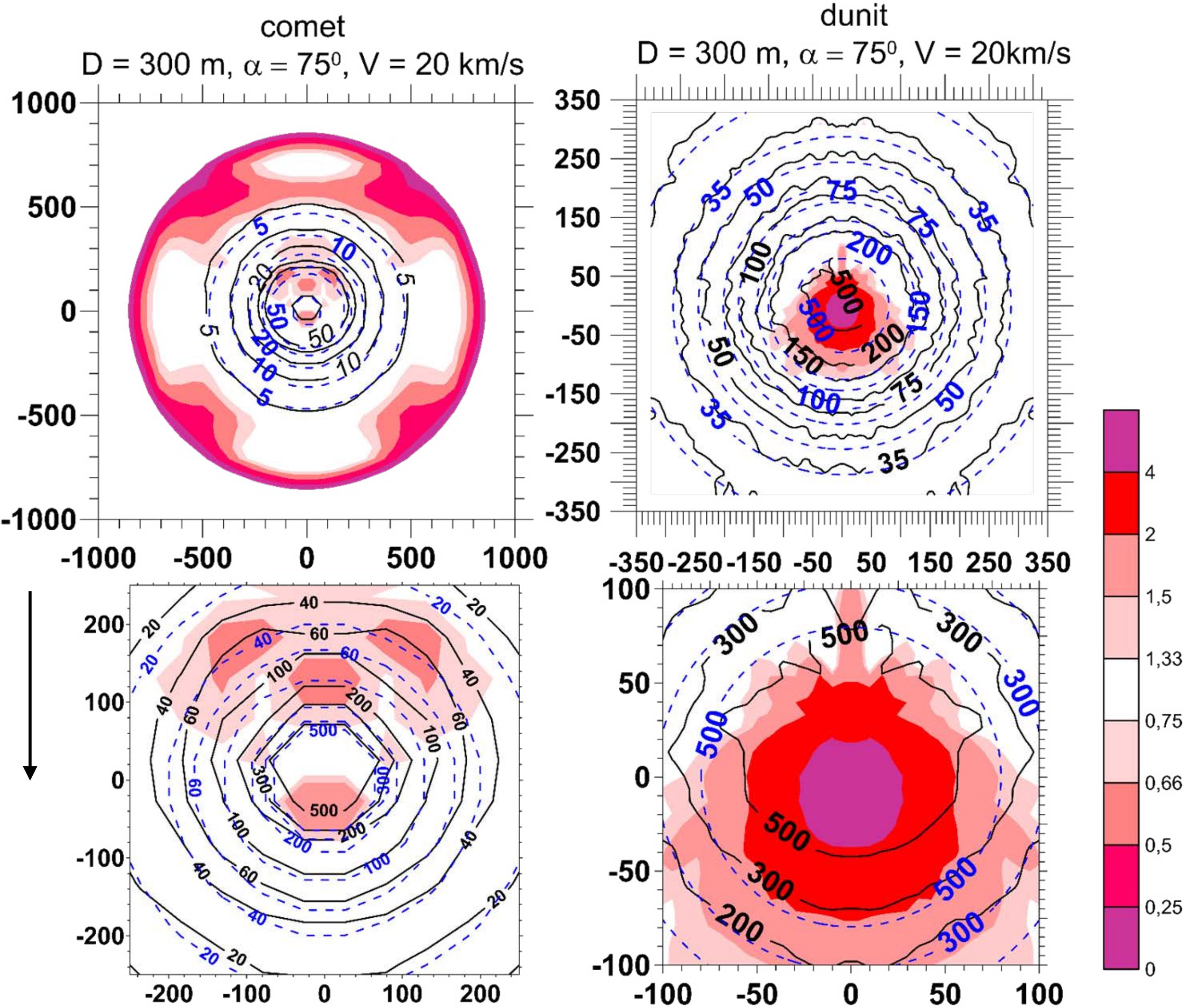

Spatial heterogeneity is excluded from Q_sc (no ellipticity)

Additional multiplier is included – to limit Q at the outer areas.

In most cases an uncertainty in estimates based on this scaling relation does not exceed 4 times in the range Q~ 10-500 J/cm^2.

Thermal exposure Q obtained in the numerical simulations - solid contours with black labels and Q_sc based on scalings (dashed contours with blue labels [J/cm2]
Bottom panels - central part on a larger scale. Color - the ratio of Q_sc/Q
Trajectory is top -bottom

PDC 2021 PROBABLE IMPACTOR RADIATION

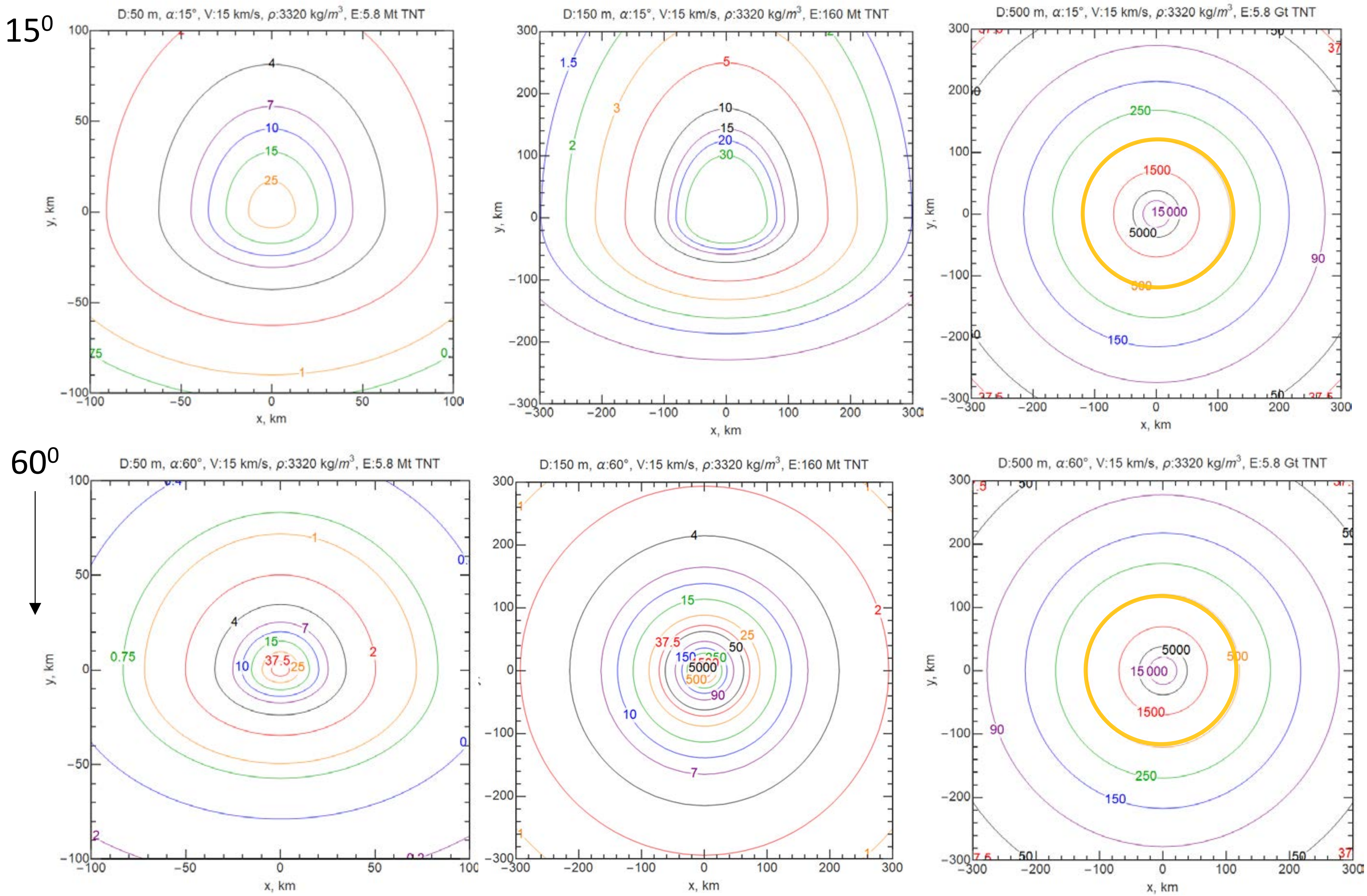

As expected the radiatively damaged area is dependent on entry angle and size

IONOSPHERIC DISTURBANCES

Impact -> plume formation -> its deceleration/oscillation at H>100 km -> energy is transformed into heat -> heated region expands laterally -> disturbances spread over thousands of km

Initial plume formation

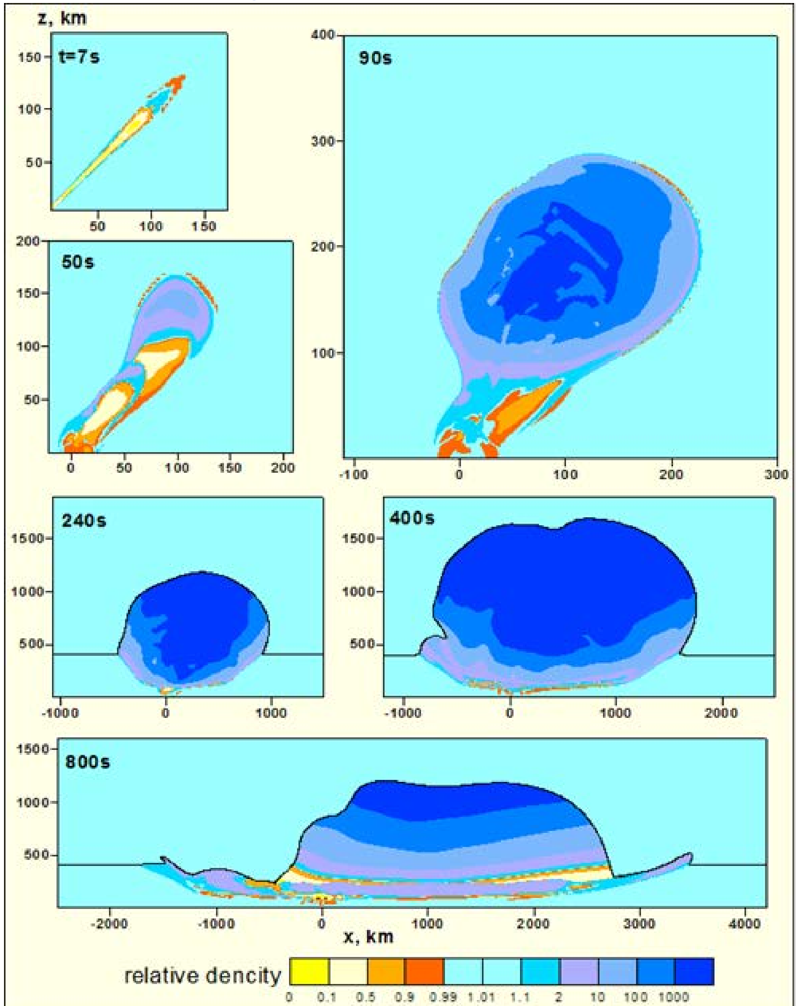

Further evolution

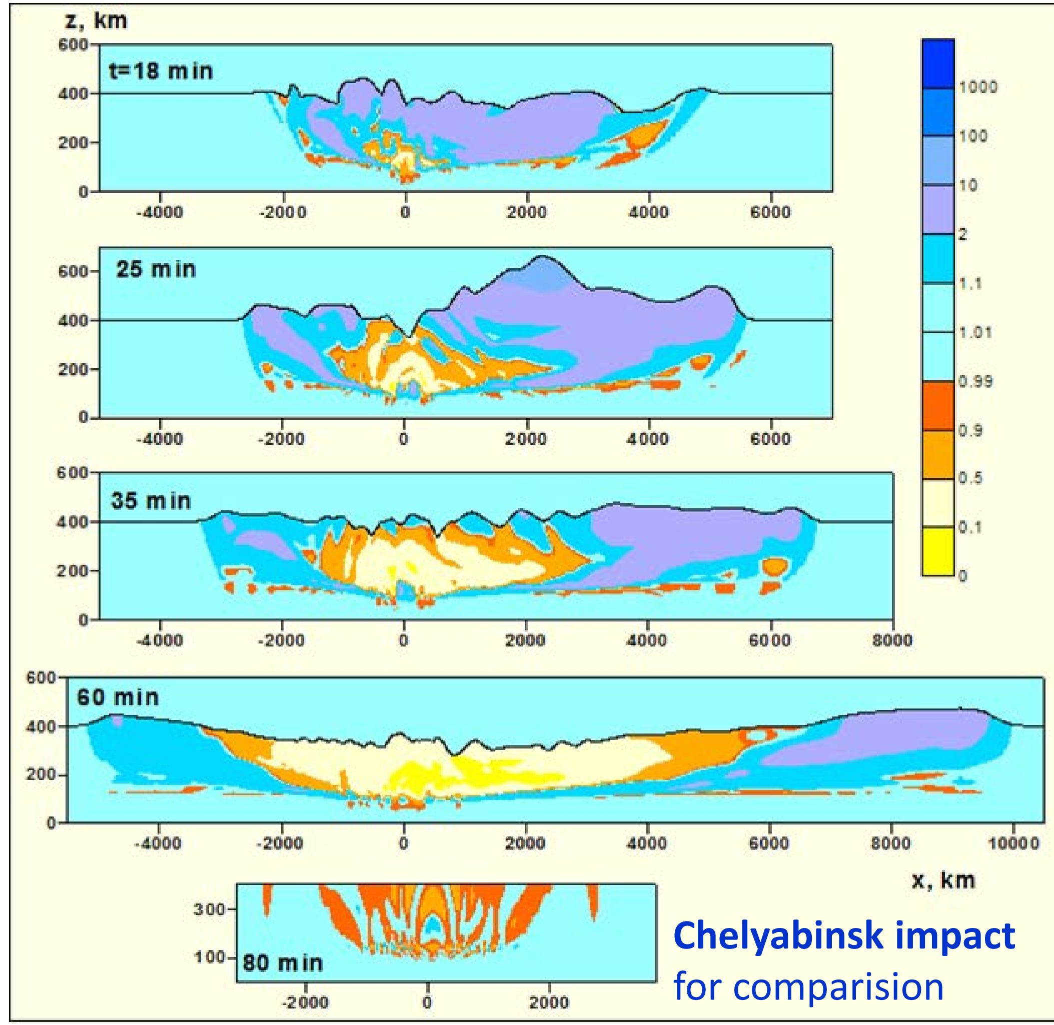

distributions of relative density ξ=max(abs(ρ/ρ^* -1)) at different time moments

$\alpha=45^0$ D=80 m V=30 km/s, comet (Shuvalov&Khazins 2017; Artemieva et al.2018)

IONOSPHERIC DISTURBANCES

Disturbances parameter ξ - relative density

ξ=max(abs(ρ/ρ* -1)) - asymmetric:

Two factors: - asymmetry of the initial disturbances; - maximum H reached by plumes.

Asymmetry is the most prominent in the 45° scenario.

Maximal ξ is largest in the vicinity of the epicenter and decreases at the scale of thousands km.

ξ is oscillating at a point (x,y).

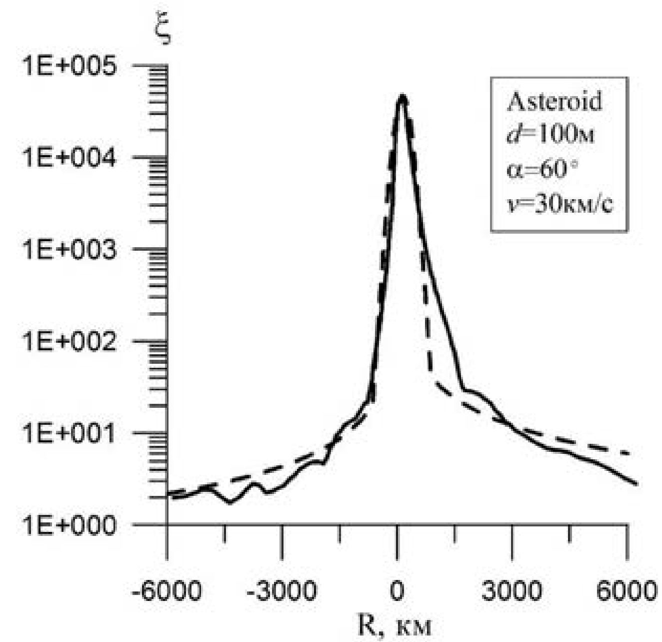

Distribution of maximal ξ at H=300 km in a plane perpendicular to the Earth's surface and passing through the impactor trajectory.

Solid - numerical modeling,
dashed - interpolation.

Shuvalov&Khazins 2017;
Artemieva et al.2018

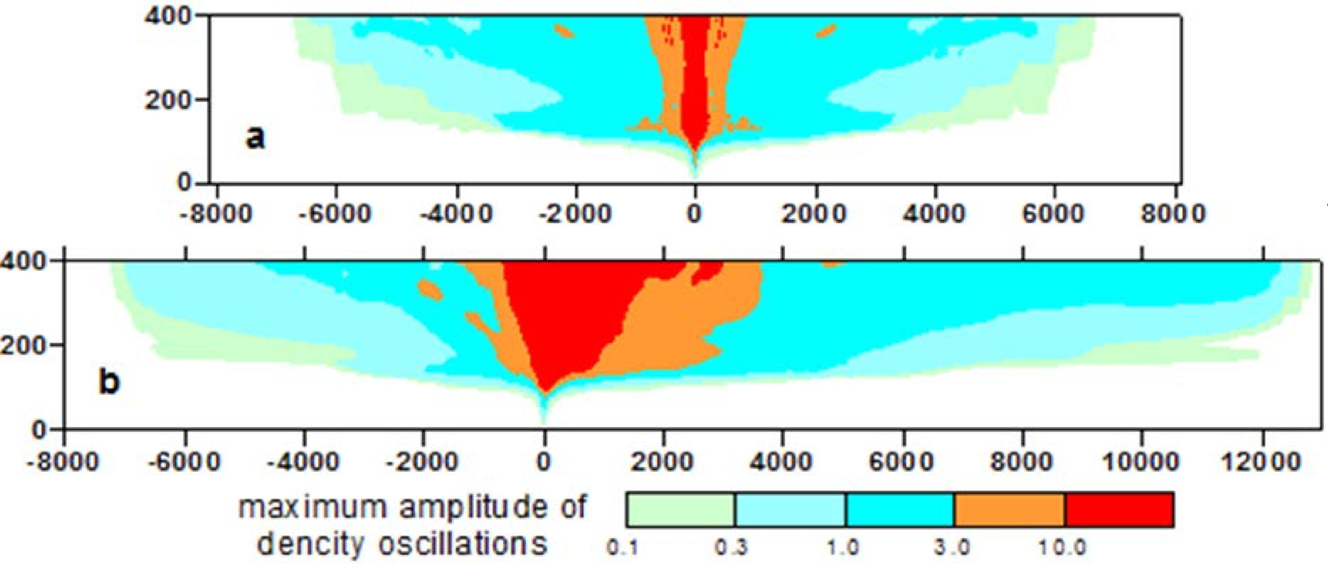

Distributions of disturbances parameter ξ : (a)13 Mt spherical explosion at H~ 10 km
(b) 13 Mt impact ($\alpha=45^0$, D=80 m, V=30 km/s, comet)
The explosion produces smaller disturbances than a real impact.

IONOSPHERIC DISTURBANCES

The only instrumental data on ionospheric disturbances – Chelyabinsk event
Well-pronounced TEC disturbances with an average period ~10 min and amplitude of 0.07–0.5 TECU (total electron content unit, 1 TECU = 10^{16} el/m^2) were detected (Perevalova et al. 2015).

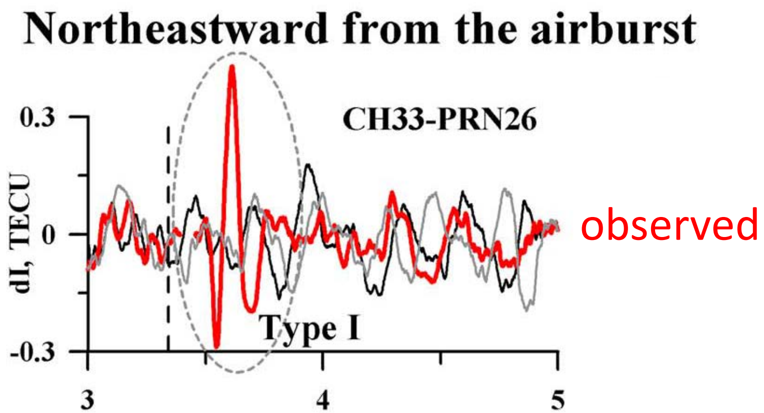

observed – grey
model at 300 km from epicenter – black
T~8-16 min

It is assumed that
TEC ~ρ~ ξ ,
value of ξ at H~300 km is considered as basis to estimate of TEC

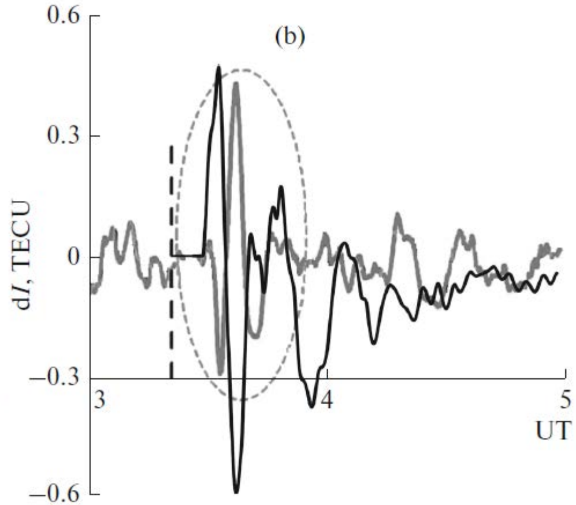

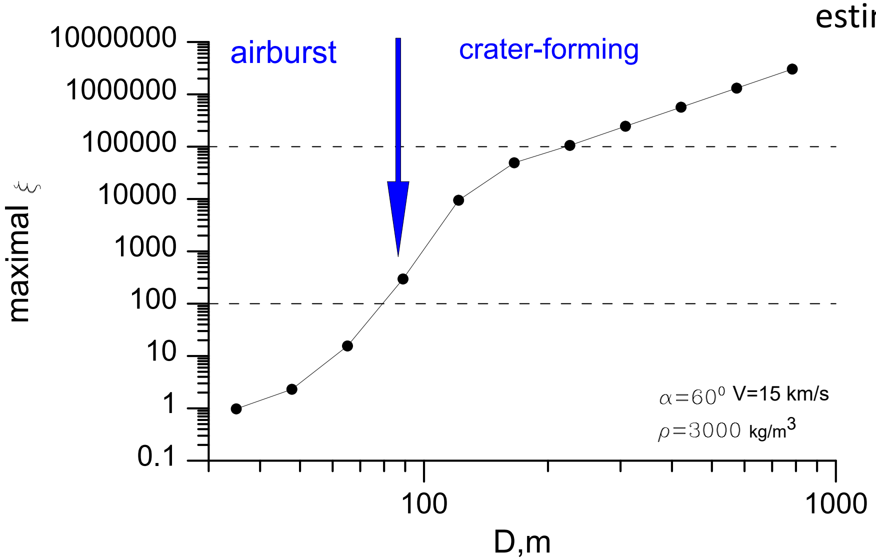

Dependence of disturbances parameter ξ on impactor size

2021 PDC probable impactor:
asteroid, V~15 km/s
D~35 - 700 m
entry angle – 3-90^0, more probable 50-80^0

SEISMIC EFFECTS

To calculate the seismic magnitude of an impact event – one needs to know "seismic efficiency" k_s

the fraction of the kinetic energy of the impact E_{kt} that ends up as seismic wave energy E_{seism}

Modeling: Svetsov et al. (2017) , Khazins et al. (2018)

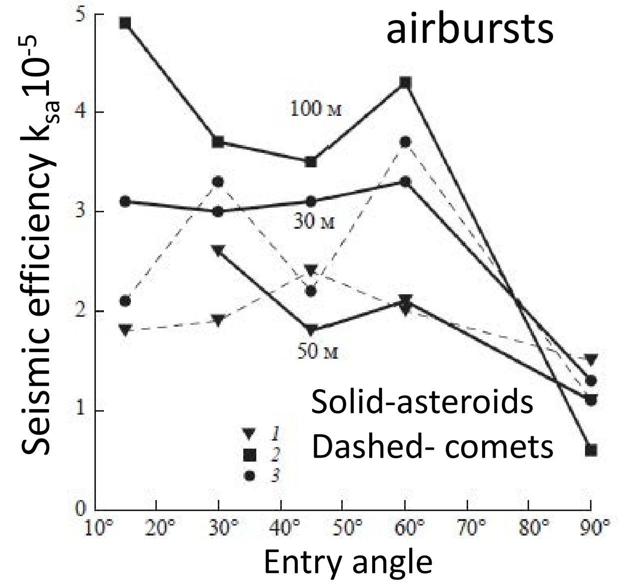

Airbursts: causes a seismic effect due to the impact of a shock wave on the surface.

Average seismic efficiency $\mathbf{k_{sa} = 2.5\ 10^{-5}}$

Lower for vertical impacts (upward motion influence)

Isolines of overpressure(p–p0, atm)

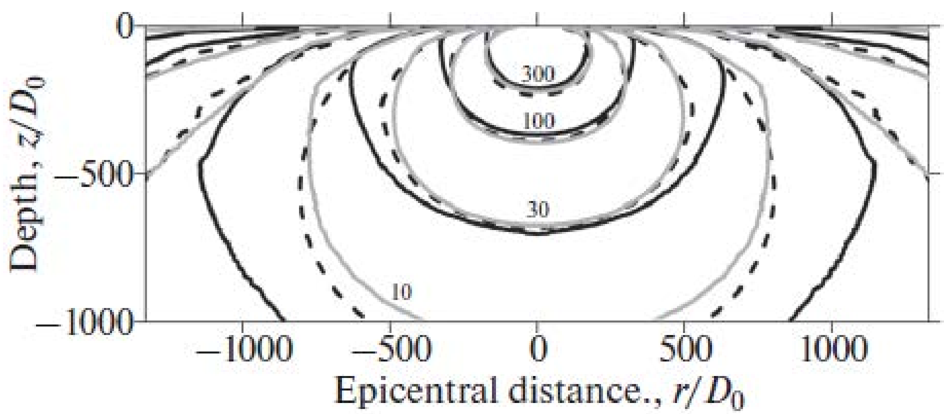

black - underground explosion with E_0 at a depth of $40D_0$

dotted - surface explosion with energy $8E_{kt}$

gray – impact with energy $2.5E_{kt}$ (vertical sizes coincide)

Crater-forming impacts:

comparative calculations of SW generation by crater-forming impacts and explosions

seismic efficiency $\mathbf{k_{sc} = 10^{-3}}$ (vertical impact)

$k_{sc}(\alpha) = k_{sc}(90°)\bullet\sin(\alpha)$

Collins et al. (2005): $k_{sc} = 10^{-4}$

Intermediate cases:

If impactor energy is dissipated both in the air (Ea) and in crater formation (Ec) then

$E_{seism} = k_{sa}Ea + k_{sc}Ec$

SEISMIC EFFECTS

Seismic effect Magnitude: 5.8

The seismic magnitude of the impact event is estimated for bothcrater forming impacts and aerial bursts.The magnitude is used for determination of the instrumental characteristicsof a seismic disturbance in the observational point.

Richter scale magnitude of the impact event: 5.8
Mercally scale intensity: IV-V
The peak ground velocity: 3.8 cm/s
The peak ground acceleration: 42 cm/s^2
Time of arrival to the observation point (started from moment of maximal energy deposition): 0:00:21

2021 PDC probable impactor: asteroid, V~15 km/s

- as small as 35 meters to as large as 700 meters
- entry angle – 3-90^0, more probable 50-80^0

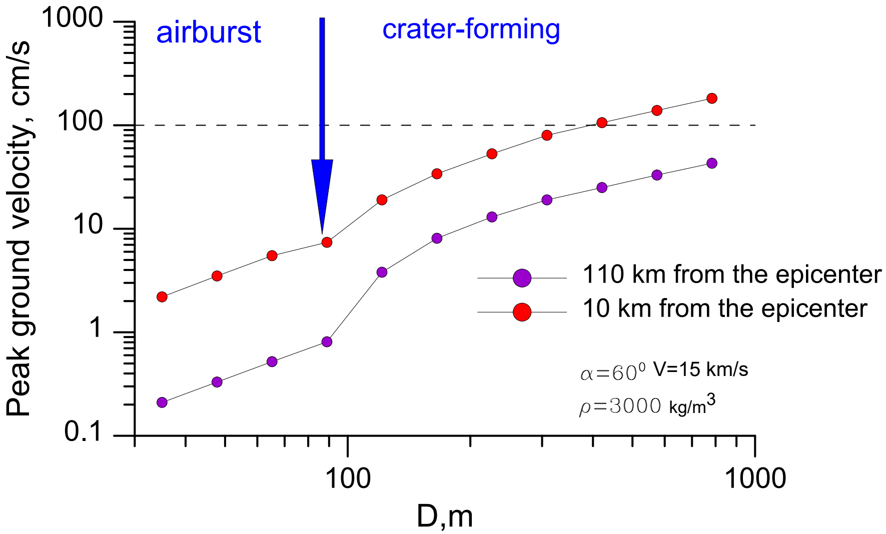

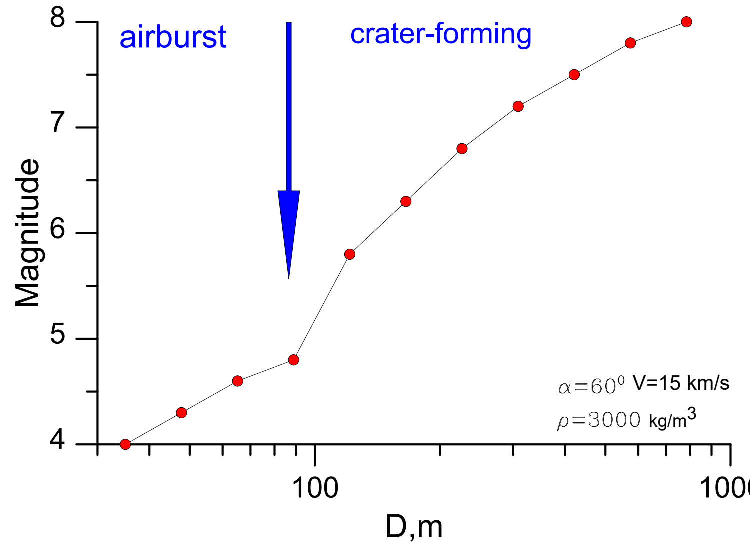

catastrophic destruction
PGV>100 cm/s

Chelyabinsk: M~3.7-4 Tunguska: M~4.8-5.2

CONCLUDING REMARKS

Serial numerical calculations of the cosmic objects impacts were conducted in a frame of special gasdynamic model with radiative transfer.

Results of these simulations allowed us to construct scaling relations, which permit one to quickly assess different dangerous consequences of impacts based on impactor parameters.

First time modeling and scalings for airbust radiation are suggested and demonstrated satisfactory agreement with existing observational data and other modeling.

First time modeling and scalings for ionispheric disturbances are suggested.

Scalings for seismic efficiency are improved based on impact modeling, the efficiency essentially differ from seismic efficiency for explosions.

Described scaling relations are implemented into web-based calculator.

Scalings in transition region of sizes/energies should be considered in more detail.

PDC probable impactor parameters are very uncertain and its impact may result in consequences of different scale.

7th IAA Planetary Defense Conference

26-30 April 2021, Online Event

Hosted by UNOOSA in collaboration with ESA

Planetary Defense Conference
PROTECTING EARTH FROM ASTEROIDS

Q&A

Session 9a: Impact Effects

UNITED NATIONS
Office for Outer Space Affairs

7th IAA Planetary Defense Conference

26-30 April 2021, Online Event

Hosted by UNOOSA in collaboration with ESA

Break

Up next: Session 10a - Disaster Management